NANYANG TECHNOLOGICAL UNIVERSITY
SINGAPORE

SYNTHESIS AND APPLICATION OF PEPTIDOGLYCAN OLIGOMERS AS METABOLIC LABELING AGENTS FOR BACTERIA

HE JINGXI

SCHOOL OF CHEMICAL AND BIOMEDICAL ENGINEERING

2019

SYNTHESIS AND APPLICATION OF PEPTIDOGLYCAN OLIGOMERS AS METABOLIC LABELING AGENTS FOR BACTERIA

HE JINGXI

School of Chemical and Biomedical Engineering

A thesis submitted to the Nanyang Technological University in partial fulfilment of the requirement for the degree of

Doctor of Philosophy

2019

Statement of Originality

I hereby certify that the work embodied in this thesis is the result of original research, is free of plagiarised materials, and has not been submitted for a higher degree to any other University or Institution.

28/09/2019 何景熙

Date He Jingxi

Supervisor Declaration Statement

I have reviewed the content and presentation style of this thesis and declare it is free of plagiarism and of sufficient grammatical clarity to be examined. To the best of my knowledge, the research and writing are those of the candidate except as acknowledged in the Author Attribution Statement. I confirm that the investigations were conducted in accord with the ethics policies and integrity standards of Nanyang Technological University and that the research data are presented honestly and without prejudice.

28/09/2019

. . . . . .

Date

. . . . . .

Prof. Chan Bee Eng Mary

Authorship Attribution Statement

This thesis contains material from 1 paper submitted in the following peer-reviewed journal(s) where I was the first author.

Chapter 3 is submitted as J.-X. He, K. Le Mai Hoang, S. H. Kho, Z. Guo, W. Zhong, K. R. V. Thappeta, R. Zamudio-Vázquez, S. N. Hoo, Q. Xiong, H. Duan, L. Yang, M. B. Chan-Park, X.-W. Liu. Synthetic Biohybrid Peptidoglycan Oligomers Enable Pan-Bacteria-Specific Labeling and Imaging: *In Vitro* and *In Vivo*. *Angew. Chem. Int. Ed.* **2019** (under revision).

The contributions of the co-authors are as follows:

- Prof. Liu, Prof. Chan, Dr. Le Mai Hoang and I conceptualized the project, Prof. Duan and Prof. Yang helped with experiment design.
- I did all chemical synthesis with assistance by Miss Hoo, and prepared sample for Cryo-TEM experiments.
- Miss Kho and Dr. Zamudio-Vázquez performed super-resolution confocal microscopic experiments.
- Dr. Thappeta and Dr. Guo performed experiments for L-form bacteria and mammalian cells, respectively.
- Dr. Xiong performed experiments with antibiotic resistant bacteria.
- Mr. Zhong did animal studies of synthesized compounds.
- I did all other experiments described, analyzed all experiment results and prepared the manuscript. Prof. Chan and Prof. Liu edited the manuscript before submission.

28/09/2019 ....

Date

何景熙 ....

He Jingxi

ACKNOWLEDGEMENT

I would like to express my heartfelt gratitude to people who have encouraged, supported and helped me during the whole period of my PhD candidature.

I am sincerely grateful to my supervisor Prof. Mary Chan-Park and co-supervisor Prof. Liu Xuewei for their extensive guidance and support. It has been a great privilege for me to work with them, who have been inspiring mentors and scientists. I would like to further extend this gratitude to Prof. Duan Hongwei, Prof. Yang Liang, Prof. Mu Yuguang, and Prof. Tan Choon Hong for their knowledge which was kindly shared with me as a great contribution to my research progress.

I would like to express my deepest acknowledgement and appreciation to the following lab mates for their generous help offered to my research projects: Dr. Kim Le Mai Hoang, Dr. Guo Zhong, Dr. Kishore Reddy Venkata Thappeta, Dr. Rubí Zamudio-Vázquez, Mr. Zhong Wenbin, Dr. Xiong Qirong, Ms. Hoo Sin Ni, Dr. Leng Wei Lin, Dr. Yao Hui, Dr. Báti Gábor, Dr. Kumar Bhaskar Pal, Dr. Ding Feiqing, Dr. Xu Yuan, Dr. Lin Yichao, Dr. Du Yu, Mr. Hou Zheng, Mr. Li Jianghua, Ms. Zhang Kaixi, and Dr. Ronny William. I would also like to express my thanks to all other colleagues in Prof. Chan's and Prof. Liu's research group for their kind encouragement and support.

I also want to thank all my friends who are always there to provide me the strong support when I needed, especially Ms. Kho Shu Hui for her invaluable help.

I am also extremely grateful to my family for their support and encouragement in my pursuits.

Table of Contents

ABSTRACT

Peptidoglycan is the core component of every bacterial cell wall, which makes it an attractive target for the development of new bacterial targeting agents and broad-spectrum antibiotics. Although many major discoveries have been made on the bacterial cell wall in the past decade, much remains uncertain about the working mechanisms of bacterial cell wall biogenesis, as well as its dynamic transformations during a bacterium's life cycle. One major bottleneck in these discoveries is the limited availability of tool compounds, derived from either natural or synthetic sources, to study the composition and dynamics of bacterial cell walls. The first part of this thesis describes an efficient and convenient approach to synthesize biohybrid peptidoglycan oligomers (PGOs), starting with the plentiful shrimp shell-derived biopolymer chitosan. The new method is the first that enabled top-down PGO synthesis as opposed to other bottom-up synthetic strategies reported. The whole process took thirteen steps in eight one-pot reactions and produced the final product in a practical gram scale. The highly water-soluble biohybrid PGOs were then synthetically conjugated to the fluorescent rhodamine dye and successfully incorporated into the peptidoglycan cell walls of both Gram-positive and Gram-negative bacteria strains. Using super-resolution STED confocal microscopy, PGO-rhodamine were found to be localized into the cell walls of all bacterial strains tested. Furthermore, the PGO-rhodamine was not taken up or incorporated into mammalian cells at all, thus confirming that PGOs can be a powerful tool for pan-bacteria-specific labeling and imaging. In the following part, mechanistic studies further supported the hypothesis of enzyme mediated metabolic labeling rather than non-specific binding to bacterial surface. The cell wall-deficient L-form strain of

enterococcus showed a drastic reduction in PGO-rhodamine incorporation, and calorimetric studies further confirmed the strong binding between our PGOs and the penicillin-binding protein 1a (PBP1a). Moreover, the potential of PGOs was demonstrated in biosensing as a diagnostic tool based on the mechanisms explored. The agent could sensitively detect the presence of low amount of bacteria, reaching as low as ~10 CFU/mL. It was also capable of identifying antibiotic resistant strains, with the aid of respective antibiotics. Animal studies confirmed the excellent specificity and utility of PGOs for use in infection models relevant to real life situation, and no toxicity was observed in all *in vivo* experiments. Besides application of modified PGOs *per se*, the bacteria targeting capability was tested in conjugation with gold nanoparticles for colorimetric analysis in a subsequent chapter. Bacteria detection was demonstrated with high sensitivity using our design, by incubation only without the need of sample washing thereafter.

Based on all the results presented in this thesis, the synthetic PGOs have been demonstrated applicable to bacterial detection and killing purposes with versatile modifications available in a feasible manner. The practical and efficient synthesis of this polymer is not an end to the project, but a starting point whereby a broad range of antibacterial applications could develop upon.

LIST OF ABBREVIATIONS

3T3	3T3 mouse fibroblast cells
Ac	Acetyl
Ala	Alanine
AMR	Antimicrobial resistant
ATCC	American type culture collection
AuNP	Gold nanoparticle
BHI	Brain heart infusion
Bn	Benzyl
Boc	*tert*-Butyloxycarbonyl
CFU	Colony-forming unit
DIPEA	*N*,*N*-diisopropylethylamine
DI water	Deionized water
DLS	Dynamic light scattering
DMF	Dimethylformamide
DMSO	Dimethyl sulfoxide
E. coli	*Escherichia coli*
EDCI	*N*-(3-Dimethylaminopropyl)-*N*′-ethylcarbodiimide hydrochloride
E. faecalis	*Enterococcus faecalis*
ESI	Electron spray ionization
Et	Ethyl
FDA	Food and Drug Administration
Fmoc	9-Fluorenylmethoxycarbonyl
FRAP	Fluorescence recovery after photobleaching
GDP	Gross domestic production
Glu	Glutamic acid

GPC	Gel permeation chromatography
HATU	1-[Bis(dimethylamino)methylene]-1*H*-1,2,3-triazolo[4,5-*b*]pyridinium 3-oxid hexafluorophosphate
HOAt	3*H*-[1,2,3]-Triazolo[4,5-*b*]pyridin-3-ol
HPLC	High performance liquid chromatography
HRMS	High resolution mass spectrometry
ITC	Isothermal titration calorimetry
K. pneumoniae	*Klebsiella pneumoniae*
LC-MS	Liquid chromatography mass spectrometry
Lys	Lysine
MDR	Multi-drug resistant
Me	Methyl
MIC	Minimum inhibitory concentration
MHB	Mueller Hinton Broth
MRSA	Methicillin-resistant *S. Staphylococcus aureus*
MTT	3-(4,5-dimethylthiazol-2-yl)-2,5-diphenyltetrazolium bromide
MWCO	Molecular weight cut-off
NAG	*N*-acetyl glucosamine
NAM	*N*-acetyl muramic acid
NHS	*N*-hydroxysuccinimide
NMR	Nuclear magnetic resonance
NPs	Nanoparticles
OD	Optical density
P. aeruginosa	*Pseudomonas aeruginosa*
PBP	Penicillin binding protein
PBS	Phosphate buffer solution
PG	Peptidoglycan

PGO	Peptidoglycan oligomer
PGT	Peptidoglycan glycosyltransferase
S. aureus	*Staphylococcus aureus*
SDS	Sodium dodecyl sulfate
STED	Stimulated Emission Depletion
Su	Succinimide
TBAF	Tetrabutylammonium fluoride
TEM	Trasmission electron microscopy
THF	Tetrahydrofuran
TIRF	Total internal refraction fluorescence
TLC	Thin layer chromatography
TOF	Time of flight
TP	Transpeptidase
TSB	Trypticase soy broth
UV−vis	Ultraviolet–visible
VRE	*Vancomycin-resistant Enterococci*
WHO	World Health Organization

LIST OF FIGURES

LIST OF SCHEMES

Chapter 1: Introduction

1.1 Current State of Antibiotic Resistance

The overuse and misuse of antibiotics have given rise to resistant bugs, and previously treatable infections have become increasingly more difficult and costlier to control. Emergence of virulent and deadly multidrug-resistant (MDR) pathogens or "superbugs" includes *Pseudomonas aeruginosa* and methicillin-resistant *Staphylococcus aureus* (MRSA).[1] The infections are becoming increasingly lethal, estimated by a report supported by UK government to reach 10 million per year worldwide by 2050, with the casualties mainly from Asia and Africa. According to an estimation by the World Bank, antimicrobial resistance (AMR) would drag global GDP by 1.1 to 3.8 percent by 2050.[2] In a report by World Health Organization in 2017, most drugs in the clinical pipeline fall under the category of modification to existing antibiotics, which were designed to have a narrow spectrum and short term before rendered ineffective from resistance. There remains a particularly strong, unmet need for novel antibiotics effective against all the AMR strains.

Since the year 2000, only five new antibiotics have been approved by FDA: linezolid (2000), daptomycin (2003), retapamulin (2007), fidaxomicin (2010) and bedaquiline (for multidrug-resistant (MDR) tuberculosis, 2012).[3] However, it must be noted that these newly approved antibiotics are only confined to the treatment of limited bacterial infections. No antibiotics with new killing mechanism or a broad spectrum have been reported for the past decades.

A resistant bacterial strain may be equipped with multiple mechanisms of antibiotic resistance, and they may originate intrinsically, by genetic mutation or from other resistant strains via horizontal gene transfer.[4] The outer membrane, which is universally present in all Gram-negative bacterial species, is one of the typical intrinsic resistances, as it blocks off a significant number of large or hydrophobic antibiotics passively.[5] On the other hand, strains such as *P. aeruginosa* are notorious for the efflux pumps they carry along on cell surface as an active means of eradicating small or hydrophilic antibiotics which have slipped through the outer membrane barrier[6]. The wide presence of these innate defense mechanisms sets up a hurdle to be overcome for effective treatment, and the acquired mechanisms further build up the difficulties.[7-8] Genetic mutation and natural selection help bacteria to develop and retain genes that render antibiotics ineffective. This is also commonly done either passively, through modifying targets of antibiotics as in the case of vancomycin-resistant enterococcus, or actively, through secreting enzymes that deactivate antibiotics as in the case of β-lactamase producing bacteria.

The resistant bacteria are not only more difficult to kill, but challenging to track as well. The defense mechanisms such as outer membrane or efflux pumps repel bacteria staining agents in the same manner as antibiotics. Identification of bacterial infections, especially those caused by AMR bacteria, in a timely fashion could promote more accurate and effective prescription, thus reducing fatality rate directly, and impeding resistance from antibiotic abuse in the long run. Currently, the diagnosis methods in practice generally rely on deduction from indirect evidences such as analysis of patient history and symptoms, which give inaccurate conclusions occasionally. In contrast, a conclusive depiction of source of illness is generally obtained from laboratory culture

test in 48-72 hours. This duration could often be too long for a patient under severe infection to endure, especially when the pathogen is an AMR strain or has developed biofilm,[9-10] thus better diagnosis options are in urgent need.

1.2 Gram Distinction and Structure of Peptidoglycan

Many methods are available to characterize an unknown sample of bacteria. Among them, Gram staining is a long established technique that can determine the bacteria of concern to be 'positive' or 'negative'.[11] Most bacteria species fall into either category and the whole experiment takes only a few minutes, so it is commonly adopted as one of the first steps of analysis. Generally, a sample is treated with crystal violet and iodine, followed by ethanol washing. It would be classified as Gram-positive if the dark violet color remains, or Gram-negative if the color disappears and that of a counterdye becomes prominent. This difference is mainly decided by a characteristic of their cell envelop structures, namely peptidoglycan (PG).[12] When there is a thick PG layer on cell surface, the large complex between crystal violet and iodine would be retained from washing, and such bacteria are Gram-positive. In contrast, Gram-negative species have a thin PG layer which are not able to block the colored complex. Through direct visualization, Gram staining is a handy tool for categorization of Gram-positive or Gram-negative bacterial cells in a bacteria sample, yet it is not capable of effectively detecting presence of bacteria in a mammalian cell sample with possible infection. Particularly, any cell type, not specific to bacteria, which does not have a thick PG layer would display pink color after staining. Furthermore, Gram staining distinguishes bacteria by their cellular structure rather than biological activities. Hence, it cannot

identify more detailed properties such as bacterial species, drug resistance or whether the cells are alive.

PG forms a mesh-like resilient structure that protects bacteria against varying osmotic pressures, and provides an anchoring platform for extracytosolic proteins.[13] At the molecular level, PG contains repeating units of *N*-acetylglucosamine (NAG) linked *N*-acetylmuramic acid (NAM), with the latter covalently linked to a pendant pentapeptide. Different bacteria strains demonstrate variance in the exact structure of the pentapeptides, which are all cross-linked to the same NAG-NAM oligosaccharide chains to generate the three-dimensional network of PG that is characteristic of all bacterial cell walls.

1.3 Biosynthesis of PG on Cell Surface

PG consists of alternating NAG-NAM sequences to form long strands. The covalent linkages between NAM units further weave the strands into rigid networks to cover the whole surface of a bacteria cell. Although the chemistry of the linkages differs among bacterial species, and the length of each strand may vary even for the same strain, the assembly of PG follows the same process for all bacteria (**Figure 1-1**).

The biosynthesis of PG starts within cytosol, where NAG first undergoes enzymatic conversion to become NAM with a lipid pyrophosphate at the anomeric position and a pentapeptide linked to the C3-lactate.[14] As an entity, the compound is known as Lipid I, comprising one sugar unit. After forming glycosidic linkage with another NAG, the disaccharide product Lipid II is flipped outside cytosol to reach cell surface.[15]

At the exterior of cell membrane, the subsequent PG assembly processes are carried out by penicillin binding proteins (PBPs). The enzymes are named after their interaction

with the renowned antibiotic family, as they are inhibited through irreversible binding and in turn leading to cell lysis.[16] They constitute two major domains which work together towards mature PG, namely peptidoglycan glycosyltransferases (PGTs) and transpeptidases (TPs). PGTs catalyze glycosylation between the anomeric position of a PG strand with a Lipid II substrate and are responsible for PG elongation. After multiple cycles of transglycosylation, a strand would be sufficiently long to activate the function

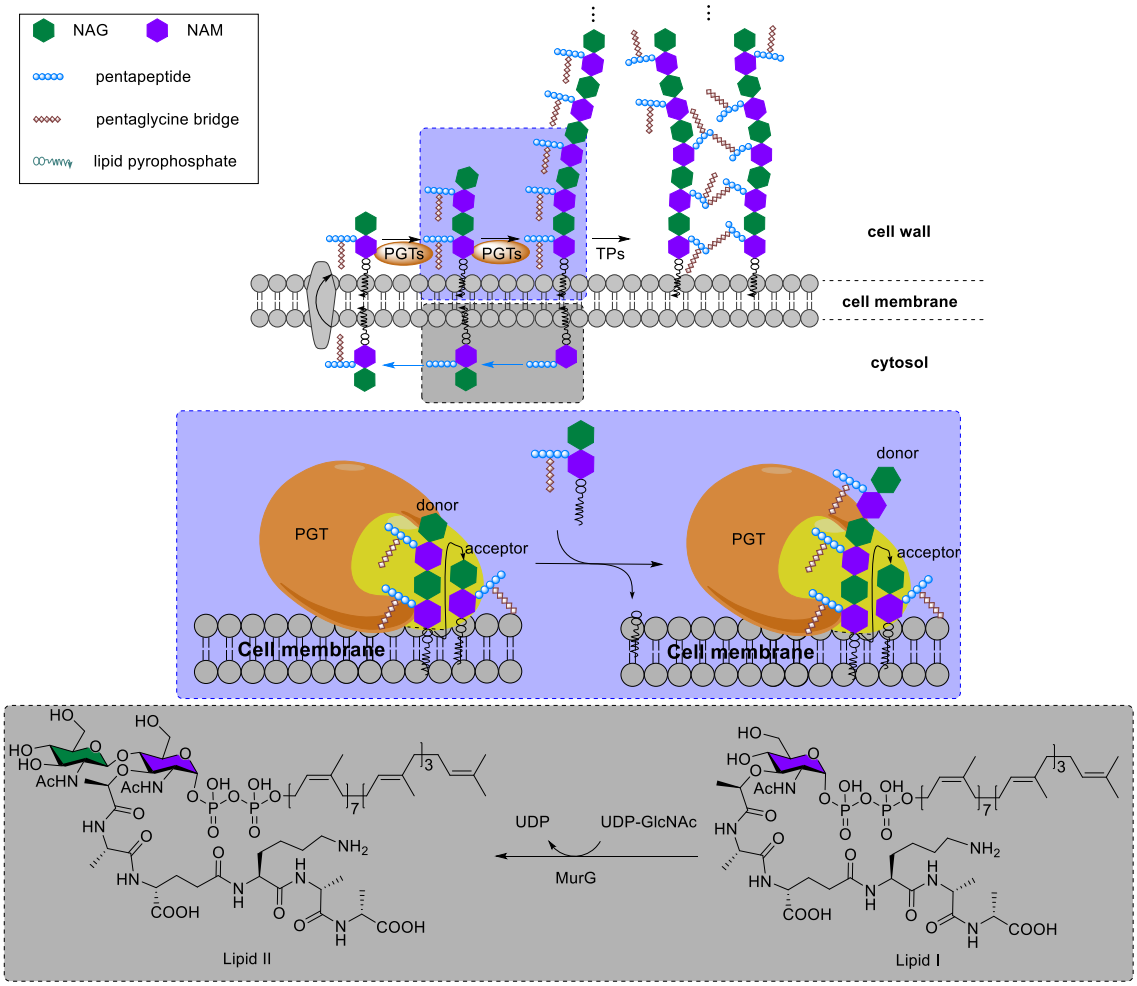

Figure 1-1. Biosynthesis of PG from Lipid I. Details of coupling reactions are drawn in blue and gray boxes for Lipid IV to Lipid VI and Lipid I to Lipid II, respectively. Chemical structures of Lipid I and II are explicitly shown and the rest follow the color code.

of TPs, which cross-link the peptides to increase the rigidity of PG. A strong PG network is required by bacteria to sustain through osmotic stress, yet a major portion of the assembly process takes place outside of bacteria, which makes it susceptible to interferences from the cell surroundings. Therefore, many common antibiotics work by impeding cell wall synthesis, such as penicillin or vancomycin.

1.4 Challenges in Access to PG Substrates

The fact that bacteria of different species follow the same process to synthesize PG and that the catalysis by PBPs takes place at the surface of bacterial cells make the PG biosynthesis promising for design of selective bacterial targeting agents. In particular, the interaction between TPs and peptide is the target of β-lactams, and that between PGTs and Lipid II is the target of vancomycin. However, progress on exploiting the potential of this process is being made slowly.

Although many PBPs have been isolated and characterized, it is impractical to speculate their bioactivities without supply of substrates. For TPs, researchers have found D-amino acids and short peptides as surrogates to activate their functions.[17-18] On the contrary, there has been no report on PGT's interaction with substrates other than Lipid I, II or longer ones. As a dynamic process, PG synthesis constantly consumes the substrates and molecules such as Lipid II are estimated to be less than 2000 per cell, which leads to very low quantity by extraction.[19] In addition, the complex chemical functional groups present on a substrate molecule makes structure modification rather challenging. Hence, chemical or chemoenzymatic synthesis of the substrates is commonly resorted to.

The earliest chemical total syntheses of Lipid I or Lipid II was reported early this century.[20-21] Nevertheless, the large number of steps needed to finish the synthesis makes it challenging even to a specialized chemist. Furthermore, this number grows rapidly with the size of substrate, which brings down the overall yield of the whole synthesis. A recent article described how a fragment of Lipid VIII, with eight sugar units, was obtained with less than 1 mg at the end.[22] Hence, investigation on activities of PGTs have been mainly carried out using Lipid II or Lipid IV derivatives, and it is not well understood how the enzymatic reaction proceeds at later stages, with longer PG strands. Particularly, it was inferred from comparison between Lipid II and Lipid IV that substrates with at least four sugar units undergo PGT catalysis more efficiently than Lipid II.[23-24] However, the limited availability of substrates is still impeding further exploration of the PG synthesis process.

1.5 Objectives

After careful examination of literature describing the synthesis of PG substrates, it was noted that the main bottleneck could be protecting group manipulation for tuning of the sugar's reactivity towards glycosylation. With larger size of a substrate, more glycosidic bonds need to be constructed and many times more hydroxyls and amines need to be chemo- and regioselectively protected or deprotected. Drawing inspiration from our group's earlier works on synthesis of chitosan-based polymers for antibacterial applications,[25] it was envisioned that a 'top-down' synthetic strategy starting from chitosan instead of conventional 'bottom-up' ones starting from glucosamine could allow for skipping most glycosylation reactions (**Figure 1-2**). Moreover, all the associated protection, deprotection and activation of positions where glycosidic bonds

are built, namely C1 and C4, are no longer needed since there are already β-1→4 glycosidic bonds chaining the whole molecule together. In this manner, plenty of time and resources could be saved and the product may be potentially enough for mechanism and application studies.

The long chain oligomeric product, once successfully obtained, would be investigated

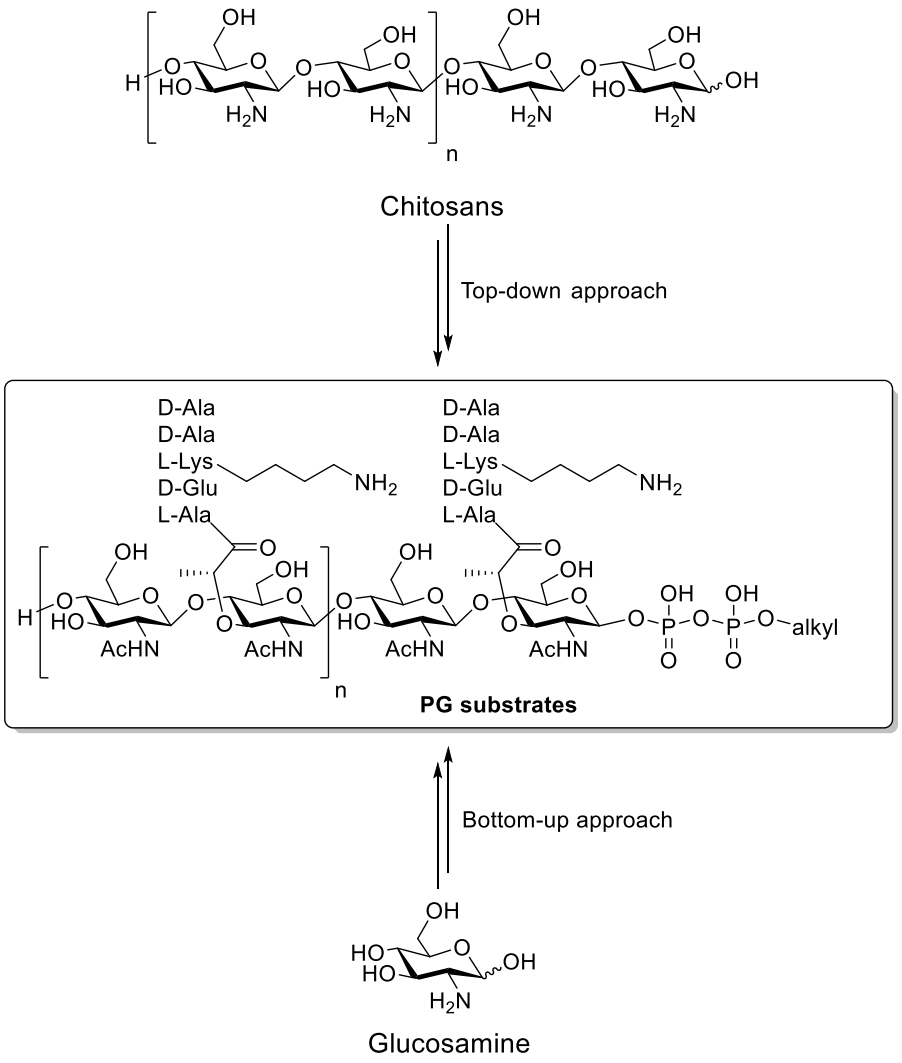

Figure 1-2. 'Bottom-up' and 'top-down' (this design) synthesis of PG substrates.

for bioactivities to demonstrate if they can still be recognized by PGTs and made into a part of bacterial cells' PG layer. In addition, it was noted that Lipid IV is more efficiently used than Lipid II by PGTs but how larger ones behave remains unknown. On the other hand, PG substrates prepared by this method can be readily extended to different sizes with chitosan precursors of appropriate degrees of polymerization, so the correlation between size and enzyme activities may be investigated for higher sugar numbers.

Eventually, the synthetic substrate may be brought to test of applications as a targeting molecule. Since PG and PBPs are only found in bacteria, targeting this process could potentially be bacteria exclusive, without significant interaction with mammalian cells. Furthermore, this targeting agent may be further manipulated for detection or killing of resistant strains specifically, which could contribute to solving the AMR problem discussed in Section 1.1. Hence, in this thesis I have the following objectives:

1. Design and optimize top-down synthetic route to access oligomeric PG substrates from chitosan starting materials.
2. Investigate how the synthetic substrate interact with bacteria and PBPs.
3. Apply the synthetic substrate in biosensing.

1.6 Organization of the Thesis

The thesis comprises six chapters, following the sequence of Introduction (Chapter 1); Literature review (Chapter 2); Synthetic peptidoglycan oligomers for bacteria-specific metabolic labeling (Chapter 3); PGOs with different sizes are recognized and used with varying efficiencies (Chapter 4); A PGO/AuNP conjugate for highly sensitive detection

of bacteria (Chapter 5); Conclusion and outlook (Chapter 6). A brief description of contents in each chapter is given as follows:

In Chapter 2, a literature review is given on how researchers have accessed PG substrates in the past and how they have been used. The concept of metabolic labeling and how it has been developed in the context of bacterial cell wall are also presented. This provides the basis for design and application of the synthetic oligomeric PG.

In Chapter 3, the top-down synthetic route of PGOs was designed and optimized to give the product in practical scales. The PGOs synthesized were conjugated with different fluorescent dyes for *in vitro* or *in vivo* metabolic labeling of bacterial cell wall with excellent selectivities. They have also been mechanistically evaluated for their interaction with PBPs and applied to screening of AMR strains.

In Chapter 4, PGOs were functionalized with sulfur moieties to improve the affinity with gold atom. Conjugates of PGO and gold nanoparticles were prepared and optimized for detection of bacteria by colorimetric assays, which could be more practical than fluorophore alone with the centrifugation and washing steps after incubation skipped. The bacterial selectivity of PGOs combined with high sensitivity of the nanoparticles towards environmental changes afforded an efficient bacteria-sensing tool.

In Chapter 5, conclusions are made from works done and presented in this thesis and an outlook is given for possible future directions.

Chapter 2. Literature Review

2.1 Reported Methods to Access PG Substrates

As described in Chapter 1, PG biosynthesis is a promising target for design of design of agents that target bacteria selectively, yet the limited availability of substrates impedes further investigation. Fragments of the full substrates, such as monosaccharides, amino acids or short peptides have been used for probing PG assembly.[26-28] However, they are not directly present in the reactions taking place on cell surface as depicted in **Figure 1-1**, which mainly involves Lipid II, which is synthesized within cytosol and transported outside thereafter, and larger molecules stemming from Lipid II. Hence, researchers are looking for new methods to obtain larger PG substrates which are more likely to participate in PG biosynthesis on cell surface.

2.1.1 PG Substrates Obtained by Chemical Synthesis

The earliest reports on chemical total synthesis of Lipid I or II are contributed by Eli Lilly and DuPont, respectively, making use of an expensive precursor, NAM.[20-21, 29] For Lipid II, the authors firstly blocked the lactate with a protected Alanine to prevent formation of undesirable product as cyclized NAM. Then protecting group manipulation was done to replace 4,6-*O*-benzylidene protection with 6-*O*-acetyl, leaving C4-OH exposed for glycosylation with NAG. While an acetyl and phthaloyl protected NAG had been prepared in parallel, β-1→4 glycosylation was preformed regio- and stereoselectively to build the NAG-NAM core structure. After another protecting group manipulation, the authors made it consistent that all amines were in the final form of acetamide, which is kept to the end to the synthesis. Also, the benzyl protection at the

reducing end was removed, followed by glycosylation with a phosphoramidite, which was oxidized *in situ* to phosphate. Eventually, the peptide and lipid phosphate moieties, also prepared in parallel, were installed onto the lactate and phosphate respectively and a global deprotection by TBAF and sodium methoxide sequentially led to Lipid II as the final product (**Figure 2-1**).

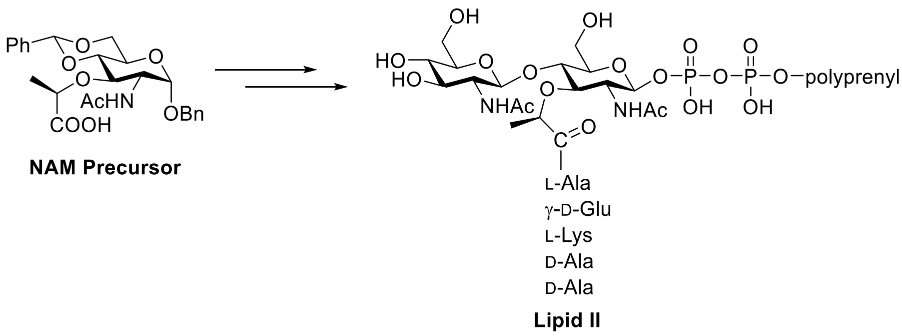

Figure 2-1. The first reported chemical total synthesis of Lipid II started from a protected NAM precursor.[20]

For larger substrates such as Lipid IV, with four sugar units, this chemistry became inefficient both economically and timely. Hence, cheaper starting materials and synthetic strategies other than the conventional glycosylation and protecting group manipulation sequences are commonly adopted.[23, 30] A fragment of Lipid IV was synthesized by Mobashery *et al.* first, with the anomeric position blocked by silyl or methyl instead of a lipid pyrophosphate.[31] Kahne and Walker reported use of thioglycosides to construct a tetrasaccharide backbone before adding on lactate, peptide and lipid pyrophosphates. The thioglycoside remained latent until oxidation into sulfoxide, so the authors could prepare monosaccharide building blocks as thioglycoside modules, then lock pairs into disaccharide modules and eventually form tetrasaccharides by further locking pairs of disaccharides (**Figure 2-2**). Cheng and Wong, on the other

hand, came up with a strategy that discriminated upon reactivities of sugars with different protecting patterns. After carefully customization of the protecting groups of each monosaccharide building block, their 'relative reactivity values' became just good that sequential glycosylations can be done with acceptable regio- and stereoselectivities when no further manipulation of protecting groups were needed in-between.

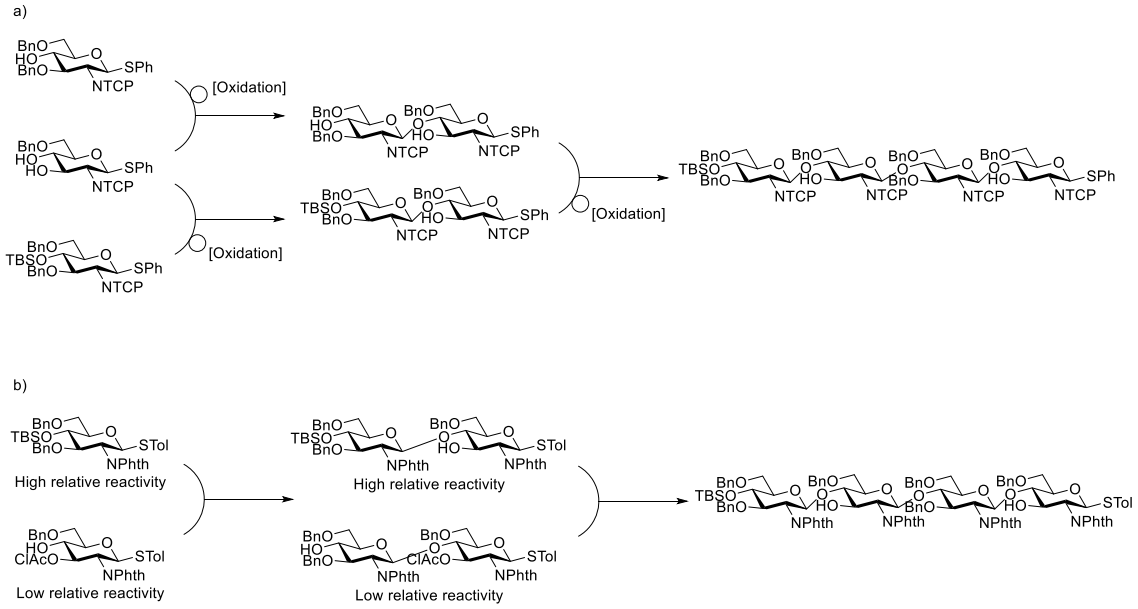

Figure 2-2. Synthesis of the tetrasaccharide core of Lipid IV by **a)** a latent thioglycoside which can be activated via oxidation separately or **b)** tuning of relative reactivity values of each molecule so activation can be done sequentially from high to low reactivity.[23, 30]

The largest substrate reported thus far is an octasaccharide as a fragment of Lipid VIII.[22] The authors used Fmoc group to protect C4-OH, which could be cleaved off readily with mild bases or even on solid support. Extending the modular synthetic strategy to locking pairs of tetrasaccharides, the authors obtained a Lipid VIII fragment without the terminal lipid pyrophosphate, having a final yield of less than 1 mg. This clearly showcases the difficulty in accessing large substrates of PG with a reasonable scale for mechanism or application investigations.

2.1.2 PG Substrates Obtained by Enzymatic Synthesis

Earlier studies on the glycosyl transfer reaction catalyzed by PBPs relied on substrates obtained by enzymatic synthesis more commonly. Lipid II, the most commonly used building block for PG biosynthesis, was first synthesized chemoenzymatically by subjecting chemically synthesized Lipid I to catalysis by a glycosyltransferase, MurG.[32] During the study, multiple analogs of Lipid I showed comparable activities in interaction with the PGT, and those with smaller lipid tails than the natural substrate were concluded as 'better' substrates since they were less prone to spontaneous aggregation in solution.

Similar studies were also reported by later, which synthesized Lipid II derivatives from analogs of Lipid I to study structure-activity relations (SARs). In 2003, Wong *et al.* furthered previous conclusion that smaller lipid tails were better for substrates and found that the sole function of that moiety in the enzymatic synthesis of Lipid II was anchoring by hydrophobic interactions.[33] In this regard, an aromatic ring or a saturated alkyl chain fulfills the requirement with similar efficiencies, and a non-branching alkyl chain with 12-14 carbons worked the best in terms of both enzymatic activities and synthetic challenges. Later, the same group did a similar study for synthesis of larger substrates using Lipid II derivatives.[34] The entirety of pentapeptide moiety was found to be not necessary for PBPs to be functional, as a truncated tripeptide served as PG substrate *in vitro* with comparable enzyme kinetics and thermodynamics. However, the product was not further applied for any studies because the length of the final product was not well controlled during the enzymatic reactions. For a similar reason, no reports

are seen which uses enzymatic reaction to prepare substrates larger than Lipid II with a practical scale for further studies.

The first fully enzymatic synthesis of Lipid II, in contrast to the previous works which all had an chemically synthesized intermediate to be subjected to enzymatic reactions, was reported in 2014.[14] An unmodified NAG was incubated with a series of enzymes from NahK to MurG, which are found in the natural synthetic route of PG substrates, in one pot to produce the final product Lipid II in up to 70% overall yield. Moreover, the enzyme UK, being responsible for phosphorylating the lipid tail, was tested for its specificity towards analogs of the natural polyprenyl moiety. High tolerance towards deviations in chemical structures was observed throughout all analogs tested, and the authors demonstrated enzymatic synthesis as a highly efficient way to obtain Lipid II and derivatives for investigations.

2.1.3 PG Substrates Obtained by Extraction

As discussed in the previous chapter, there are limited number of molecules of PG substrates per bacterial cell, and they have a wide range of chain lengths, being a mixture of Lipid II, IV, VI, VIII, etc. Hence, direct extraction of PG substrates from bacterial cells had been out of consideration for researchers trying to access the compounds.

Recently, Kahne and Walker conceived that antibiotics which function by blocking cell wall synthesis, especially inhibiting PGTs and thus polymerization of Lipid II, might lead to accumulation of PG substrates which are prohibited from assembly.[35] Results of Western blotting showed that the amount of Lipid II had a ten-fold increase in *S. aureus* after treatment with moenomycin and that had a thirty-fold increase in *B. subtilis* after

treatment with vancomycin. The authors extracted the cell culture with chloroform and methanol, and washed the interface lipid layer with pyridinium acetate/butanol/water to give native Lipid II in up to 500 μg/L. Although the isolated compound can hardly be further modified by chemical reactions compared to the appropriately protected intermediates in chemical synthesis, this serves as an efficient alternative route to access Lipid II when native substrates are needed for mechanism studies of PG biosynthesis.

2.2 Metabolic Labeling

It was during the comparisons between chemical and enzymatical synthesis of PG substrates, as discussed in the previous section, that researchers have noted the specificity of enzymes towards the chemical structure of substrate. This proved to be one of the advantages of chemical approach when a diversity of analogous compounds is needed, since the reserve of chemical reactions available for structure modification is far larger and more developed than that of enzymatic reactions. However, the natural metabolism pathway of cell wall synthesis could also tolerate deviations to the defined substrate structures when intercepted by a synthetic substrate with structure closely enough mimicking native ones. Bertozzi *et al.* pioneered the application of carbohydrate substrates for metabolic labelling of eukaryotic cells. They showed that ketone functionalized mannose could be metabolically incorporated into human cancer cells.[36] The chemical reactivity of modified cell surface towards hydrazide was then significantly improved and the engineered cells allowed for active targeting by this reactivity while alive. Similarly, Grimes *et al.* showed that azide functionalized glucosamines could label the carbohydrate core of PG in bacteria.[28] While labeling efficacies have been observed in many species, the vast number of glucosamine

derivatives investigated (ranging from a simple substitution of methyl to a large fluorophore) have yet to display particular selectivity against bacteria over other species.

2.2.1 Metabolic Labeling Bacterial Cell Wall via TPs

The metabolic labelling of bacteria through swapping of terminal D-amino acids on PG's peptide stem with synthetic analogues has been pioneered by Kahne and VanNieuwenhze. Kahne *et al.* found, as they reported in 2011, that while TPs were well known for their cross-linking functions, their substrates were not limited to large PG fragments.[18] It was noted that only one participant for the enzymatic reaction had to be a polymeric substrate, and the other one could be as small as an amino acid with D-stereochemistry on the α-carbon. Besides the mechanistic investigation on this reaction, VanNieuwenhze *et al.* established the basis for applications of this reaction only one year later.[26] Fluorophore functionalized D-amino acids (**Figure 2-3**) were

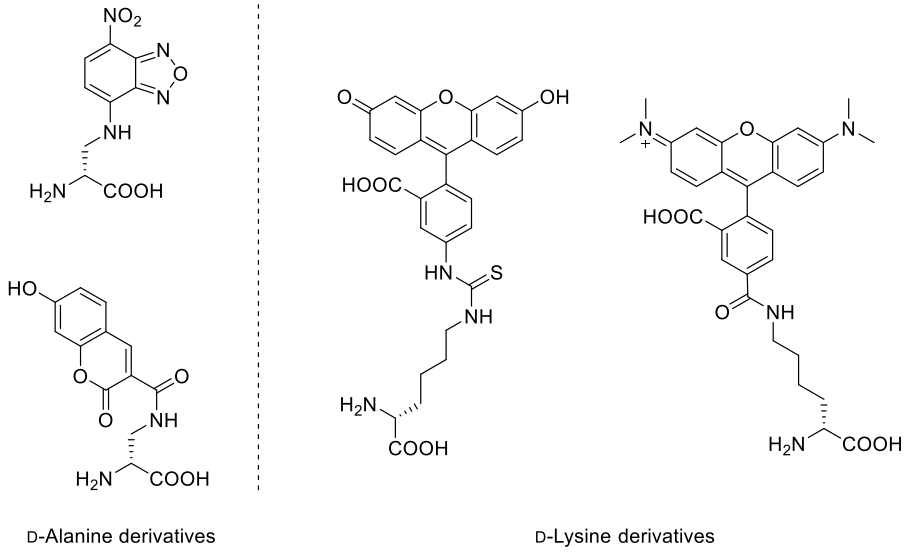

Figure 2-3. Fluorescent labeled D-amino acids that have been successfully demonstrated for cell wall metabolic labeling.[26]

incubated with whole bacteria and the cell wall was successfully labeled fluorescently. Moreover, alkyne or azide modifications on the side chain allowed for installation of fluorophores post-labelling, via click reactions.

Many uses have been found for TPs catalyzed metabolic labeling of cell wall. In 2014, Liechti and co-workers substantiated that D-amino acids could be incorporated into Chlamydia *tricomatis* by the same procedure applicable to other common species.[27] Whether cell wall existed in this strain has long been a topic of interest to researchers, and observing functional TPs provided a strong positive support. On the other hand, Pires *et al.* did not focus on a single strain, but utilized the activities of TPs to distinguish among different bacterial species.[37-38] Taking advantage of the significant discrepancy between uptake efficiencies of Gram-positive and Gram-negative strains, the authors were able to tell the Gram distinction of a strain of interest upon labeling using a standardized condition. The discrepancy, as hypothesized by the authors, was due to low permeability of the outer membrane barrier, which was present only in Gram-negative species, leading to the restricted access to TPs of the compounds, as well as the inherent compositional variations of TPs across different strains.

As small molecules, functionalized D-amino acids could be readily synthesized to a practical scale for far more application studies than those enumerated here.[39-43] However, the small size of D-amino acid molecule implicates that any modification (*e.g.* with a fluorescent dye) would significantly alter the recognition and incorporation of D-amino acid by bacteria. Hence, the metabolic labeling process might need relatively high concentrations to enable cellular uptake, as it was noted that the minimal concentration to reach an acceptable signal to noise ratio of 3 was around 0.5 mM of D-amino acid

with at least 3 washes.[44] Furthermore, TPs have a high tendency swap the terminal D-Ala with other D-amino acids in the surroundings, and this terminus is also subject to hydrolytic removal by the same class of enzymes during PG remodeling.[17] This leads to spontaneously and uncontrollably diminishing amount of incorporated D-amino acid agents upon discontinuation of supply in the culture media, even when the cell is being washed by growth media.[44]

2.2.2 Metabolic Labeling Bacterial Cell Wall via PGTs

The activity and application of TPs have been extensively studied so far with a handy tool of D-amino acid, which could be synthesized and modified with ease. Moreover, many antibiotics have been developed against TPs, with the most well-known representative of penicillin. On the contrary, there has been no report on shortcuts to access substrates of PGTs, as the polymerization process they are in charge of only involved a peptidoglycan oligomer and a molecule of Lipid II. Although a handful of reports on the activities of this class of enzymes have been published, they are mostly on Lipid II derivatives as the minimal active structures.[45-49] In addition, the application of PGTs has not been effectively developed, and the only known antibiotic targeting PGTs is moenomycin, which has not been approved for treatment of bacterial infection in human due to its poor pharmacokinetics.[50]

For the metabolic labeling application via PGTs, pioneering works by Nishimura *et al.* revealed that live bacteria cells might be labeled utilizing fluorescein labeled Lipid I or Lipid II derivatives with varying efficiencies.[51] Namely, lactobacillus had efficient incorporation of the compounds when incubated *in vitro*. However, with the unresolved synthetic challenges as described in the previous section, the route of PGTs proved to be

discouraging compared to TPs, which has D-amino acids as shortcuts. Meanwhile, it was reported that longer NAG-NAM sequences, such as Lipid IV with at least four sugar units, has even higher efficiencies in the incorporation into PG in comparison to Lipid II, with two sugar units.[23-24, 30] It was found in the studies that while PGTs such as PBP1b could only catalyze PG polymerization by adding one molecule of Lipid II each time, some such as PBP1a could directly couple peptidoglycan oligomers (PGOs). Hence, the higher uptake efficiency of PGOs probably arose from their participation in more enzymatic reactions.

Nontheless, the synthetic yield of PGOs drops drastically with increasing lengths, as discussed in the previous section. No study is available on how the oligomers perform as metabolic labeling agents.

2.3 Summary and Conclusions

The rise of AMR increased the demand of bacteria-selective targeting agents, and the universal-yet-specific presence of PG in bacteria drove the development of more efficient methods to access PG substrates for the metabolic labeling of cell wall. Compared to the more understood TPs, PGTs have been far less investigated and exploited, leaving a wide gap to be explored. Hence, recent advances in strategies to obtain molecules larger than Lipid I have been discussed with examples given in section 2.1.

Synthesis of Lipid I or II were rather straightforward, especially when the most complex component, NAM, was purchased with customized protections. However, it becomes far more difficult when the target of synthesis is Lipid IV, with three glycosylation

reactions necessitated instead of one. Hence, chemists generally design the protecting pattern and anomeric leaving group of monosaccharide building blocks such that they could be assembled modularly into disaccharides and tetrasaccharide sequentially, without further protecting group manipulations in-between. After obtaining the tetramer core, peptides and lipids were attached, followed by a final global deprotection to yield Lipid IV or its derivatives. However, another doubling of NAM-NAG sequences proved to have an even more drastic increase in synthetic difficulty. Without a breakthrough in the design of synthetic methodology, researchers have no access to full Lipid VIII or higher at a sufficiently practical synthetic efficiency for mechanistic or application investigations.

Alternatives have been adopted, including enzymatic synthesis or extraction from bacterial cells. They could produce Lipid II with high efficiencies, and the chemical structure of product was the same as native ones present in live bacteria, so various biological studies could be carried out with the PG substrates obtained as such. However, they also shared the same drawback as they could only produce Lipid II in the native form. Only limited modifications could be done on such a complex structure without orthogonal protecting groups, and this precluded experiments which required a few analogs. Furthermore, these alternative approaches have only produced compounds up to the size of Lipid II, as anything larger would involve catalysis of functional PGTs, and their polymerization could be hardly controlled to stop at a certain point.

In section 2.2, the concept of metabolic labeling of bacterial cell wall has been described with examples demonstrating how the technique can be applied.

PBPs are responsible for the second stage of PG biosynthesis, which distinguishes itself from the first stage by occurring only on cell surface, utilizing materials, as the end products of the first stage synthesis, transported there from cytosol by flippases.[52-54] The two constituent domains, PGTs and TPs, are naturally targets for agents which strive for bacterial selectivity due to their universal presence in bacteria, complete absence in mammals, particularly humans, as well as their ease of access, being conveniently residing on the exterior of bacterial cells.

Since the discovery of TPs' capability to swap terminal D-amino acids on PG substrates, researchers have been able to exploit this function to both investigate biological proceesses involving TP catalysis and develop bacteria-specifc agents for biosensing or antibacterial applications. However, no such interaction with small molecules have been found for PGTs, which are still predominantly known for its role in transglycosylation of Lipid II molecules and the elongation of PG chain in turn.

Hence, the biological pathways involving PGTs remains largely unexplored, and bacterial species with inherent AMR against TP-targeting antibiotics, such as MRSA with its binding pockets of TPs mutated, find themselves difficult to be metabolically labeled. With more facile and practical methods to access substrates of Lipid II series, especially as oligomers of peptidoglycan, we would be able to expand our knowledge of PGTs and extend our reach in the diversity of bacterial species with the tool of metabolic labeling.

Chapter 3: Synthesis of Peptidoglycan Oligomers as Bacteria-specific Metabolic Labeling Agents

3.1 INTRODUCTION

The rise of multidrug-resistant bacteria pathogens is becoming a global threat to public health, thus driving the relentless search for new and more effective antibiotics.[55-57] The biosynthesis pathway for bacterial cell walls remains an attractive family of drug targets, due to its ubiquitous presence across all bacterial phyla and its complete absence in human cells.[16, 58-60] In fact, many of the most successful broad-spectrum antibiotics such as vancomycin, penicillin, and the associated beta-lactam families specifically disrupt various stages of bacterial cell wall biogenesis.[61-62] Further, this feature may also be the target of bacteria-specific targeting agents underpinning various biosensing agents.

The major constituent of bacterial cell walls, in both Gram-positive and Gram-negative bacteria, is the network of peptidoglycan (PG). The PG network forms a resilient structure that protects bacteria against varying osmotic pressures, and provides an anchoring platform for extracytosolic proteins such as Braun's lipoprotein.[13] At the molecular level, PG contains repeating units of *N*-acetyl-glucosamine (NAG) linked *N*-acetyl-muramic acid (NAM), with the latter covalently linked to a pendant pentapeptide. Different bacteria strains demonstrate variance in the exact structure of the pentapeptides, which are all cross-linked to the same NAG-NAM oligosaccharide chains to generate the three-dimensional network of PG that is characteristic of all bacterial cell walls.

NAG-NAM oligosaccharide elongation and peptide cross-linking are thus shared processes in all bacteria, mediated by a variety of peptidoglycan glycosyltransferases (PGTs) and transpeptidases (TPs) respectively. TPs, in particular, have been the target for several modern broad-spectrum antibiotics such as penicillin and vancomycin, with derivatives of D-amino acids developed for mechanistic or application studies.[18, 26, 37, 42] However, little is known about the PGTs and their enzymatic properties, in part due to the limited availability of both relevant substrates, which has no shortcuts like D-amino acids for TPs, and appropriate *in vitro* assays. Towards this end, some encouraging efforts have been devoted to synthesizing the lipid II-VIII compounds as PGT substrates, through chemical or enzymatic pathways.[14, 22, 30, 35, 63] Through these substrates, researchers have gathered invaluable information on PGT enzymatic properties, and made early attempts to chemically engineer the substrates into potential inhibitors for mechanistic studies, structure-activity relationship studies, and novel antibiotic designs.[32-34, 64] However, one of the major obstacles inhibiting further progress was the difficulty in obtaining substrates derivatives, which has to be prepared through carefully designed orthogonal chemical protections. An overwhelming number of steps are required to obtain just the tetrasaccharide unit, reported at nearly 63 steps starting from monosaccharides,[49] even though the tetrasaccharide is still suboptimal. Longer N-saccharide oligomers are likely to be more biologically relevant substrates for PGTs and TPs (**Figure 1-1**).[23-24, 30] Here we present an efficient 9-step approach for synthesizing biohybrid peptidoglycan oligomers (PGOs) from chitosan, a plentiful biopolymer readily available from all crustacean wastes (**Scheme 3-1**). We also demonstrated that our biohybrid PGOs are successfully incorporated into the cell walls

of various bacteria strains. Our PGOs can be customized for various needs in mechanistic studies, bacterial bioimaging and novel drug designs.

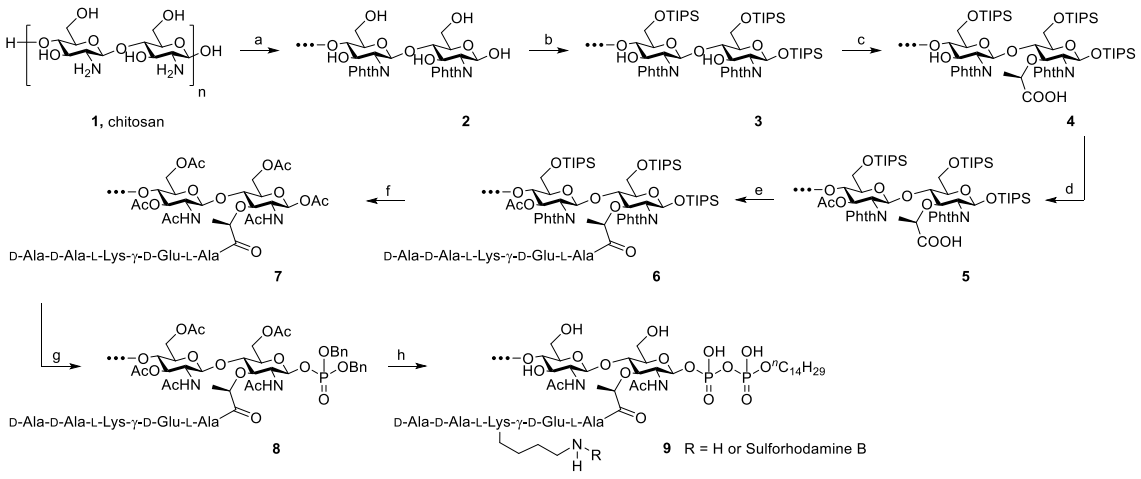

Scheme 3-1. Total synthesis of PGO **9** and rhodamine-labelled PGO **9** from low molecular weight chitosan **1**. Synthetic steps are described in detail in Section 3.2.2.

3.2 EXPERIMENT METHODS

3.2.1 Materials and Equipment

Chitosan (Mw ⩽ 3000 Da, degree of deacetylation > 85%) was purchased from Carbosynth Ltd. (Berkshire, UK). *N*-(3-Dimethylaminopropyl)-*N*′-ethylcarbodiimide hydrochloride (EDCI), 1-[Bis(dimethylamino)methylene]-1*H*-1,2,3-triazolo[4,5-*b*]pyridinium 3-oxid hexafluorophosphate (HATU), 3*H*-[1,2,3]-Triazolo[4,5-*b*]pyridin-3-ol (HOAt) and all amino acids used in synthesis were purchased from GL Biochem Ltd. (Shanghai, China). Membrane dye FM 1-43fx was purchased from Thermo Fisher Scientific Inc. (Waltham, USA). All other chemicals used in synthesis were purchased from Sigma-Aldrich Co. LLC. (St. Louis, USA). Bacterial strains (*Escherichia coli* ATCC 29425, ATCC958,

ATCC8739, *Pseudomonas aeruginosa* ATCC 27853, *Staphylococcus aureus* ATCC BAA-40, ATCC 1556, ATCC29213 *Enterococcus faecalis* ATCC 700802, and *Bacillus Subtilis* ATCC 6633) were purchased from the American Type Culture Collection (Manassas, USA) and stored at -80 ºC. Mueller-Hinton broth (MHB, Difco), brain heart infusion broth (BHI, Difco) and trypticase soy broth (TSB, Difco) were purchased from Beckton, Dickinson and company (Franklin Lakes, USA). Enzyme was purchased from Cusabio (Texas, USA). Dialysis tubing was purchased from Spectra/Por (Singapore).

The reactions were all performed under nitrogen atmosphere. Starting materials and reagents were all purchased commercially and used as received. Solvents used in reactions were all purified according to standard procedures in literature. Thin layer chromatography (TLC) with Merck TLC silica gel 60 F254 plate was used to check reaction progress. UV, or potassium permanganate staining if necessary, was used to visualize compounds on TLC plates. Flash column chromatography with silica gel 60 (0.010-0.063 mm) and gradient solvent system was used to isolate products. ^{1}H and ^{13}C NMR spectra were obtained using 400 MHz Bruker AVIII 400 spectrometer or 500 MHz Bruker AV 500 spectrometer. Tetramethylsilane (TMS) was used as internal standard in measurement of chemical shifts (ppm). Multiplicities were reported as s (singlet), d (doublet), t (triplet), q (quartet), m (multiplet or unsolved), br s (broad singlet) or dd (doublet of doublets). The number of protons (n) corresponding to a resonance signal was indicated as nH and coupling constants were reported as J values in units of Hz. Characterization data for known compounds were checked in comparison with literature for consistency and not presented in this report. Polymeric substrates were purified by dialysis using a dialysis tubing cellulose membrane (3.5 kDa MWCO) for 2 days. Shimadzu LCsolution (Shimadzu Corporation, Kyoto, Japan) and Kromasil

100-5C8 reverse phase column (Kromasil, Bohus, Sweden) was used for HPLC analysis with deuterium lamp at 280 nm. Dynamic light scattering was done using Malvern Zetasizer Nano (Malvern Panalytical, Malvern, UK).

3.2.2 Experimental for Chemical Synthesis

Protection of chitosan was done following protocols similar to those reported by Ifuku *et al* and Gagnon *et al*.[65-66] Coupling with peptide, glycosylation and deprotection followed protocols similar to those reported by Kahne *et al* and Wong *et al*.[23, 33-34] Whereas substrates were prepared following to literature, ^{1}H NMR for substrates were attached below for reference. In addition, ^{13}C NMR and HRMS were given for newly prepared peptides. Calculations are based on repeating monosaccharide units on the oligomers.

Synthesis of polymer **2**.

Chitosan **1** (2.0 g, 12.5 mmol) was dissolved in 100 mL mixture of AcOH/H_2O (v/v, 1:9). Phthalic anhydride (5.6 g, 37.5 mmol) was then added and the solution was stirred at 120 ºC for 24 hours before cooling down to room temperature. The solvent was removed under reduced pressure and residue washed with ethanol and diethyl ether to give product **2** (3.3 g, 88%) as an off white solid.

Synthesis of polymer **3**

Polymer **2** (1.5 g, 5 mmol) was dissolved in 100 mL DMF. Imidazole (2.7 g, 40 mmol) was added, followed by triisopropylsilyl chloride (6.8 g, 35 mmol) dropwise at 0 ºC. The reaction mixture was slowly warmly up to room temperature and stirred for 48

hours before solvent was removed under reduced pressure. The residue was washed with ethanol and diethyl ether to give product **3** (1.7 g, 71%) as a yellow solid.

Synthesis of polymer **4**

Polymer **3** (0.96 g, 2 mmol) was dissolved in 20 mL DMF at 0 ºC. Sodium hydride (200 mg, 5 mmol) was added portionwise and then (*S*)-(−)-2-Bromopropionic acid (153 mg, 1 mmol) was added dropwise. The reaction mixture was slowly warmed up to room temperature and stirred for 48 hours before quenching with methanol. The solvent was removed under reduced pressure and residue washed with water and ethanol consecutively to give product **4** (0.69 g, 69%) as a yellow solid.

Synthesis of polymer **5**

Polymer **4** (0.50 g, 1 mmol) and 4-dimethylaminopyridine (244 mg, 2 mmol) were dissolved in 20 mL pyridine at 0 ºC. Acetic anhydride (510 mg, 5 mmol) was added to the solution dropwise with stirring. The reaction was slowly warmed up to room temperature and stirred for 48 hours. Then solvent was removed under reduced pressure and the residue was washed with saturated ammonium chloride solution, followed by water to give product **5** (0.46 g, 92%) as an off white solid.

Synthesis of polymer **6**

To a solution of pentapeptide **12** (91 mg, 0.1 mmol) in 20 mL CH_2Cl_2 was added 4 mL 2.0 M HCl in Et_2O and the mixture was stirred at room temperature for 4 hours. After checking full consumption of **12** by TLC, the solvent was removed *in vacuo* and the crude H-Ala-D-*iso*-Glu(OBn)-Lys(Fmoc)-D-Ala-D-Ala-OMe·HCl **13** was used without further purification. Polymer **5** (100 mg, 0.2 mmol) and DIPEA (52 mg, 0.4 mmol) were

dissolved in 25 mL DMF at room temperature. To the stirring solution was added HATU (190 mg, 0.5 mmol) and HOAt (68 mg, 0.5 mmol). After 5 min, H-Ala-D-*iso*-Glu(OBn)-Lys(Fmoc)-D-Ala-D-Ala-OMe·HCl (170 mg, 0.2 mmol) was added and the reaction mixture was left stirring overnight. After removing solvent under reduced pressure, the residue was washed with saturated ammonium chloride solution and water to give product **6** (146 mg, 79%) as a brown solid.

Synthesis of polymer **7**

Polymer **6** (92 mg, 0.1 mmol) was dissolved in 30 mL methanol. Acetic acid (120 mg, 2 mmol), tetrabutylammonium fluoride (1.0 M THF solution, 2.0 mL) and hydrazine (64 mg, 2 mmol) were added consecutively. The mixture was stirred at room temperature for 48 hours before solvent was removed under reduced pressure. The residue was washed with saturated ammonium chloride solution and water, then dried and redissolved in pyridine together with 4-dimethylaminopyridine (25 mg, 0.2 mmol). Acetic anhydride (51 mg, 0.5 mmol) was added to the solution dropwise at 0 ^{o}C with stirring. The reaction was slowly warmed up to room temperature and stirred for 48 h. Then solvent was removed under reduced pressure and the residue was washed with saturated ammonium chloride solution, followed by water to give product **7** as a yellow oil. The crude oil was used without further purification.

Synthesis of polymer **8**

Crude polymer **7** was dissolved in 15 mL THF at 0 ^{o}C. Methylamine (1.0 M THF solution, 0.3 mL) was added dropwise and the mixture was slowly warmed up to room temperature with stirring. After 24 hours, the solvent was removed under reduced pressure. The residue was washed with saturated ammonium chloride solution and water,

then evaporated to dryness and dissolved in 30 mL dichloromethane. To this solution was added 1*H*-tetrazole (21 mg, 0.3 mmol) and dibenzyl *N,N*-diisopropylphosphoramidite (70 mg, 0.2 mmol) at 0 ºC. The mixture was warmed up and stirred at room temperature for 5 hours before cooling to -50 ºC. Then *tert*-butyl hydroperoxide (70%, 1 mL) was added and the mixture was left stirring overnight. After removing solvent under reduced pressure, the residue was washed with saturated ammonium chloride solution, saturated sodium bicarbonate solution and water to give product **8** as a yellow oil. The crude was used for next step without further purification.

Synthesis of polymer **9**

Tetradecyl monophosphate (59 mg, 0.2 mmol) was dissolved in 10 mL mixture of DMF and THF (v/v, 1:1) under room temperature. Then CDI (162 mg, 1 mmol) was added and the solution was stirred for 2 h before 1 mL dried methanol was added. The mixture was stirred for another 1 hour and dried to give activated tetradecyl phosphoroimidazolidate (C_{14}PIm). To a solution of crude polymer **8** in 10 mL MeOH was added 8 mg Pd on activated charcoal. The suspension was stirred under H_2 atmosphere at room temperature overnight before filtration through a pad of celite. The solution was dried, and redissoved in 10 mL DMF before transferring to C_{14}PIm. Subsequently, 1*H*-tetrazole (14 mg, 0.2 mmol) was added and the mixture was stirred for 24 hours before evaporation to dryness. Then the residue was dispersed in 20 mL mixture of methanol and water (v/v, 1:1) and LiOH (1 M aqueous solution, 1 mL) was added. The mixture was stirred for 2 hours before dialysis and lyophilization to give the final product **9** (50 mg, 50% for three steps) as a yellow solid. HPLC analysis was performed using NH_4OH/MeOH from 0/100 to 10/90 in 60 min and **9** had a retention

time of 7 min. Tagging by sulforhodamine B was done following literature procedures.[67] Generally, 10 mg **9** was dissolved in 2 mL carbonate buffer (0.1 M, pH = 9) and a solution of sulforhodamine B acid chloride in DMF (2 mg/mL, 100 μL) was added. The mixture was left to stir in dark at room temperature for 2 hours and dialyzed afterwards to give PGOs-rhodamine.

The pentapeptide **13** for coupling to chitosan backbone was synthesized by a condensation reaction between Boc-Ala-D-*iso*-Glu(OBn)-OH and H-Lys(Fmoc)-D-Ala-D-Ala-OMe followed by Boc removal with hydrogen chloride according to methods reported in literature.[18]

Synthesis of compound **11**, Boc-Lys(Fmoc)-D-Ala-D-Ala-OMe

H-D-Ala-D-Ala-OH (320 mg, 2.00 mmol) was dissolved in 20 mL MeOH at 0 ºC and acetyl chloride (785 mg, 10.0 mmol) was added dropwise. The reaction was stirred for 15 min before slowly warming up to room temperature and stirring overnight. After removing solvents *in vacuo*, crude H-D-Ala-D-Ala-OMe **10** was dissolved in 10 mL anhydrous DMF followed by addition of DIPEA (646 mg, 5.00 mmol). Subsequently, Boc-Lys(Fmoc)-OH (937 mg, 2.00 mmol), HOAt (408 mg, 3.00 mmol) and EDCI (575 mg, 3.00 mmol) were added and the mixture was stirred for 2 hours before pouring into 50 mL water. Then EtOAc (30 mL x 2) was used for extraction and the combined organic layer was washed with water (50 mL x 5), brine (50 mL) and dried with Na_2SO_4. The crude was purified by flash column chromatography (50% CH_2Cl_2/EtOAc) to give compound **11** as a white solid (0.99 g, 79%). ^{1}H NMR (400 MHz, DMSO-d_6) δ 8.18 (d, J = 7.2 Hz, 1H), 7.99 (d, J = 7.9 Hz, 1H), 7.88 (d, J = 7.5 Hz, 2H), 7.68 (d, J = 7.5 Hz, 2H), 7.41 (t, J = 7.5 Hz, 2H), 7.33 (t, J = 7.5 Hz, 2H), 7.25 (t, J = 5.9 Hz, 1H), 6.92 (d, J

= 7.3 Hz, 1H), 4.40 – 4.15 (m, 6H), 3.60 (s, 3H), 2.95 (q, *J* = 6.6 Hz, 2H), 1.63 – 1.06 (m, 21H). ^{13}C NMR (101 MHz, DMSO-d_6) δ 173.22, 172.44, 172.24, 156.52, 155.94, 144.39, 141.19, 128.04, 127.49, 125.58, 120.56, 78.60, 65.65, 54.93, 52.31, 48.00, 47.92, 47.24, 32.56, 31.79, 30.06, 29.52, 28.61, 23.18, 18.64, 17.23. HRMS (ESI) calcd. for C33H45N4O8 [M+H]: 625.3237, found: 625.3237.

Synthesis of compound **12**, Boc-Ala-D-*iso*-Glu(OBn)-Lys(Fmoc)-D-Ala-D-Ala-OMe.

To a solution of **11** (624 mg, 1.00 mmol) in 30 mL CH_2Cl_2 was added 5 mL 2.0 M HCl in Et_2O and the mixture was stirred at room temperature for 4 hours. After checking full consumption of **11** by TLC, the solvent was removed *in vacuo* and the crude H-Lys(Fmoc)-D-Ala-D-Ala-OMe·HCl was used without further purification. Boc-Ala-OSu (286 mg, 1.00 mmol) and H-D-Glu(OH)-OBn (237 mg, 1.00 mmol) were dissolved in 10 mL DMF and 2 mL saturated $NaHCO_3$ (aq.) solution was added to the mixture. After stirring at room temperature overnight, 30 mL water was added and pH of the solution was adjusted to 2 by careful addition of HCl. The solution was extracted with EtOAc (20 mL x 2) and the combined organic layer was washed with 1 mM aq. HCl (30 mL x 2), water (30 mL x 2) and brine (30 mL). After drying over Na_2SO_4, the solvent was removed *in vacuo* and the crude Boc-Ala-D-*iso*-Glu(OBn)-OH was dissolved in 20 mL DMF. To the solution was added DIPEA (388 mg, 3.00 mmol), crude H-Lys(Fmoc)-D-Ala-D-Ala-OMe·HCl, HATU (760 mg, 2.00 mmol) and HOAt (272 mg, 2.00 mmol). The mixture was stirred at room temperature overnight before 60 mL water was added. Then it was extracted with EtOAc (50 mL x 2) and the combined organic layer was washed with water (80 mL x 5) and brine (80 mL). After removing solvent *in vacuo*, the crude was purified by flash column chromatography (60%

CH_2Cl_2/Acetone) to give compound **12** (730 mg, 77%) as a white solid. ^{1}H NMR (400 MHz, DMSO-d_6) δ 8.27 (d, J = 7.8 Hz, 1H), 8.18 (d, J = 7.5 Hz, 2H), 8.02 (d, J = 7.2 Hz, 1H), 7.88 (d, J = 7.5 Hz, 2H), 7.84 (d, J = 7.5 Hz, 2H), 7.41 (t, J = 7.5 Hz, 2H), 7.38 – 7.24 (m, 8H), 6.86 (d, J = 7.7 Hz, 1H), 6.60 (t, J = 5.9 Hz, 1H), 6.28 (d, J = 1.5 Hz, 2H), 5.11 (s, 2H), 4.27 (dh, 3H), 4.15 (q, J = 7.2 Hz, 1H), 4.02 (p, J = 7.2 Hz, 1H), 3.59 (s, 3H), 2.88 (q, J = 6.6 Hz, 2H), 2.19 (q, J = 7.7 Hz, 2H), 1.97 (h, J = 7.3, 6.6 Hz, 1H), 1.83 (dq, J = 15.0, 8.4, 7.6 Hz, 1H), 1.65 – 0.97 (m, 24H). ^{13}C NMR (101 MHz, DMSO-d_6) δ 173.49, 173.28, 172.52, 171.99, 157.77, 155.44, 143.03, 139.87, 137.88, 136.35, 129.38, 128.84, 128.43, 128.18, 127.74, 121.83, 120.48, 110.19, 78.54, 66.39, 53.50, 52.25, 52.04, 50.13, 48.07, 48.02, 31.85, 31.67, 30.06, 29.84, 28.63, 27.37, 23.11, 18.92, 18.40, 17.22. HRMS (ESI) calcd. for C48H63N6O12 [M+H]: 915.4504, found: 915.4513.

Rhodamine labeled pentapeptide **14** was synthesized by replacing Fmoc on lysine side chain with rhodamine B, followed by removal of Boc with hydrogen chloride using the same procedure as **13** and removal of OBn and OMe with LiOH using the same procedure as **9**. The product was dialyzed using 100-500 MWCO dialysis tubing and lyophilized without further purification.

Synthesis of compound **15**, Boc-Ala-D-*iso*-Glu(OBn)-Lys(Rhodamine)-D-Ala-D-Ala-OMe.

To a solution of **12** (91.4 mg, 0.10 mmol) in 10 mL DMF was added 2 mL diethylamine and the mixture was stirred at room temperature for 1 hour. After checking full consumption of **12** by TLC, diethylamine was removed *in vacuo* and rhodamine B (71.9 mg, 0.15 mmol), HOAt (20.4 mg, 0.15 mmol) and EDCI (28.8 mg, 0.15 mmol) were

added. Then DIPEA (38.8 mg, 0.30 mmol) was added into the solution and it was left to stir at room temperature overnight before 30 mL water was added. Then it was extracted with EtOAc (30 mL x 2) and the combined organic layer was washed with water (50 mL x 5) and brine (50 mL). After removing solvent *in vacuo*, the crude was purified by flash column chromatography (40% CH_2Cl_2/Acetone) to give compound **15** (73.6 mg, 64%) as a red solid. ^{1}H NMR (500 MHz, Chloroform-d) δ 8.34 (d, J = 7.9 Hz, 1H), 7.82 (s, 1H), 7.74 (s, 3H), 7.55 (q, J = 3.8 Hz, 2H), 7.33 (dd, J = 14.2, 5.8 Hz, 4H), 7.24 (d, J = 15.1 Hz, 2H), 7.09 – 6.99 (m, 4H), 6.85 (d, J = 9.8 Hz, 2H), 6.77 (s, 2H), 5.01 (s, 2H), 4.24 (t, J = 7.2 Hz, 3H), 3.66 (q, J = 7.5 Hz, 10H), 3.38 – 3.31 (m, 1H), 2.94 (d, J = 37.7, 35.0 Hz, 1H), 2.33 (s, 1H), 2.14 (s, 1H), 2.02 (s, 2H), 1.74 – 1.60 (m, 4H), 1.48 – 1.40 (m, 10H), 1.39 – 1.33 (m, 23H), 1.32 – 1.23 (m, 18H), 1.22 – 1.15 (m, 4H), 0.97 – 0.82 (m, 16H). ^{13}C NMR (101 MHz, Chloroform-d) δ 167.88, 165.14, 157.75, 155.61, 134.57, 133.46, 133.23, 132.60, 131.58, 131.33, 131.00, 130.51, 130.38, 128.93, 128.68, 128.65, 128.58, 128.40, 114.23, 113.65, 96.59, 68.30, 67.65, 46.27, 38.89, 30.51, 29.83, 29.07, 28.52, 23.90, 23.11, 14.17, 12.81, 11.09, 1.15.

Synthesis of polymer **16**, chitosan-pentapeptide conjugate with rhodamine tag

To a solution of pentapeptide **15** (23.0 mg, 0.02 mmol) in 20 mL CH_2Cl_2 was added 4 mL 2.0 M HCl in Et_2O and the mixture was stirred at room temperature for 4 hours. After checking full consumption of **15** by TLC, the solvent was removed *in vacuo* and DIPEA (12.9 mg, 0.1 mmol) in 20 mL DMF was added at room temperature. Then polymer **5** (10.0 mg, 0.02 mmol), HATU (19.0 mg, 0.05 mmol) and HOAt (6.8 mg, 0.05 mmol) were added into the solution and the reaction was left to stir overnight. After removing solvent under reduced pressure, the residue was washed with saturated

ammonium chloride solution and water to give a crude of protected chitosan-pentapeptide conjugate. The crude was redispersed in 10 mL MeOH, followed by addition of tetrabutylammonium fluoride (261 mg, 1 mmol), hydrazine (32 mg, 1 mmol) and LiOH (1 M aqueous solution, 0.1 mL). The mixture was stirred for another 12 hours before dialysis and lyophilization to give the final product **16** as a red solid.

Synthesis of inhibitor **17**

Crude polymer **7** was dissolved in 15 mL THF at 0 ºC. Methylamine (1.0 M THF solution, 0.3 mL) was added dropwise and the mixture was slowly warmed up to room temperature with stirring. After 24 hours, the solvent was removed under reduced pressure. The residue was washed with saturated ammonium chloride solution and water, then evaporated to dryness and dissolved in 30 mL dichloromethane. To this solution was added 1*H*-tetrazole (21 mg, 0.3 mmol) and methyl (2R)-3-(((benzyloxy)(diisopropylamino)phosphanyl)oxy)-2-(dodecyloxy)propanoate[68] (102 mg, 0.2 mmol) at 0 ºC. The mixture was warmed up and stirred at room temperature for 5 hours before cooling to -50 ºC. Then *tert*-butyl hydroperoxide (70%, 1 mL) was added and the mixture was left stirring overnight. After removing solvent under reduced pressure, the residue was washed with saturated ammonium chloride solution, saturated sodium bicarbonate solution and water to give crude product **17**. Then the residue was dispersed in 20 mL mixture of methanol and water (v/v, 1:1) and LiOH (1 M aqueous solution, 1 mL) was added. The mixture was stirred for 2 hours before dialysis and lyophilization to give the final product **17** (70 mg, 70% for two steps) as a yellow solid.

3.2.3 General Procedure for Gel Permeation Chromatography (GPC)

Shodex SB-803 HQ and SB-805 HQ columns (Showa Denko, Tokyo, Japan) were connected in series for GPC in Agilent 1260 infinity system (Agilent, CA, USA). Samples were dissolved in deionized water at 1 mg/mL and eluted at 0.5 mL/s through columns. The elution was done using 0.05 M NaCl in deionized water at 40 ºC, and signals were detected using the RI detector of Agilent 1260 infinity system.

3.2.4 General Procedure for Dynamic Light Scattering

Dynamic light scattering experiments were done using Malvern Zetasizer (Malvern Instruments Ltd, Malvern, UK). Samples were prepared at 100 μg/mL in deionized water and measured at 25 ºC. Backscattering at 173 degrees was adopted as the measuring angle.

Zetasizer software was used to analyze and generate a graph of size distribution.

3.2.5 Lysozyme Degradation Assay

To prepare crude for mass analysis, 2 mg substrate was dissolved in 0.2 mL 10 mM acetate buffer (pH = 5.0) before addition of 0.4 mg lysozyme (from egg white, Sigma-Aldrich Co. LLC., St. Louis, USA) and incubation at 38 ºC for 24 hours. Then the enzyme was pelleted by centrifugation at 1,500 X *g* for 5 min, and the solution of crude metabolites was collected, diluted to 2 mL with 0.1 % formic acid in deionized water and analyzed by ESI-TOF.

3.2.6 General Procedure for Fluorophore Labeling Assay

Labeling by sulforhodamine B acid chloride (Sigma-Aldrich Co. LLC., St. Louis, USA) was performed on PGOs following protocols given by the supplier. Briefly, 10 mg

PGOs was dissolved in 1 mL carbonate buffer (0.05 M $NaHCO_3$/ Na_2CO_3 in deionized water, pH = 9). Then a solution of 1 mg sulforhodamine B acid chloride in 0.1 mL DMF was added, and the mixture was shielded from light through aluminum foil wrapping. After stirring at room temperature for 2 hours, the solution was dialyzed for three days while keeping the dialysis container wrapped with aluminum foil. The product was obtained by lyophilization as a red solid.

Labeling by Sulfo-Cyanine7.5 *N*-hydroxysuccinimide (NHS) ester (Lumiprobe, Maryland, USA) followed a similar protocol, also offered by the supplier. Briefly, 10 mg PGOs was dissolved in 1 mL solution of sodium bicarbonate (0.1 M in deionized water). Then a solution of 1 mg Sulfo-Cyanine7.5 NHS ester in 0.1 mL DMF was added, and the mixture was shielded from light through aluminum foil wrapping. After stirring at room temperature for 2 hours, the solution was dialyzed for three days while keeping the dialysis container wrapped with aluminum foil. The product was obtained by lyophilization as a green solid.

3.2.7 General Procedure for Stimulated Emission Depletion (STED) Microscopy

3.2.7.1 Sample Preparation and Image Taking for STED Microscopy

To prepare samples for super resolution STED microscopy, overnight broth cultures were subsequently grown in 5 ml of fresh culture broth (1:100 dilution) to prepare logarithmic phase cultures after incubation at 37 ºC for 4 hours in a shaking incubator (225 rpm). Then, bacteria cells were pelleted by centrifugation at 1,500 X *g* for 5 min, suspended in culture media at a concentration of 10^8 CFU ml^{-1} and incubated for 1 h in

the dark in the presence of 100 μg/ml of rhodamine-labeled derivative of **9** at 37 ºC with agitation (225 rpm). Bacterial cells were next incubated with the membrane stain FM1-43FX (Life Technologies) at a final concentration of 5 μg/ml for 5 min, as suggested by the manufacturer, and subsequently washed three times with PBS and resuspended in a fixative solution of 2% paraformaldehyde in PBS (pH = 7.0). Cells were fixed for 1 h at 37 ºC in a shaking incubator (225 rpm), washed three times in PBS and applied to a sterile glass bottom collagen coated dish (MatTek Corporation). STED super resolution microscopy was performed on a Leica TCS SP8 STED-3X microscope (Leica Microsystems, Wetzlar, Germany) at SingHealth Advanced Biomaging Core. 479 nm and 556 nm lasers were used for fluorescence excitation, while 660 nm STED laser was used for depletion. In order to achieve maximum lateral resolution, all images were acquired in 2D STED mode. Further image processing required deconvolution, which was done using Huygens Professional software (Scientific Volume Imaging, Hilversum, Netherlands). ImageJ was utilized for further image processing.

3.2.7.2 Measurement of Fluorescence Intensity Using Images Taken from STED Microscopy

Calculation was done using Fiji ImageJ according to the procedure reported by Burgess.[69-70] Both the laser power and STED power were kept constant throughout the experiments for the acquisition of the images for calculation purposes. To minimize crosstalk, the excitation wavelength of the red channel was set at 570 nm, with the emission photons collected from 580 nm to 620 nm. Only the cells that were in focus were taken into account for calculation, and the channels of the images (not processed by deconvolution) were split prior to calculation; calculating only those from the red

channel. The area with fluorescence on each bacterial cell surface was drawn (**Figure 3-1**) and the total intensity was normalized by the number of pixels found in the area (mean). A total of hundred or more cells per bacterial strain were computed, and the average was taken for comparison.

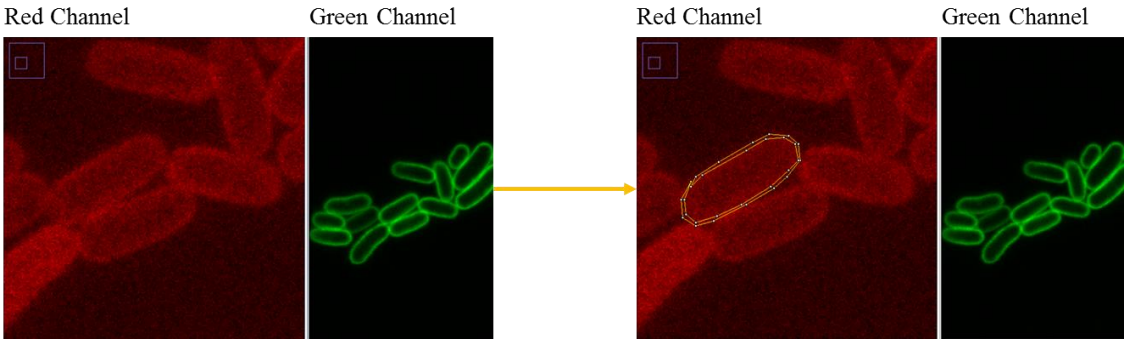

Figure 3-1. Schematic illustration of intensity calculation method. Only the surface part of bacterial cells was measured to compare the amount of substrate incorporated onto cell wall.

3.2.8 Preparation of Stable L-form Mutant of *E. faecalis*

L-forms were generated using DM3 agar by modified methods from reported protocol.[71] DM3 medium consists of 1.2 % agar, 0.5 % Tryptone, 0.5 % yeast extract, 1 M Succinate(pH 7.3), 3.5 % K_2HPO_4 and 1.5 % KH_2PO_4, 20% Glucose, 1 M $MgCl_2$ AND 2% BSA. Parental strain *E. faecalis* OG1RF was grown overnight at 37 °C in DM3 broth. 100 µL of an overnight culture was directly plated on DM3 agar plates supplemented with 200 µg/mL penicillin G. The plates were incubated at 37 °C. Small fried egg-like shaped colonies appeared after 5 days. The colonies were restreaked on DM3 agar with 200 µg/ml penicillin G for a few times to get pure colonies, and serial passaging of pure colonies in DM3 agar with decreasing penicillin G concentrations to generate stable L-forms. The stable L-forms were stored at -80 °C in 20 % glycerol.

3.2.9 General Procedure for Total Internal Refraction Fluorescence (TIRF) Microscopy

Fluorescence microscopy was performed on Nikon TIRF microscope (Nikon instruments, NY, USA). BODIPY FL and sulforhodamine B were excited at 488 and 560 nm and emitted at 512 and 580 nm respectively. Three days old L-forms grown in DM3 broth was washed and incubated with 1 µL of Polymyxin B or Boc-FL (1 mg/mL) and 2 µL substrate (2 mg/mL) for 30 min at 37 ℃. After 30 min, cells were washed thrice with 1 mL of liquid DM3. The final pellet was suspended in 30 µL liquid DM3. 5 µL of cells were placed on poly-lysine coated slides and observed under TIRF microscope. Image processing was done using MetaMorph Microscopy Automation & Image Analysis Software (Photometrics, AZ, USA). ImageJ was utilized for further image processing.

For FRET studies, 488 nm laser was used for fluorescence excitation, while emissions from both BODIPY FL (512 nm) and sulforhodamine B (580 nm) were collected simultaneously. Samples were photobleached with Fluorescence Recovery after Photobleaching (FRAP) device using 561 nm laser for 1 second while fluorescence intensity was monitored for both channels for 100 seconds in total.

3.2.10 General Procedure for Cryo-Transition Electron Microscopy (cryo-TEM)

To prepare samples for cryo-TEM, overnight TSB cultures were subsequently grown in 5 ml of fresh culture broth (1:100 dilution) to prepare logarithmic phase cultures after incubation at 37 ºC for 4 hours in a shaking incubator (225 rpm). Then, *E. faecalis*

bacteria cells were pelleted by centrifugation at 1,500 X *g* for 5 min, suspended in TSB culture media at a concentration of 10^8 CFU ml^{-1} and incubated for 2 h in the dark in the presence of 1 mg/mL of PGOs-rhodamine at 37 ºC with agitation (225 rpm). The cells were subsequently washed three times with PBS and frozen onto copper grid by liquid nitrogen. Cryo-TEM was performed using FEI Titan Krios (300kV, FEG, Falcon II direct detector, and Gatan Tridiem GIF with 2k x 2k post-GIF Gatan CCD) at NUS Centre for BioImaging Sciences. The images were taken at 14,000x magnification and processed subsequently by ImageJ.

3.2.11 General Procedure for Isothermal Titration Calorimetry (ITC)

ITC experiments were performed using Microcal PEAQ-ITC instrument (Malvern Instruments Ltd, Malvern, UK). The solutions of PGOs (30 μM) and PBP1a (300 nM) in deionized water were prepared fresh before each experiment and three replicates were performed for each setting. 0.4 μL of PGOs solution was titrated into 300 μL *E. coli* PBP1a solution followed by twelve 3-μL injections at 150 seconds intervals. The reaction cell was stirred at 750 rpm and reference was set at 10 μcal/s. The data were all obtained and analysed using Microcal softwares.

3.2.12 General Procedure for Determination of Minimal Inhibition Concentration (MIC)

Bacteria cells were grown overnight at 37 °C in Mueller−Hinton broth (MHB) to mid log phase and diluted to 10^5 - 10^6 CFU mL^{-1} in MHB. A 2-fold dilution series of 100 μL of polymer solution in medium was made in 96-well microplates, followed by the addition of 100 μL of the bacterial suspension (10^5 - 10^6 CFU mL^{-1}). The plates were incubated at 37 °C for 18 - 24 h, and the absorbance at 600 nm was measured with a

microplate reader (BIO-RAD Benchmark Plus). A positive control with 1 μg/mL vancomycin, a negative control without polymer, and a blank without bacteria were included. MICs were determined as the lowest concentration that inhibited cell growth by more than 90%.

3.2.13 General Procedure for Evaluation of Cytotoxicity

NIH 3T3 cells (1×10^4 cells/well) were seeded with complete medium on a 96-well plate and cultured overnight. The old medium was replaced with fresh medium containing polymer for 24 hours. Then, 10 μL MTT solutions were added to the media. After incubation for 2 hours, the OD_{450nm} of the media was measured by using a microplate reader. The cell viability was calculated using the formula:

$$\% \text{ cell viability} = (\text{AbsTest} - \text{AbsBlank}) / (\text{AbsControl} - \text{AbsBlank}) \times 100\%.$$

3.2.14 Bacterial Detection with PGOs

The potential of PGOs in diagnostic applications for bacterial infections was evaluated by the agent's abilities to detect low concentrations of bacteria within a short period and to distinguish AMR strains from susceptible ones.

3.2.14.1 Determination of the Limit of Detection of Bacteria at Varying Concentrations Using PGOs

For limit of detection, 1 mL *E. coli* EC958 was prepared at different concentrations each, and PGOs-rhodamine (200 μg) was added for metabolic labeling for 1 hour at 37 ℃. All the bacteria were harvested by centrifugation at 5000 rpm for 15 min and washed with

PBS for 3 times. The bacteria pellet was finally dispersed in 1 mL PBS for fluorescence analysis with fluorospectrometer.

3.2.14.2 Identification of AMR Strains from Susceptible Strains under the Treatment of Antibiotics

For resistant strain detection, 1 mL of drug-sensitive and drug-resistant bacteria (10^6 CFU/mL) were treated with different concentration of antibiotics (Penicillin G sodium salt) ranging from 0 to 1000 μg/ml for 2 h. PGOs-rhodamine (50 μg) were then added for metabolic labeling for 1 hour at 37 ℃. All the bacteria were harvested by centrifugation at 5000 rpm for 15 min and washed with PBS for 3 times. The bacteria pellet was finally dispersed in 1ml PBS for fluorescence analysis with fluorospectrometer.

3.2.15 General Procedure for *in vivo* Imaging of Fluorescence from Bacterial Infections

PGOs-Cy7.5 was prepared according to the protocol described in Section 3.2.6. *S. aureus* (ATCC29213) was intraperitoneally injected into mice to develop bacterial infection in most organs of mice, including liver and kidney. At 2 hours post-infection, 5 mg/kg of PGOs-Cy7.5 was intravenously administrated to non-infected and infected mice. Non-invasive image was taken at varied time point using IVIS SpectrumCT (PerkinElmer, USA) to track fluorescence difference. At 10 hours post-infection, mice were euthanized and dissected, and fluorescence intensity of varied organs were imaged and quantified for the fluorescence intensity. Eventually, organs were homogenized and serial diluted to get the exact bacterial CFU count.

3.2.16 General Procedure for Evaluation of Toxicology of PGOs *in vivo*

5 mg/kg and 20 mg/kg of PGOs were injected into female Balb/c mice (five mice per group) respectively via intravenous route. Mice receiving the same volume of saline were used as control. Mice weight were monitored daily, at 7 days post-injection, mice blood was collected from submandibular vein for blood biochemistry assay using Blood Chemistry Analyzer (Pointcare V2, MNCHIP). The blood biochemical levels were analyzed with one-way classification analysis of variance (ANOVA).

3.3 RESULTS AND DISCUSSIONS

3.3.1 Facile and Practical Synthesis of PGOs

Starting from low molecular weight chitosan **1**, phthaloyl group was first used to protect the free amino group at C-2 from subsequent transformation (**Scheme 3-1**). The bulky triisopropylsilyl group was delivered to the primary alcohol and anomeric hydroxyl group at the reducing terminal successfully. C-3 hydroxy groups on chitosan are relatively inert towards this reaction unless harsher conditions are applied. This results in the formation of substrate **3**. Next, 2-bromopropanoate was introduced at C-3 by S_N2 chemistry, with a molar ratio of 2:1 for glucosamine unit : 2-bromopropanoate, approximating the alternating pattern of the peptidoglycan repeat motif, to give us the desired substrate **4**. The remaining hydroxyl groups were then capped by acetyl esterification. We noted the improvement in organic solvent solubility along the protection scheme, from substrate **2** forming a dispersion in DMF, to substrate **5** dissolving in CH_2Cl_2 as well as other commonly used organic solvents.

The pentapeptide was prepared based on established literature, following the sequence found in *S. aureus* and *E. faecalis*.[18] The protecting groups on side chain and terminal functionalities were selected to be Fmoc for amine and benzyl or methyl ester for carboxylic acids, so that global deprotection can be realized at the end of synthesis with lithium hydroxide. The amide linkage between the pentapeptide and substrate **5** was achieved under HATU/HOAt/DIPEA coupling conditions. Following partial cleavage and global protection with acetic anhydride, dibenzyl monophosphate can be introduced at the reducing terminus. Hydrogenation was used to liberate the phosphate so that it can be coupled with a second lipid-linked monophosphate, to yield the desired oligosaccharide pyrophosphate **9** (**Scheme 3-1**). We opted to employ the tetradecanyl lipid linker in place of the natural polyprenyl lipid to simplify preparation routes, taking into consideration that the tetradecanyl linker has been found to display a better binding affinity to MurG, one of the key PGTs.[33] The crude mixture was dialyzed with

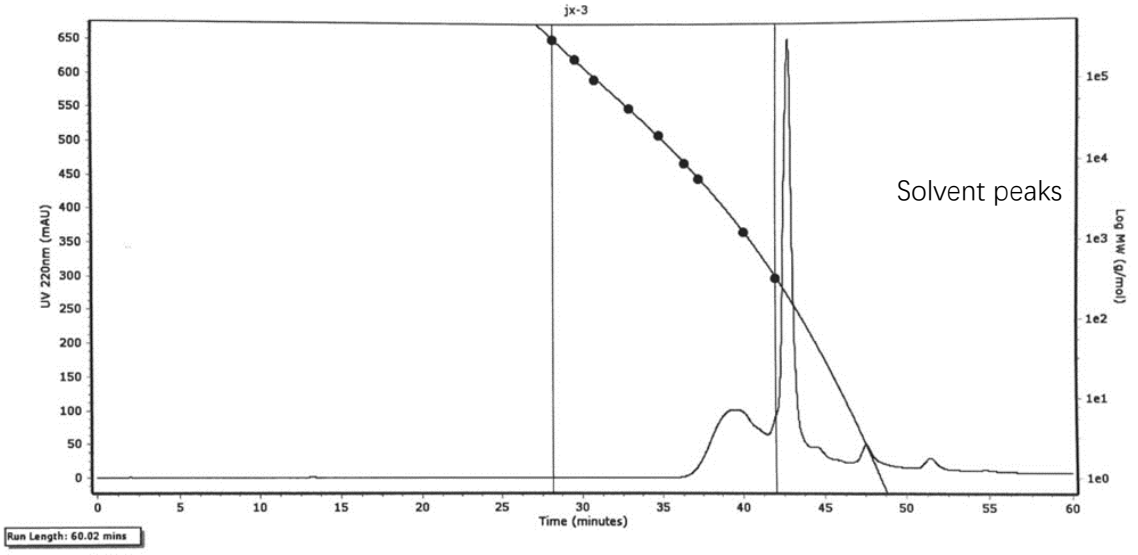

Figure 3-2. GPC chromatogram of PGOs.

deionized water, filtered and lyophilized to furnish the pure oligomeric final product as a beige solid.

The product's composition was analyzed with GPC. As peak broadening was observed and the elution time was shorter than expected in the chromatogram, existence of self-assemblies with increased hydrodynamic radius was inferred (**Figure 3-2**). This was confirmed by DLS of PGOs in solution, which showed nanoparticles of around 80 nm in diameter (**Figure 3-3**).

Then the molecular structure of **9** was examined by NMR. Comparison of integration values from sugar, peptide and lipid moieties suggested a statistical ratio of 1:0.5:0.1, which totaled around 5 kDa molecular weight on average. This result agreed well with the theoretical outcome, as our synthesis started from chitosan of < 3 kDa molecular weight and finished with a design that half of sugar repeating units being grafted by peptide. Finally, the finer structure of PGOs was evaluated with the lysozyme

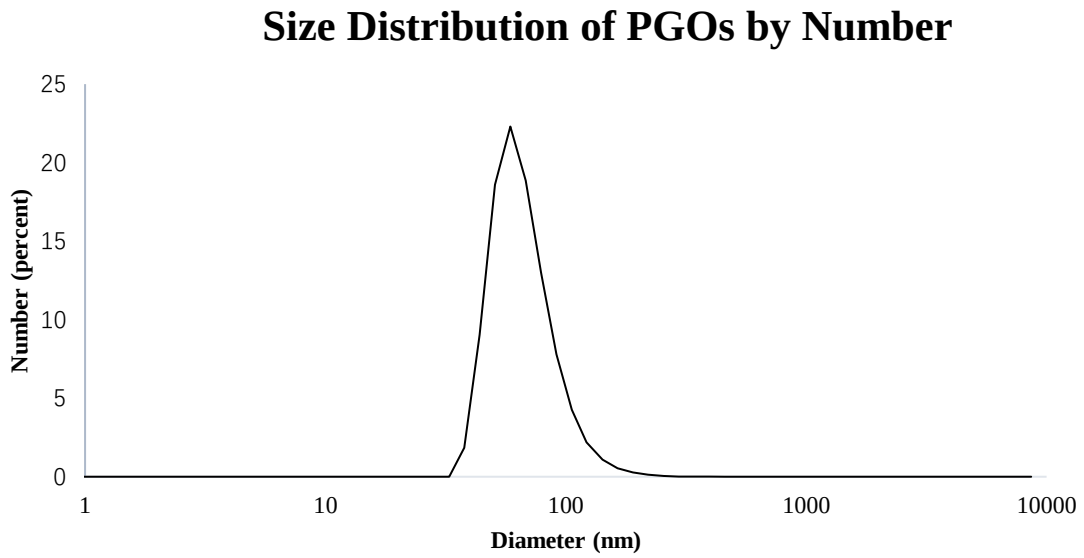

Figure 3-3. Results from DLS on the hydrodynamic radius of PGOs.

degradation assay. Lysozyme binds to tetrasaccharides, or longer motifs, in peptidoglycan and cleaves the glycosidic linkages in the middle. LC-ESI-TOF MS analysis revealed the presence of a m/z fragment consisting of a NAG-NAM with pendant pentapeptide (**Figure 3-4**). The presence of this fragment, but not NAG-NAG or NAM-NAM fragments, supported our hypothesis that the oligomeric product **9** has an alternating NAG-NAM pattern, as expected for a PGO.

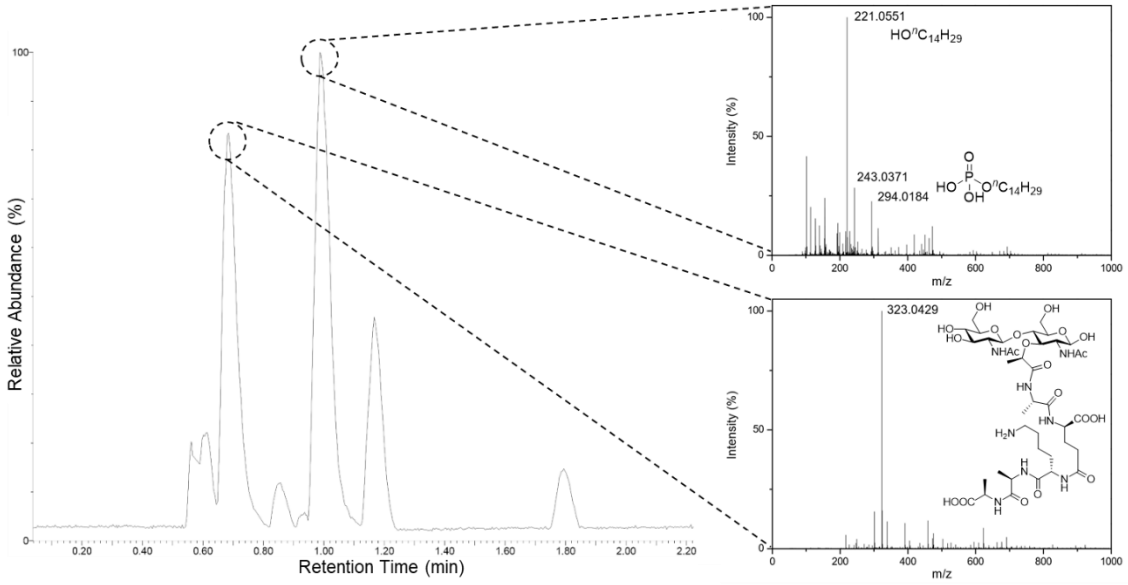

Figure 3-4. LC-ESI-TOF of metabolites from lysozyme degradation assay. Two major resultant peaks at t = 0.69 min and t = 0.99 min correspond to the NAG-NAM subunit and the phospholipid respectively. The remaining peaks were from metabolites from the enzyme and the buffer used in the lysozyme degradation assay.

3.3.2 PGOs as Highly Specific Metabolic Labeling Agents for Bacterial Cell Wall

Sulforhodamine B acid chloride (rhodamine) was covalently bound to the free amine on the side chain of lysine moieties of our soluble PGOs **9**.[67] The lysine residue has been extensively modified without significant influence on substrates' enzymatic activities or

viability of bacteria in turn.[34, 51] Furthermore, the dye of choice, rhodamine, can be easily coupled to the lysine amine and has a wavelength suitable for the stimulated emission depletion (STED) technique in super-resolution microscopy studies. We cultured bacteria strains in the presence of PGOs-rhodamine. Nutrient-rich media such as MHB and BHI were introduced, and the PGOs-rhodamine was incubated at varying concentrations and durations. The optimal incubation time was found to be an hour long, with 100 μg/mL of PGOs-rhodamine. A total of 6 bacteria strains were evaluated for this study, of which 4 were Gram-positive and 2 were Gram-negative (**Figure a17**). Among these, MRSA, vancomycin-resistant *E. faecalis* and *P. aeruginosa* are clinically relevant strains that represent multi-drug resistant (MDR) bacteria. The membrane dye

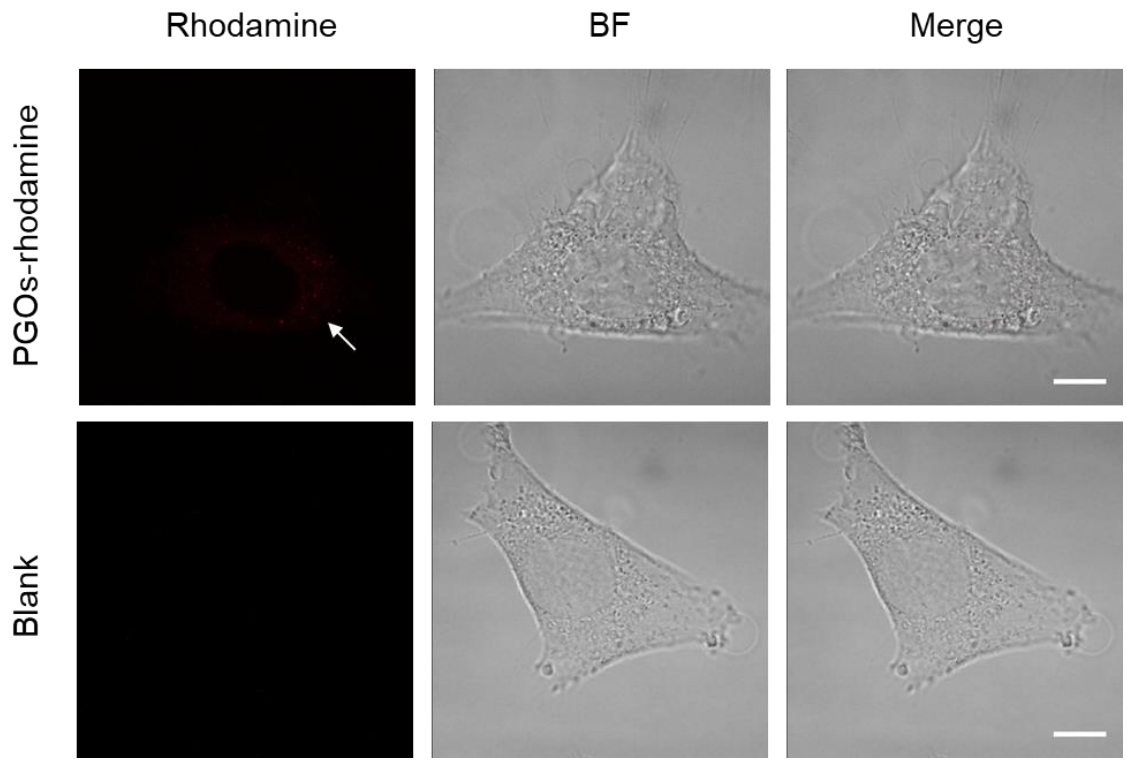

Figure 3-5. Confocal microscopic images of 3T3 cells incubated with (top row) and without (bottom row) PGOs-rhodamine. No significant fluorescent signals were detected in treated cells, with trace amount (white arrow) hypothetically from non-specific adsorption and endocytosis. Scale bar = 10 μm.

FM 1-43fx was used as an indicator dye for bacterial cell surface localization.

Based on our super-resolution STED microscopy studies, PGOs-rhodamine was colocalized with FM 1-43fx in all of the strains tested, suggesting PGOs were successfully incorporated into the bacterial cell walls of all 6 tested strains. In addition, we confirmed that the PGOs-rhodamine does not get into mammalian 3T3 cells (**Figure 3-5**), demonstrating the utility of PGOs-rhodamine as a bacteria-specific indicator.

Being aware that D-amino acids have far less efficiency when labeling Gram-negative strains, hypothetically due to inherent structural variation across strains,[37] we went on to

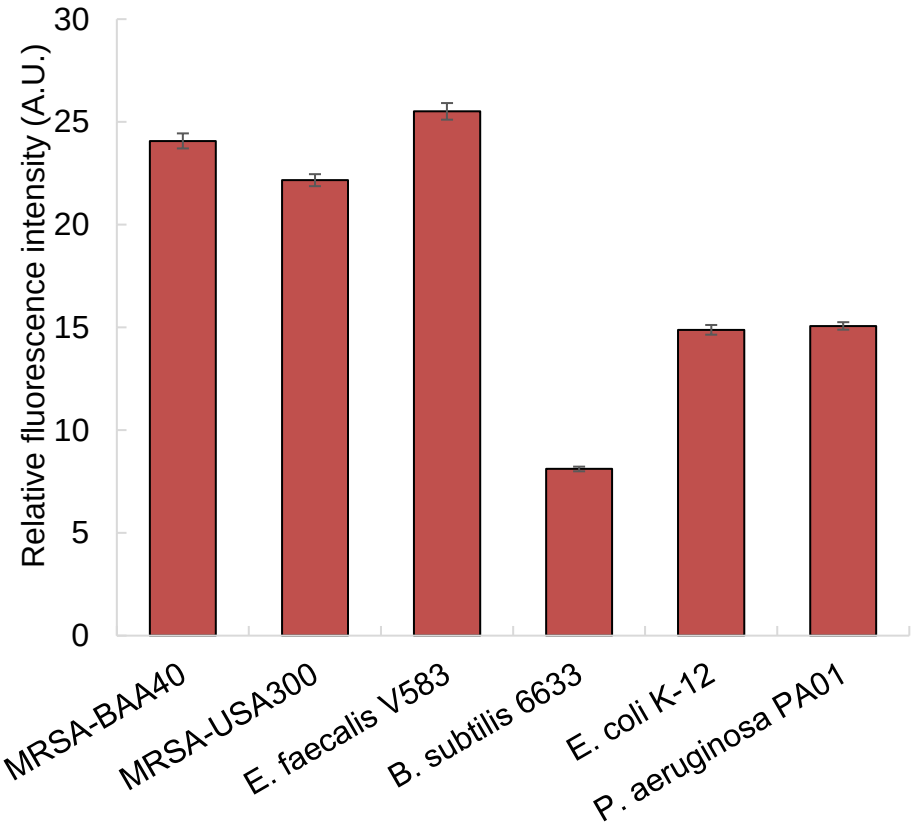

Figure 3-6. Relative fluorescence intensity on bacterial surfaces after incorporation of PGOs. A total of above one hundred cells from each strain were used for measurements, and the average PGOs-rhodamine fluorescence signal per cell was measured for comparison.

investigate whether PGOs, as substrate of PGTs, could have improved incorporation from multivalent binding. Quantification of fluorescence signal, following method reported by Burgess *et al*., demonstrated that both Gram-negative and Gram-positive species showed significant uptake and labeling by our PGOs (**Figure 3-6**).[69-70] The broad spectrum of efficient uptake and incorporation exhibited by PGOs, makes it a potentially useful substrate for further designs of a new class of bacterial bioimaging reagents.

3.3.3 Mechanistic Study on the Enzymatic Interactions of PGOs for Metabolic Labeling

To confirm and verify which component of the PGOs led to robust uptake and incorporation, we used the rhodamine fluorophore to label the entire PGOs, the peptide conjugated-chitosan, and the pentapeptide. The rhodamine-labeled substrates, and rhodamine alone, were incubated together with E. faecalis, and incorporation was measured by quantifying bacterial cell surface fluorescence intensity. The total intensity was normalized by the area of fluorescence.

Of all the substrates tested, only bacteria incubated with the rhodamine-labeled PGOs showed high fluorescence intensities (**Figure 3-7**). These results are consistent with a previous crystal structure report which suggested that every moiety, including the oligosaccharide chain and the pentapeptide of PGOs, are required for effective binding to the active site of PGT enzymes[45]. Thus our results proved that the accumulation of PGO-rhodamine was due to the biological incorporation of PGOs into the bacterial cell surface, and not due to trivial accumulation of any of the components or breakdown products of PGOs-rhodamine.

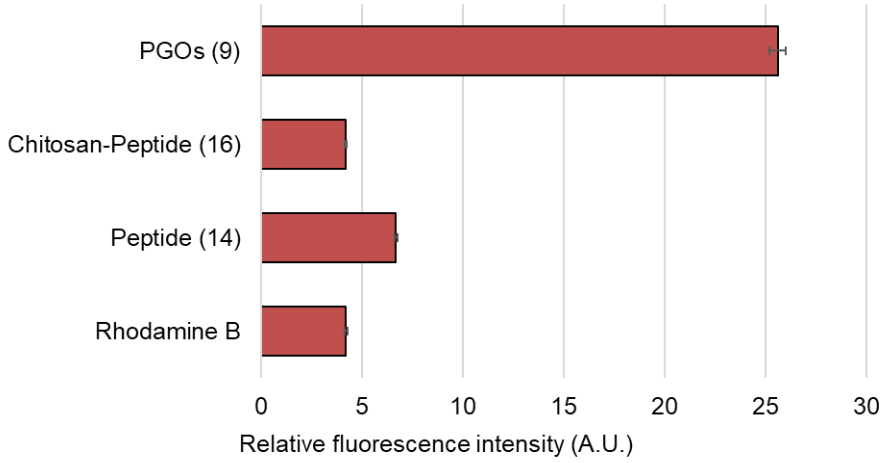

Figure 3-7. Cell surface relative fluorescence intensity of *E. faecalis* after incubation with different substrates.

To characterize the modified bacterial cell wall with PGOs incorporated, we took images of higher resolution with STED confocal microscopy. Cells of *S. aureus* and *E.*

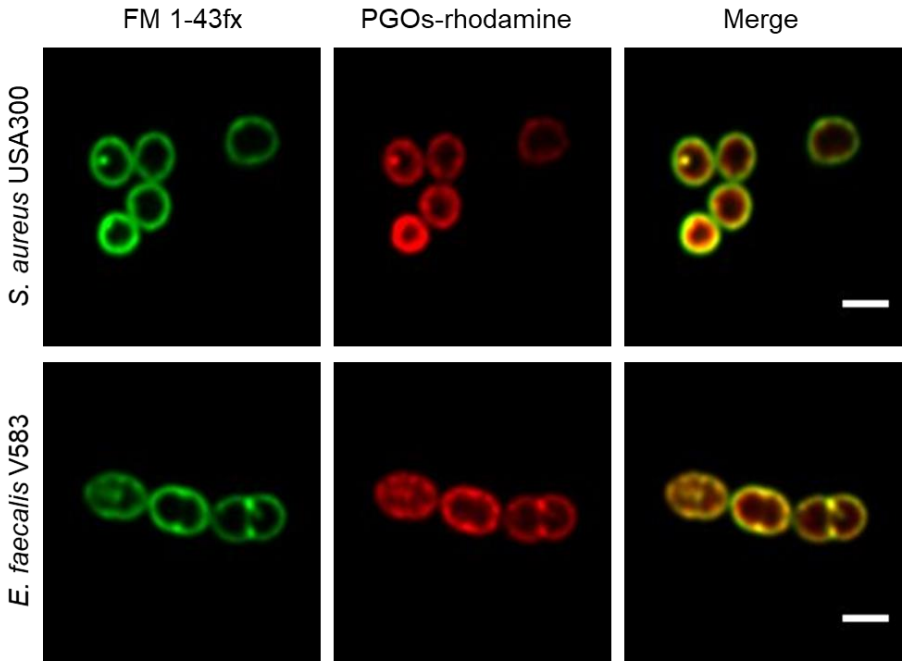

Figure 3-8. Super resolution STED confocal microscopic images of *S. aureus* and *E. faecalis*, scale bar = 1 μm.

faecalis showed thick cell walls as reflected by signals of PGOs-rhodamine (**Figure 3-8**). Upon closer observation, we noticed that PGOs-rhodamine resided on the inner part of the cell surface compared to FM 1-43fx, which was adsorbed directly onto the bacterial cell surface. Thisincomplete colocalization of FM1-43fx and PGO-rhodamine further ruled out the possibility that the PGOs-rhodamine had been only physically adsorbed onto the exterior of bacterial cells, and indicated that it was specifically transported into the bacterial cell surface layer. This was also supported by cryo-electron microscopic studies of the PGOs-rhodamine labeled bacteria cell wall, which showed a slightly thicker layer indicative of the incorporation of rhodamine into the PG network (**Figure 3-9**).

We also used L-form of the Gram-positive *Enterococcus* bacteria to further study the biological role of PGOs incorporation into bacterial cell walls. L-form bacteria are deficient in cell wall components/fragments on their surface.[71] Here we used BOCILLIN FL (Boc-FL), a fluorescent penicillin derivative, to label PBPs and cell

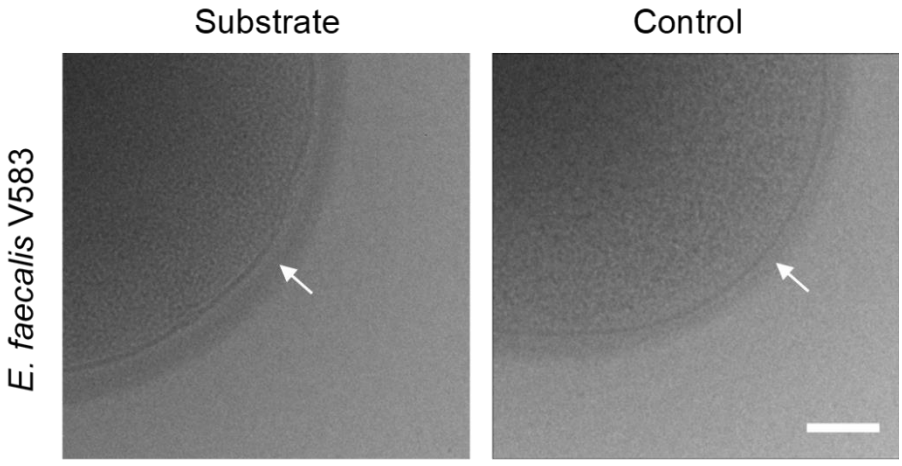

Figure 3-9. Cryo-TEM images of *E. faecalis* sample, scale bar = 100 nm. Dark line represented cell membrane and white arrow marks where low density of PG was observed.

walls specifically. Incubation of PGOs-rhodamine (red) and Boc-FL (green) with the wild type cells resulted in an intense fluorescence due to PGO and penicillin respectively at the septum region and also the circumferential cell surface (**Figure 3-10**, top row), whereas L-form cell surfaces showed only a few distinct fluorescent punctae that are overlapping from both PGOs-rhodamine and Boc-FL (**Figure 3-10**, bottom row). The images always showed colocalization of PGOs and penicillin derivatives, whether it is the division septa of the wild type strain or the distinctive punctae in the L-form strain's cell surfaces. We also attempted to compare the localization of PGOs to the membrane dye Polymyxin B-BODIPY FL. Strong uniform membranous staining by Polymyxin B derivative was observed in the L-form cells, including the region with dense membrane material as indicated (**Figure 3-11**, bottom row). In comparison, the

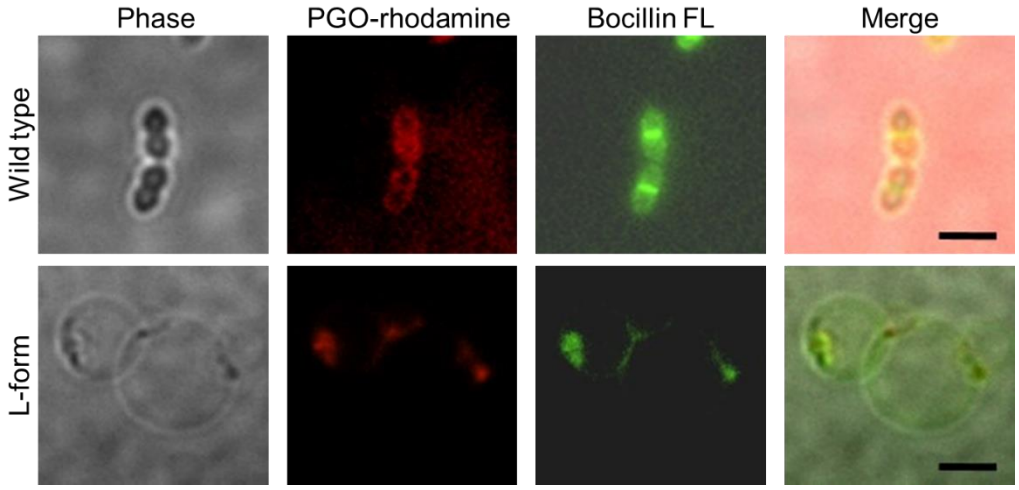

Figure 3-10. Localization of PGOs-rhodamine and Boc-FL in wild-type and L-form *E. faecalis* OG1RF imaged with TIRF microscopy. Scale bar = 1 μm for wild-type and 10 μm for L-form respectively. PGOs-rhodamine (red) and Boc-FL (green) are colocalized in the septa of wild-type cells, and the punctae of L-form cells.

PGOs localized in discrete punctae on the L-form cell surfaces. Hence, we can conclude that PGOs' localization patterns within bacterial cell walls closely resemble native PG substrates.

Furthermore, we used ITC to check the binding interactions between PGOs and PGT proteins. We used *E. coli* K12 PBP1a, since we have shown that *E. coli* K12 avidly incorporate PGOs, and *E. coli* K12 PBP1a is known to recognize large PG substrates.[23-24, 30] Interestingly, the interaction between PGOs and PBP1a had an exceptionally high exothermic enthalpy (ΔH) of -33 kcal/mol which defied a perfect fit into binding models. As an earlier work by Wong and Cheng showed a similar trend in the raw heat graph (without curve fitting and calculation) of Lipid II's interaction with PGT, we deemed this result plausible, probably due to the extensive hydrogen bonding interaction present in multivalent binding of the oligomers.[34] We found that the binding

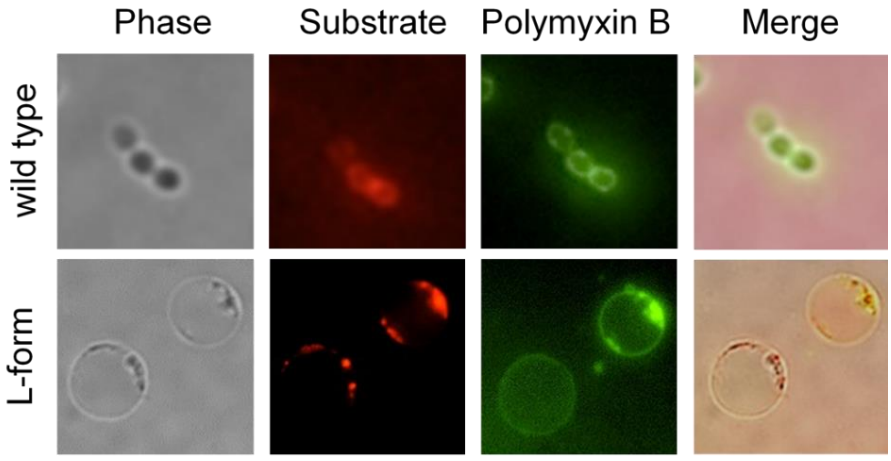

Figure 3-11. TIRF images of wild type and L-form *E.faecalis* OG1RF. The bacterial cells grown in DM3 medium were incubated with PGOs-rhodamine and membrane dye Polymyxin B-BODIPY FL. Scale bars, 1 μm and 10 μm for wild type and L-forms respectively.

energy for PGOs and *E. coli* K12 PBP1a had $\Delta G = -9.8 \pm 0.2$ kcal/mol and Kd of 83 nM, which is stronger than literature reports, being -4 to -6 kcal/mol and around 10 μM respectively.

3.3.4 Evaluation on the Diagnostic and Therapeutic Potential of PGOs

After mechanistic studies, the potential of the synthetic PGOs in application as a diagnostic tool was further explored. Such tool has to be sensitive to low bacteria concentration and to generate results fast enough to be sufficiently practical. Hence, varying bacteria concentrations have been incubated with of PGOs-rhodamine for 1 hour, and then subject to quantification by fluorospectrometer (**Figure 3-12**). Significant fluorescence was observed in bacteria with concentration even as low as 10^1 CFU/mL when compared to PBS control, and the intensity aligned well with bacteria concentration.

Knowing that detection of bacteria with PGOs-rhodamine incorporated had a low limit, we then moved on to address a concern closely pertaining to real life circumstances, which are the antibiotic resistant strains. Infections caused by such bacteria required far more careful treatment due to their complexity, and high lethality in turn. Therefore, enormous investment is being dedicated to development of methods to timely diagnose bacterial infection involving antibiotic resistance. The broad spectrum of bacteria recognizing PGOs as substrate was demonstrated in earlier experiments, thus we conceived it was possible to identify the presence of resistant strains in a rapid manner using PGOs. As the effective uptake of the synthetic PG substrate relied heavily on cell growth and metabolism, bacteria samples were treated with antibiotics first to inhibit

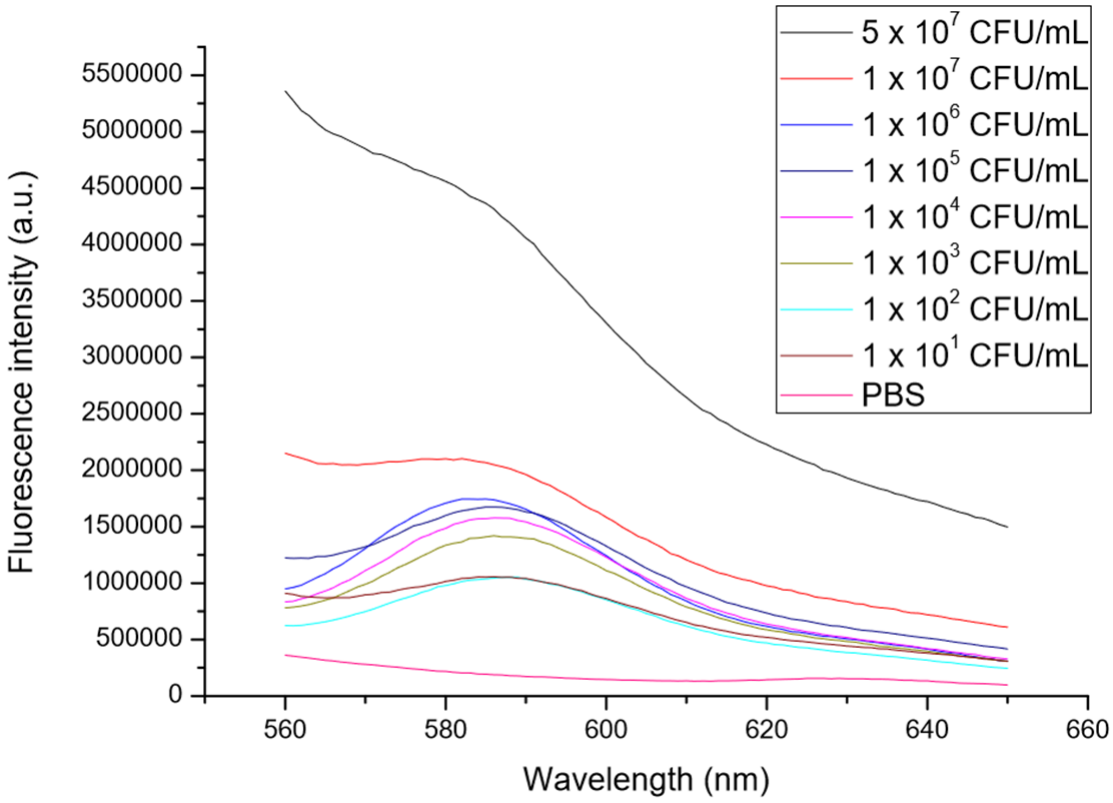

Figure 3-12. Fluorescence intensity of *E. coli* EC958 suspension labelled with PGOs-rhodamine. All suspension (including PBS control) was incubated with PGOs-rhodamine at 200 μg/mL for 1 hour and washed with PBS three times before measurement of fluorescence with fluorospectrometer.

growth of susceptible cells. Subsequently, PGOs-rhodamine was added for fluorescence analysis. Notably, a significant and consistent difference in fluorescence intensity was observed between resistant and susceptible strains for the two bacteria species tested, namely *E. coli* and *S. aureus* (**Figure 3-13**, The MICs of penicillin G sodium salt against *E. coli* 8739, *E. coli* 958, *S. aureus* 29213 and *S. aureus* USA300 were 32, 4000, 78, and 2500 μg/mL respectively.). The selective labelling of resistant bacterial strains, *E. coli* 958 and *S. aureus* USA300, in combination with the PGOs' excellent selectivity of bacterial cells in contrast to mammalian cells, would allow us to identify the presence

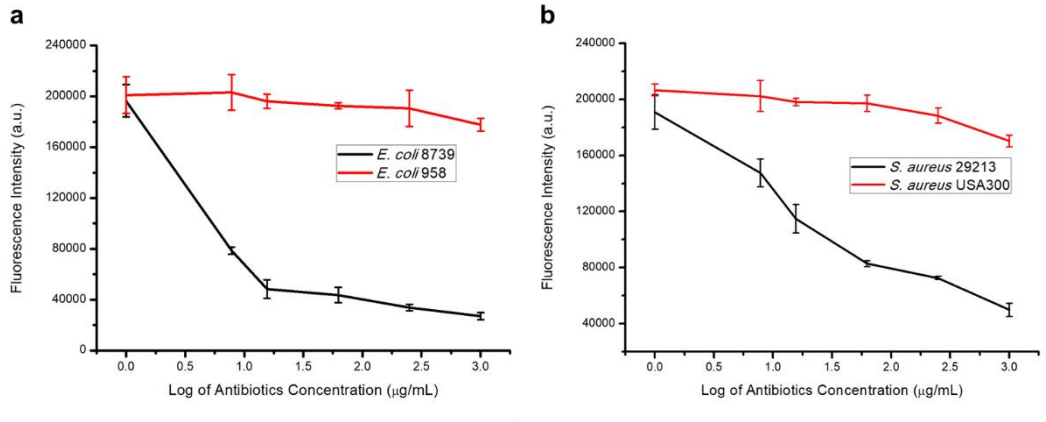

Figure 3-13. Fluorescence intensity comparison of resistant and susceptible *E. coli* and *S. aureus* respectively at 10^6 CFU/mL. The samples were incubated with 0-1000 μg/mL penicillin G sodium salt for 2 hours, washed, and then 50 μg/mL PGOs-rhodamine for 1 hour consecutively. Eventually, the bacteria samples were washed and resuspended in 1 mL PBS for analysis by fluorospectrometer.

of antibiotic resistant bacteria from samples of infection in a facile and practical manner, without the need of culturing potentially hazardous samples of infection.

In addition, we explored the therapeutic potential of PGOs with minimal modifications. The PG biosynthesis process has been a critical target for antibiotics since the advent of penicillin, which inhibits TPs, and in turn stopping PG cross-linking. In contrast, few antibiotics have been marketed as PGT inhibitors, with the most well studied being the moenomycin family. The compounds have excellent activity and no report of induced resistance, yet are not applicable to human due to their poor pharmacokinetic properties caused by a long lipid tail.[50] Nevertheless, an earlier study showed that substrates with shorter alkyl moieties retained antibacterial activities when using Lipid I/II scaffolds.[68] Intrigued by this finding, we sought to test on the PGOs' potential for antibacterial applications through simple conversion of pyrophosphate aglycone to a

phosphoglycerate, resembling a key functionality for effective binding of moenomycins and their analogues (**Figure 3-14**).

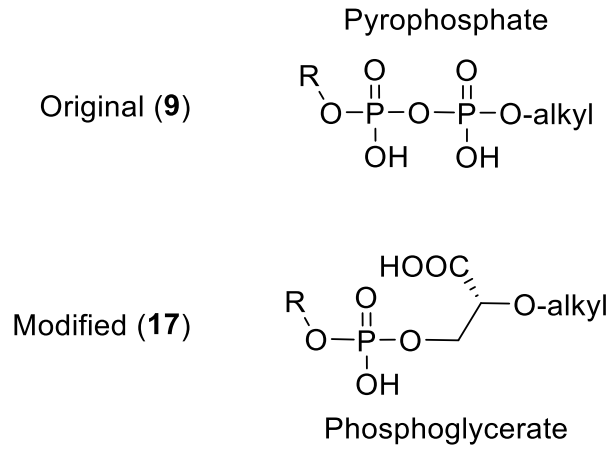

Figure 3-14. A modification to pyrophosphate moiety of original PGOs made the agent bacterial inhibitory.

As we further shortened the lipid length from C16 in the reported substrate to C12 on the PGOs scaffold, the new product had promising MIC values compared with literature reports,[68] being 32 μg/mL against both antibiotic susceptible *S. aureus* ATCC29213 and a resistant strain MRSA USA300. The decrease in activity from less hydrophobic moiety was probably compensated by the improved binding of PGOs with more binding capability in comparison with Lipid I or II. Also, the PGOs based product exhibited tolerance towards antibiotic resistance, which was a shared feature with moenomycin family antibiotics. On the contrary, the cytotoxicity against mammalian cells was found to be very low, with an IC_{50} value of 2048 μg/mL. This contrast illustrates the potential of PGOs as a platform to build on for development of novel antibacterial agents.

Based on the exploration of PGOs' diagnostic and therapeutic potential *in vitro*, we advanced to *in vivo* studies to test on its capability of detecting bacteria. The mice were infested with bacteria via the intraperitoneal injection of bacteria, followed with

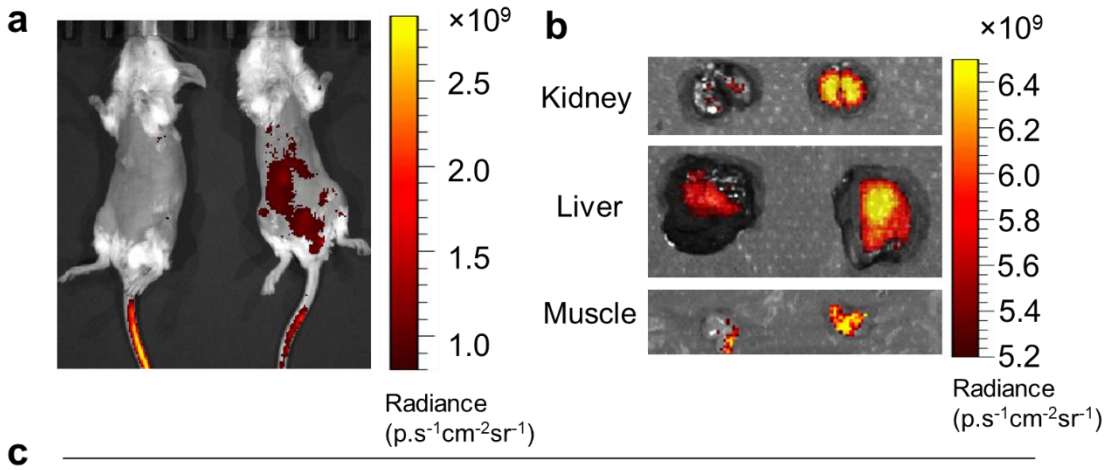

c

Bacteria CFU in varied organs

Organs	Non-infected mice	Infected mice
Liver	0.00E+00	1.67E+07
Kidney	8.33E+01	7.50E+05
Muscle	8.33E+03	1.50E+06

Figure 3-15. Imaging of PGOs-Cy7.5 in vivo. **a**, Representative image for non-infected mice (left) and infected mice (right), 8 hours after receiving intravenous injection of PGOs-Cy7.5. **b** and **c**, Fluorescence and CFU count respectively from excised kidney, liver and muscle (leg) of non-infected mice (left column) and infected mice (right).

intravenous injection of PGOs tagged by an NIR dye Cy7.5. As shown in **Figure 3-15**, PGOs-Cy7.5 was cleared faster in non-infected mice (left) compared to infected ones (right mice). Liver and kidney are two major organs infected in sepsis model, and we can clearly see that clearance of PGOs was retarded due to bacterial infection, demonstrated by strong fluorescence in liver area for infected mice in comparison with insignificant fluorescence for non-infected ones. To confirm the correlation between observed fluorescence intensity and bacterial CFU count, we dissected the mice 8 hours after injection of PGO-Cy7.5. Stronger fluorescence, along with higher bacterial count was found in kidney, liver and muscle (leg) of infected mice compared to non-infected

controls. The results of comparison well demonstrated the *in vivo* bacterial targeting effect, and in turn the applicability as a diagnostic tool, of our PGOs with minor modification by Cy7.5 dye.

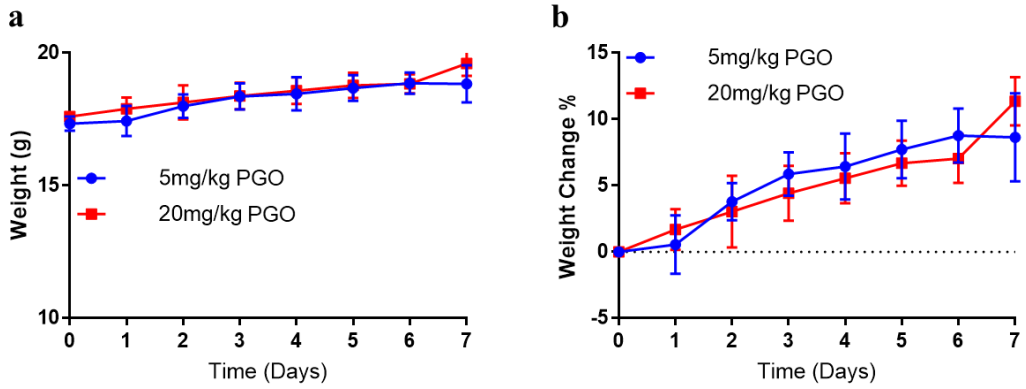

Figure 3-16. Mice weight monitor till 7 days post *i.v.* injection of 5 mg/kg or 20 mg/kg of PGO. Weight tracking (**a**) or weight change (**b**) percentage was compared to day 0 mice weight. The average weight or weight change from each group in different days were plotted with error bars representing the deviation within an experimental group of each day.

The *in vivo* toxicity of PGOs was evaluated via *i.v.* injecting 5 mg/kg or 20 mg/kg polymer followed by blood biochemistry analysis at 7 days post injection. Mice kept growing healthily and their weight increased by around 10% at day 7 after receiving intravenous injection of polymer at both dosages. (**Figure 3-16**) No nephro- or hepato-toxicity was induced by injection of the polymer, as demonstrated by the negligible variation of ALT, AST and BUN level for treated groups (**Figure 3-17**). These clearly support the excellent biocompatibility of chitosan modified even at 20 mg/kg, four times of the concentration used in bacterial targeting.

Real time *in vivo* imaging provides a practical tool to gather information about a lesion in an accurate and timely manner, so doctors would be able to advise treatments more

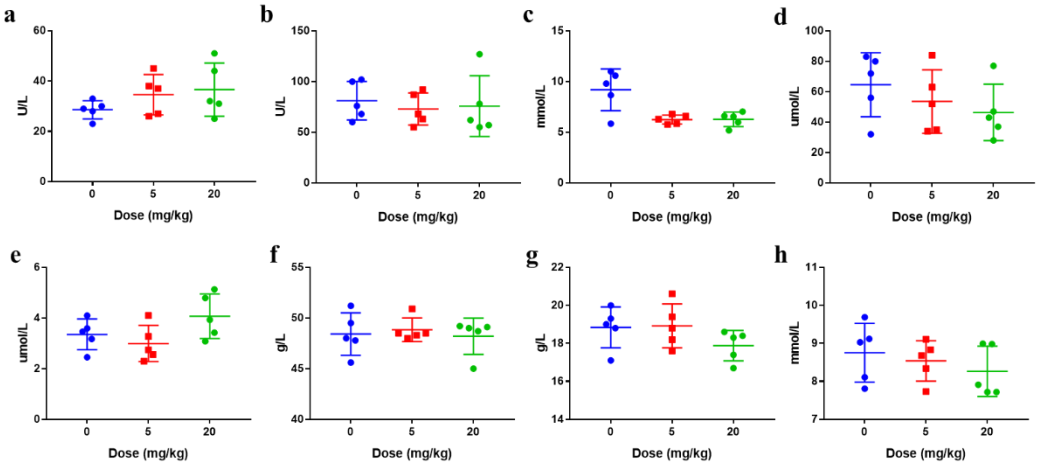

Figure 3-17. Blood biochemistry analysis at 7 days post *i.v.* injection of 5 mg/kg or 20 mg/kg of PGO. **a**, Alanine Aminotransferase (ALT), **b**, Aspartate Aminotransferase (AST), **c**, Blood urea nitrogen (BUN), **d**, Creatinine (CRE), **e**, Total bilirubin (TBIL), **f**, total protein (TP), **g**, globulin, **h**, glucose (GLU). Blood biochemical parameters from each mouse are plotted as individual points and error bars represent the deviation within an experimental group.

efficiently, yet it is more developed for anticancer studies.[72] More constraints, however, are seen when the target of interest is bacterial infection. Antibiotics have been adopted for targeting bacteria through specific binding,[73] although they are always haunted by the concern of AMR, which could be both the cause of a false negative result and the outcome of using such agents *per se*. On the other hand, monoclonal antibodies or antimicrobial peptides have also been commonly used for bacteria targeting, but they suffer from high cost or short duration of contact before metabolized or cleared. More recently, metabolic labelling has been realized *in vivo*, but it required high concentration and topical application, presumably due to a similarly short duration to take effect within body.[43, 74] In contrast, PGOs have demonstrated high sensitivity and selectivity to bacterial infection, while demanding low dosage and short time to take effect.

3.4 CONCLUSION

In contrast to reported strategies on bottom-up assembly of PG substrates, we have developed a top-down facile transformation of the inexpensive chitosan into biohybrid PGOs that can be successfully incorporated into the cell walls of different bacteria strains. The whole synthesis could be accomplished with eight one-pot chemical reactions in a convergent manner, with yield scalable to grams. The PGOs thus obtained could be conveniently modified for biosensing applications, as labeling with commcercially available rhodamine or cyanine dyes allowed for *in vitro* or *in vivo* imaging of bacteria alive. Further mechanistic studies revealed the necessity of multivalent binding for sufficient labeling activities, as well as the excellent specificity of PGOs when targeting bacteria. Our bio-synthetic hybrid PGOs could constitute a versatile platform to facilitate further mechanistic studies of the biosynthesis process of bacterial cell walls, or to be developed, after minor modifications, into diagnostic or therapeutic tools.

Chapter 4: Conjugates of PGO and Gold Nanoparticles Enable Sensitive Colorimetric Detection of Bacteria

4.1 INTRODUCTION

Bacterial infection has been a major cause of death in human civilization until the discovery of antibiotic in the last century. Nevertheless, the continuing mutations of bacteria or the acquiring of genes through horizontal gene transfer gives rise to AMR strains, which are far more complicated and lethal in turn. Identification of bacterial infections, including those caused by AMR species specifically, in a timely fashion could promote more accurate and effective prescription, thus reducing fatality rate directly, and impeding resistance from antibiotic abuse in the long run.

Currently, the diagnosis methods in practice generally rely on deduction from indirect evidences such as analysis of patient history and symptoms, which give inaccurate conclusions occasionally. In contrast, a conclusive depiction of source of illness is generally obtained from laboratory culture test in 48-72 hours. This duration could often be too long for a patient under severe infection to endure, especially when the pathogen is an AMR strain or has developed biofilm,[9-10] thus better diagnosis options are in urgent need.

Peptidoglycan (PG), with a ubiquitous and only presence in bacteria, has drawn attention from researchers as a target for identifying bacteria. Thus far, a few agents, based on antibiotic, D-amino acid or monosaccharide, have been reported or marketed for PG labeling, all requiring only a few hours to detect bacteria. However, they suffer

from drawbacks, including but not limited to narrow spectrum, low sensitivity or selectivity. PGOs, on the contrary, ensembles the full structure of PG, comprising oligosaccharides, peptides and phospholipids, which has yet to be synthesized for its daunting synthetic challenges. The main problem with commonly practiced carbohydrate synthesis is that sugar building blocks attach to each other in myriad ways to create a dazzling variety of branched structures.[22] In Chapter 3, the development of a top-down synthetic approach was described, which allowed for facile access to PGOs with excellent selectivity demonstrated in bacteria targeting. Hence, we sought to design the agent into a more practical detection tool with high sensitivity.

Gold nanoparticles (AuNPs) based colorimetric analysis has been extensively adopted for diverse biosensing applications, due to the ease of preparing and conjugating AuNPs, their high sensitivity towards subtle environmental changes, and the simple detection of extinction differences.[75-76] Aggregation of AuNPs causes the color to change from pink to violet, with a redshift in the extinction wavelength from localized surface plasmon resonance, which eventually diminishes as the size of aggregates continues to grow.[77-79] This spontaneous color change or disappearance do not require washing or microscopic imaging for identification as in the case of PGO-rhodamine for bacterial labeling. Hence, it was proposed that a combination of highly selective targeting from PGOs and highly sensitive detection of AuNPs would result in an efficient sensing tool for bacteria.

In this chapter the synthesis of AuNPs is described following a method reported in literature.[80] The NPs obtained conjugated with PGOs after characterization, and the PGO-AuNP conjugate was subject to incubation with bacteria, followed by colorimetric analysis on the extent of aggregation (**Figure 4-1**).

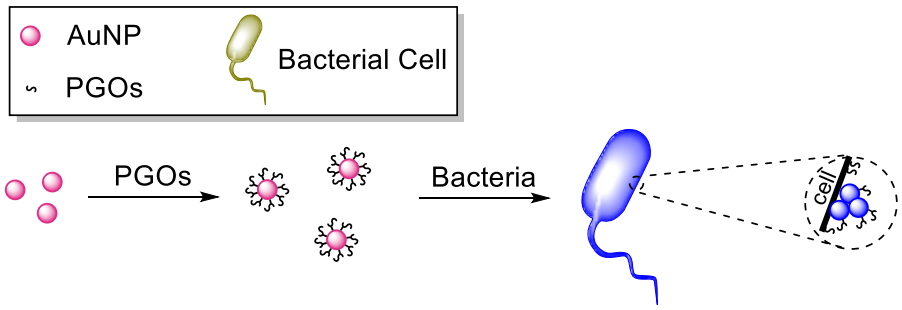

Figure 4-1. Schematic illustration of colorimetric detection of bacteria. PGOs could conjugate with AuNPs after sulfur functionalization, and the conjugate NPs aggregate towards surface of bacteria through PGOs' enzymatic interactions. The disappearance of pink color (light absorption at 520 nm) signifies presence of bacteria.

4.2. EXPERIMENTAL METHODS

4.2.1 Materials and Equipment

All chemicals used in synthesis were purchased from Sigma-Aldrich Co. LLC. (St. Louis, USA). Bacterial strains (*Escherichia coli* K12 ATCC10798, *Staphylococcus aureus* ATCC29213) were purchased from the American Type Culture Collection (Manassas, USA) and stored at -80 °C. Mueller-Hinton broth (MHB, Difco) was purchased from Beckton, Dickinson and company (Franklin Lakes, USA).

The reactions were all performed under nitrogen atmosphere. Starting materials and reagents were all purchased commercially and used as received. Solvents used in reactions were all purified according to standard procedures in literature. Thin layer chromatography (TLC) with Merck TLC silica gel 60 F254 plate was used to check reaction progress. UV, or potassium permanganate staining if necessary, was used to visualize compounds on TLC plates. ^{1}H and ^{13}C NMR spectra were obtained using 400 MHz Bruker AVIII 400 spectrometer or 500 MHz Bruker AV 500 spectrometer.

Tetramethylsilane (TMS) was used as internal standard in measurement of chemical shifts (ppm).

Shimadzu UV-3600 (Shimadzu Corporation, Kyoto, Japan) was used for UV-vis spectroscopy. Dynamic light scattering was done using Malvern Zetasizer Nano (Malvern Panalytical, Malvern, UK). TEM was done using JEOL JEM-1400 (JEOL Ltd., Tokyo, Japan)

4.2.2 Experimental for Chemical Synthesis

Synthesis of lipoic acid NHS ester **18**,

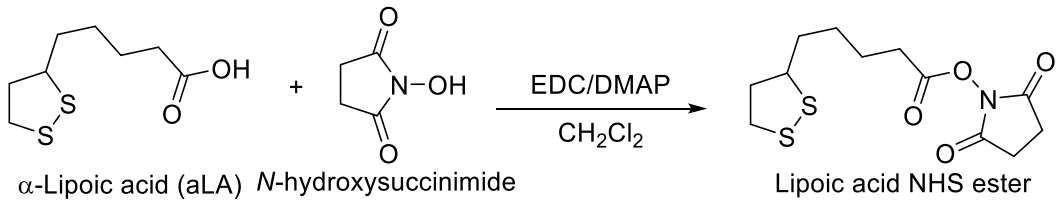

Scheme 4-1. Synthesis of lipoic acid NHS ester for PGO tagging and subsequent formation of conjugates with AuNPs.

Following **Scheme 4-1**, to a solution of α-lipoic acid (aLA, 206 mg, 1.0 mmol) in 20 mL CH_2Cl_2 was added *N*-hydroxysuccinimide (NHS, 138 mg, 1.2 mmol), 1-Ethyl-3-(3-dimethylaminopropyl)carbodiimide (EDC, 230 mg, 1.2 mmol) and 4-dimethylaminopyridine (DMAP, 122 mg, 1.0 mmol). The mixture was stirred at room temperature for 8 hours, and after checking full consumption of lipoic acid by TLC, the solution was washed with aqueous HCl (0.01 M, 20 mL x 3) and water (20 mL x 2). The organic layer was dried over brine and sodium sulfate sequentially, then the solvent was evaporated *in vacuo* to give the product **18** as a yellow solid (263 mg, 82%). ^{1}H NMR (500 MHz, Chloroform-*d*) δ 3.58 (dq, *J* = 8.4, 6.3 Hz, 1H), 3.19 (ddd, *J* = 11.1, 7.1, 5.4

Hz, 1H), 3.12 (dt, *J* = 11.0, 6.9 Hz, 1H), 2.84 (d, *J* = 4.2 Hz, 4H), 2.63 (t, *J* = 7.4 Hz, 2H), 2.47 (dtd, *J* = 12.1, 6.6, 5.4 Hz, 1H), 1.93 (dq, *J* = 13.6, 6.9 Hz, 1H), 1.84 – 1.65 (m, 4H), 1.64 – 1.48 (m, 2H). ^{13}C NMR (126 MHz, $CDCl_3$) δ 169.05, 168.28, 55.96, 40.01, 38.38, 34.25, 30.62, 28.16, 25.46, 24.21.

4.2.3 Sulfur Tagging on PGOs

Tagging by lipoic acid NHS ester followed a similar protocol as Sulfocyanine7.5 NHS ester which was described in section 3.2.6. Briefly, 10 mg PGOs was dissolved in 1 mL solution of sodium bicarbonate (0.1 M in deionized water). Then a solution of 1 mg lipoic acid NHS ester in 0.1 mL DMF was added, and the mixture was stirred at room temperature for 2 hours. After that, the solution was dialyzed for three days in deionized water, and the product was obtained by lyophilization as a beige solid.

4.2.4 Preparation of AuNPs

AuNPs were prepared by the citrate reduction method reported in literature.[80] Generally, gold(III) chloride trihydrate (60.0 mg, 0.15 mmol) was dissolved in 196 mL deionized water, and the solution was heated to reflux. Then a solution of trisodium citrate dihydrate (216 mg, 0.74 mmol) in 4 mL deionized water was added quickly while stirring. After stirring and refluxing for an additional 30 minutes, the solution was cooled to room temperature and characterized by UV-vis spectroscopy, DLS and TEM, kept refrigerated before using for further experiments.

4.2.5 General Procedure for Preparation of Conjugates from Varying Amounts of PGOs and AuNPs

The concentration of AuNP stock solution was first calculated according to literature,[81] and varying amounts of the solution were used for optimization of conjugate compositions following a similar methods as reported in literature.[82]

Briefly, to prepare a conjugate with the final concentration of AuNP at around 10 nM, 10 pmol AuNP and 0.5-8 nmol PGO-aLA (50-800 loading equivalence) were mixed together, and deionized water was added to a total volume of 1 mL. The conjugation was done on an orbital shaker at room temperature and 150 rpm, where the solution was left to stand for 48 hours. Subsequently, the mixture was subject to centrifugation at 12,000 rpm for 30 minutes, and the supernatant was discarded. After adding 1 mL deionized water, the washing step was repeated once, and the concentration of AuNPs in the final solution was evaluated by UV-vis spectroscopy.

4.2.6 General Procedure for Incubation of PGO-AuNP Conjugates with Bacteria

Bacterial strains to be tested were cultured overnight in MHB first and subsequently grown in 5 mL of fresh culture broth (1:100 dilution) to prepare logarithmic phase cultures after incubation at 37 ºC for 4 hours in a shaking incubator (225 rpm). Then bacteria cells were pelleted by centrifugation at 1,500 X *g* for 5 min and washed with PBS three times before resuspending in culture media. The bacteria suspension was diluted to the concentration to be tested and incubated for 1 hour in the presence of PGO-AuNP conjugate of varying concentrations with agitation (225 rpm).

4.3 RESULTS AND DISCUSSIONS

4.3.1 Synthesis of Sulfur Functionalized PGOs

As described in Chapter 3, the side chain amino group of lysine, which is the third amino acid of the peptide stem on PGO, has been demonstrated in many works as a site for modification without significant influence on the substrate molecule's enzymatic recognition. Hence, the design of this work still had its functionalization at this position, with only the fluorophore used in experiments in Chapter 3 being replaced by a sulfur-containing moiety for conjugation with AuNPs.

The presence of multiple nucleophilic moieties on a PGO scaffold brought concerns over the chemistry of choice, with which a sulfur-containing moiety could be tagged. With a similar situation, sulfuryl chloride or NHS ester were successfully adopted for fluorophore labeling as explained in section 3.2.6, and their ease of operation encouraged us to continue using them for this work. However, thiol functionalities are generally good nucleophiles themselves and may compete with the amino groups as designed during coupling, if not properly protected, leading to formation of thioesters instead of amides. Therefore, α-lipoic acid, an alkyl sulfide commonly seen for gold conjugation,[83-85] was chosen for linking PGOs and AuNPs in this work.

After a brief screening on coupling reagents, bases and solvents for activation of aLA, the carboxylic acid moiety of aLA was conveniently activated by NHS under optimized conditions as described in section 4.2.2. The identity of the product obtained was subsequently confirmed by NMR, and we went on to carry out sulfur tagging using a

similar protocol as commercially available NHS functionalized fluorescent dyes. The product, after lyophilization, was stored for interaction with AuNPs.

4.3.2 Preparation of AuNP Conjugates

AuNPs at approximately 10 nm in size were frequently used for colorimetric analysis of bacteria or cancer cells in a given sample, where the cell type of interest induced aggregation of AuNPs and shift or loss of light extinction.[86-88] Particularly, bacterial detection was commonly realized with the targeting capability of aptamers, which were normally specific to a specie or strain of bacteria.[89-91] The synthetic PGOs, however, might enable broad spectrum yet specific detection of bacteria as they bring the conjugated AuNPs to the surface of bacteria during incubation.

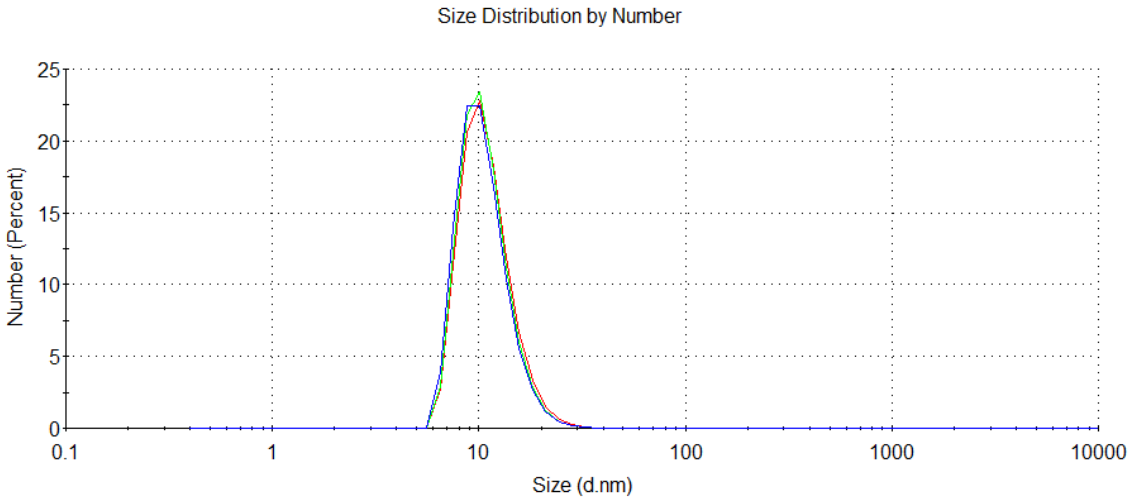

Figure 4-2. The size distribution results of AuNPs synthesized by the citrate reduction method. The average diameter given by DLS was 10.3 nm.

Following the citrate reduction method as described in section 4.2.4, an intense pink color was observed from the solution of AuNPs prepared. Then the diameter of the particles was measured by DLS (**Figure 4-2**) and TEM (**Figure 4-3**). Both gave a

similar result, being approximately 11 nm, and images of TEM further illustrated the morphology of AuNPs prepared, which was spherical in general.

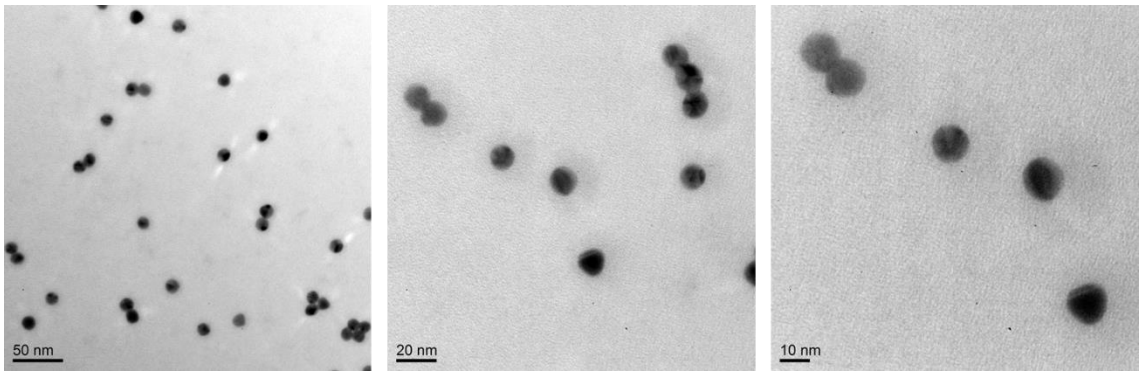

Figure 4-3. TEM images of AuNPs synthesized by the citrate reduction method. The average diameter was 10.0 nm.

After the consistency had been demonstrated on the size of nanoparticles obtained from both methods, the value was then used to calculate the molar extinction coefficient, ε, which was 1.42×10^{8} $M^{-1}\cdot cm^{-1}$ for an average diameter of 11 nm according literature.[81] This coefficient, in turn, allowed us to infer the concentration of AuNPs in solution by Beer-Lambert Law. As shown in **Figure 4-4**, the solution of AuNPs had an extinction of 2.393 at 520 nm, which corresponded to 16.9 nM as the NPs' concentration.

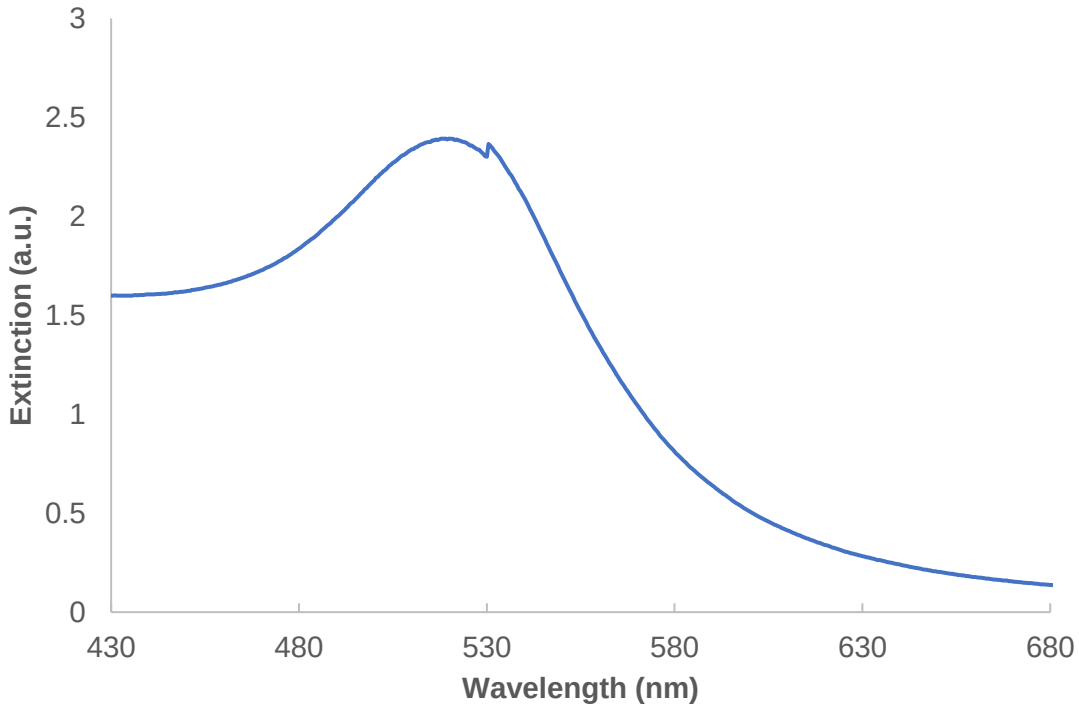

Figure 4-4. Extinction spectrum of AuNPs prepared. At 520 nm, AuNPs had an extinction of 2.393, which translated to 16.9 nM as the concentration in solution.

By calculating the concentration of AuNPs in solution, we were able to prepare PGO-AuNP conjugates at varying molar ratios according to the protocol detailed in section 4.2.5. It was noted that the size increase of NPs, as shown by DLS (**Figure 4-5**), did not lead to shift or disappearance of the peak at 520 nm in the extinction spectrum, implying AuNP cores' retention of size at around 10 nm. Therefore, it could only be due to a layer of PGOs coated on the surface, as the molecules did not have absorption of visible light.

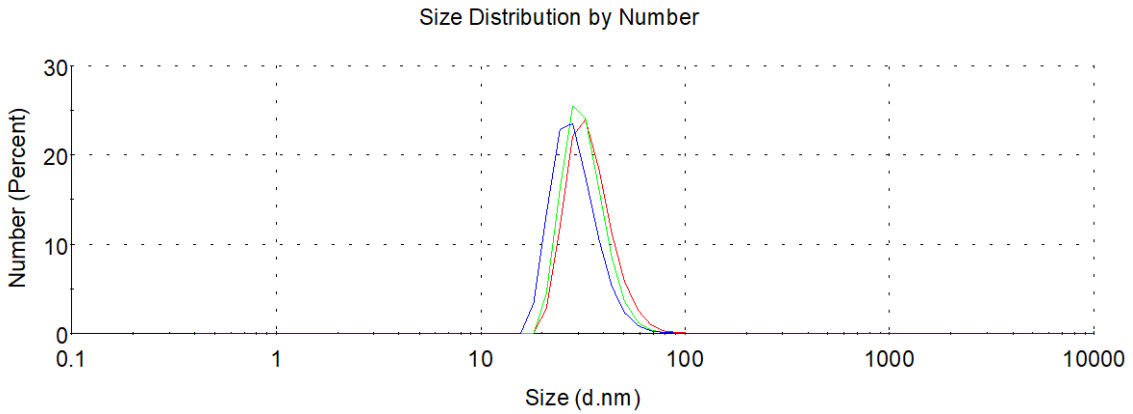

Figure 4-5. DLS results of PGO-AuNP conjugate at a ratio of 400 : 1 in deionized water. The average diameter was 26.9 nm.

Then the protective capability of PGO coating was subject to test against high salt concentrations in buffer the compositions with a PGO : AuNP ratio of no more than 200 : 1 aggregated spontaneously in PBS and MHB, turning into diminishingly pale blue color in a few hours. In contrast, higher concentrations of PGO-aLA in solution effectively stabilized AuNPs in the presence of buffer or media.

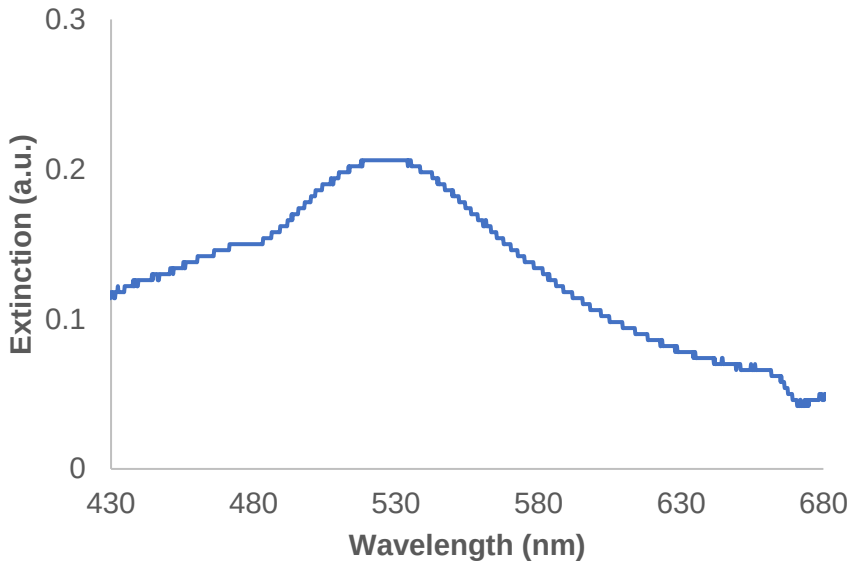

Figure 4-6. Extinction of PGO-AuNP conjugate in MHB. 2 nM conjugate was incubated at 37 ℃ for 24 hours and absorption of MHB alone was taken as control.

After a 24-hour incubation in MHB at 37 °C, the extinction profile of the conjugate only had a moderate peak broadening, with significant absorption at 520 nm remaining (**Figure 4-6**). Hence, we chose to adopt a ratio of PGO : AuNP at 400 : 1 to ensure the stability of PGO-AuNP conjugate, using a minimal amount of PGO, before contact with bacteria and to avoid potential false positive results during bacteria detection.

4.3.3 Detection of Bacteria with PGO-AuNP Conjugates

The use of AuNPs for detection of bacteria has been extensively reported,[92-95] through conjugation with targeting molecules such as antibodies or aptamers.[96-97] Recognition from these molecules were commonly associated with high specificity, being selective for limited species or strains.[88, 98-99] In contrast, PGOs have demonstrated recognition and uptake in a broad spectrum of bacterial species as shown in Chapter 3. Hence, after the composition of PGO-AuNP conjugates had been optimized, its sensitivity was subject to test against *S. aureus* and *E. coli*, one bacterial specie each from both Gram-positive and Gram-negative distinctions.

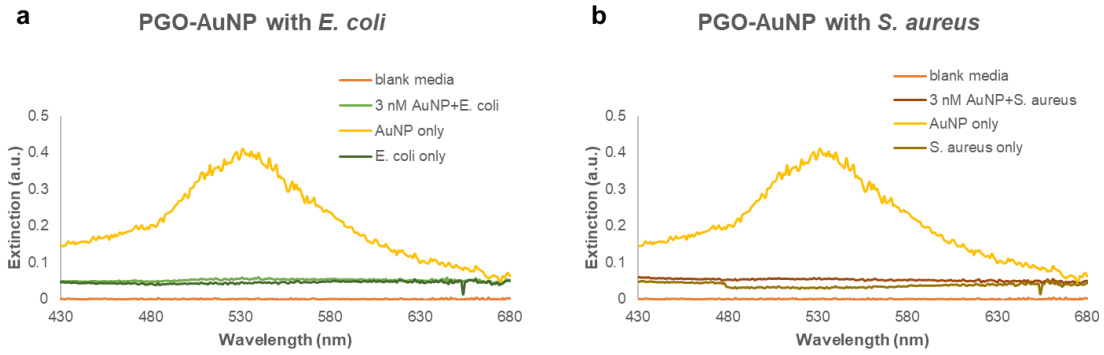

Figure 4-7. Extinction spectrum of PGO-AuNP incubated in MHB for 1 hour at 37 °C, with and without addition of **a**, *E. coli* and **b**, *S. aureus*. Blank media marked MHB incubated without NPs or bacteria, the concentration of AuNP was noted in the plot, and bacterial suspensions incubated in MHB alone were used as controls. The bacteria were added into MHB at 10^6 CFU/mL before incubation.

The concentration of AuNPs needed for detection was briefly screened first. Following the conditions adopted for PGO-rhodamine, the conjugate PGO-AuNP was incubated with bacteria in MHB for 1 hour at 37 ℃. It was found that the extinction of AuNPs at less than 1 nM was too low to have a clear contrast from that of bacteria alone. On the other hand, concentrations more than 10 nM were too high to have a complete aggregation, leaving significant absorption of light at around 520 nm after 1-hour incubation with bacteria. The optimal concentration of AuNP was determined to be 3 nM, which could be fully aggregated within 1 hour to eliminate absorption at 520 nm, while having a significant difference between samples with and without addition of bacteria (**Figure 4-7**).

Subsequently, the limit of detection of PGO-AuNP conjugate was evaluated against the two strains used for concentration optimization. Bacterial suspensions of varying concentrations were prepared by serial dilution and incubated with 3 nM of PGO-AuNP

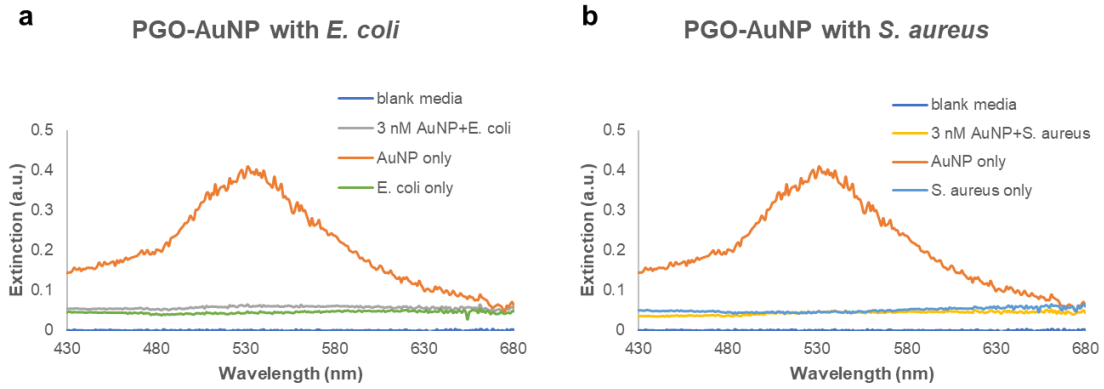

Figure 4-8. Extinction spectrum of PGO-AuNP incubated in MHB for 1 hour at 37 ℃, with and without addition of **a**, *E. coli* and **b**, *S. aureus*. Blank media marked MHB incubated without NPs or bacteria, the concentration of AuNP was noted in the plot, and bacterial suspensions incubated in MHB alone were used as controls. The bacteria were added into MHB at 10^2 CFU/mL before incubation.

conjugate solution. After incubation, we were able to observe the absence of extinction of AuNP at 520 nm, via UV-vis spectroscopy, till 10^2 CFU/mL of bacterial cells (**Figure 4-8**). This result demonstrated a high sensitivity of the conjugate in the application of bacteria detection.

4.4 CONCLUSION

Fluorescent dye modified PGOs have been shown to be capable of metabolically labeling bacteria with high sensitivity and selectivity in Chapter 3. Particularly, PGO-rhodamine was able to bring a significant increase to fluorescence intensity of bacteria as observed in spectrofluorometer. On the contrary, mammalian cells such as 3T3 mouse fibroblast exhibited negligible incorporation of the substrate, which was proposed to be from non-specific interactions and subsequent endocytosis.

Although these results well illustrated the potential of PGOs as a platform to develop on for bacterial sensing or diagnosis, we sought to further improve the operational simplicity of the overall procedure. Fluorescent labeling required multiple centrifugation and resuspension steps to suppress absorption signals from substrates in the background, as the fluorophores remained in the bacterial suspension throughout the whole incubation process. Whether dispersed in solution or concentrated onto bacterial cell wall, their excitation and emission processes did not have a significant difference. However, these washing steps might be skipped by using colorimetric methods, as local concentration had a significant influence on AuNP's extinction spectrum.

Through chemical modification, PGOs synthesized as described in the previous chapter were tagged by α-lipoic acid, which contained sulfur moieties. PGO-aLA could

spontaneously conjugate with AuNP in aqueous solution, while keeping the gold core away from each other and retaining extinction at 520 nm. With optimized composition, the conjugate was sufficiently stable to withstand salt and other nutrients in the culture media and did not aggregate. In contrast, a change in extinction profile, along with the loss of pink color, occurred upon incubation with bacteria. This detection worked for strains from both Gram-positive and Gram-negative distinctions, and had a low limit of detection, which may be applied for directly probing the presence of bacteria in a clear water sample.

Chapter 5: Summary, Conclusion and Outlooks

5.1 Summary and Conclusion

Antibiotics have greatly reduced illness and deaths resulting from infectious diseases since their introduction into medicine in the 1940s. However, conventional antibiotics used widely in medicine, agriculture, and veterinary industry are becoming increasingly ineffective in the face of multidrug-resistant "superbugs".[100] The overuse/misuse of antibiotics and the slow development of new antibiotics in the past decades make the situation even more challenging. Particularly, the number of AMR infection in Singapore has risen rapidly in the past decade. From surveillance culture investigations in hospitals in Singapore, the incidence of infection by carbapenem-resistant Enterobacteriaceae per 100,000 patient-days has dramatically increased from 0.76 in 2010 to 16.0 in 2015.[101] The infections frequently necessitated treatments by polymyxin or colistin, which are highly toxic to healthy human cells as well, while the excessive hospitalization duration and cost are also growing out of control. To address this issue, Singapore launched National Strategic Action Plan in November 2017 to prompt intensive investigation on new diagnostic and therapeutic solutions for bacterial infections, particularly those by AMR strains.

PG, as a major constituent of bacterial cell wall, has been a critical target for bacteria identification and eradication due to its universal-yet-specific presence in bacteria. Gram staining, as a common starting point for developing identity of an unknown bacterial specie, is mainly based on physical parameters of PG. On the other hand, β-lactams, as one of the earliest and most frequently prescribed antibiotics,

demonstrated its activities from chemical reactions with enzymes responsible for PG biosynthesis. Even recently, antibacterial agents with new mechanisms against the assembly of PG entirety are still being extensively investigated.[48, 62] In addition, derivatives of PG components, such as monosaccharide,[102] D-amino acid,[74] or glycolipid surrogates,[103] have been applied for bacterial detection via metabolic labeling in the past few years.

Despite the great efforts dedicated by researchers, PG substrates developed for bacteria targeting are predominantly small molecules thus far, which are easy to prepare but suffer from limited sensitivity, selectivity or spectrum of bacteria targets. Hence, the reported uses have been mainly restricted to mechanistic investigations in simplified experimental setups. Larger substrates, from Lipid II onwards, have more functional groups for multivalent binding with PG associated enzymes, guaranteeing better targeting activities. However, their unsatisfactory availability has been the major impedance against their application substantiations.

Three main methods have been reported for preparation of the large PG substrates, namely by chemical synthesis, enzymatic synthesis or overproduction/extraction. Particularly, chemical synthesis has offered the highest maneuverability for modifying substrates to analogs or derivatives, yet it has also been the most challenging among the three. Expensive starting materials or long-winding synthetic steps have precluded access to the substrates, thus investigation of mechanisms, by most researchers. Hence, we sought to address this concern by development of a practical way to obtain large PG substrates.

Identifying the bottleneck of commonly practiced syntheses to be the protection, deprotection and activation steps required for effective glycosylation, which links two sugar moieties via a glycosidic bond, our synthetic design skipped the majority of these steps by starting from oligomeric chitosans. The mass-produced starting materials are readily available at an affordable price, and naturally comprise β-1→4 glycosidic bonds, allowing us to obtain oligomeric PG substrates with a reasonable cost and scale.

After characterization of PGOs' physical properties, we were able to demonstrate the biological activities of PGOs in images obtained by STED confocal microscopy, which showed signal of fluorescent labeled PGOs on the surface of bacterial cells. While incorporation of PGOs was observed in all bacterial strains tested, encompassing both Gram-positive and Gram-negative species, negligible signal was seen in mammalian cells when incubated under the same conditions. Furthermore, we also compared, under the same incubation conditions, activities of PGOs with lipid or sugar moieties truncated, which confirmed the necessity of the entirety of PGOs for effective recognition by bacteria.

Subsequently, mechanistic investigations were done with a mutant strain and recombinant PGT. The fluorescent dye conjugated PGOs and penicillin G colocalized well on discrete PG residues after incubation with L-form enterococcus, which strongly supported our hypothesized activity mechanism and ruled out possibilities of non-specific binding to cell surface. The results substantiated PGOs' potential to probe biological processes of PGT as a highly specific enzyme substrate. Besides mechanism studies, PGOs may also be further developed for diagnostic applications both *in vitro* and *in vivo*. With the aid of antibiotics, the presence of AMR strains could be detected in

a given sample in a relatively short duration. In addition, PGOs were able to map infections *in vivo* after conjugation with an NIR dye, while being non-toxic at dosages even several times higher.

Eventually, we sought to further simplify the operational procedures for detection of bacteria through conjugation with AuNPs. At optimized conditions, the conjugates were sufficiently stable to withstand salt and other nutrients in culture media during incubation. In contrast, presence of low concentrations of bacteria could rapidly induce aggregation, which could be readily detected through colorimetric analysis. This demonstrated PGOs as a versatile platform to be developed on for diverse applications.

5.2 Outlooks

5.2.1 PGO Conjugates for Bacterial Sensing or Antibacterial Applications

As shown in Chapter 3 and 4, the bacterial specificity of PGO may be combined with fluorescent dyes or gold nanoparticles for detection of bacteria, via microscopic imaging, spectroscopic measurement or colorimetric analysis. The amine handles on pendant peptide moieties could effectively react with acid chloride or NHS ester using reported protocols, making conjugates for diverse applications available. Moreover, this conjugation process has not been associated with influence on binding interactions with PGTs or cell toxicity *per se*. We can further utilize this chemistry to attach antibacterial agents to kill bacteria in a similar manner to the more established antibody-drug conjugate strategy,[104-105] or to attach other nanoparticles for bacterial sensing

applications under different mechanisms from the PGO-AuNP conjugate described in Chapter 4.[106]

5.2.2 PGO Derivatives for Mechanistic Investigation of the Biosynthesis Process of Bacterial Cell Wall

As described in Chapter 1 and 2, the biosynthesis process of bacterial cell wall has been the target of many critical antibiotics, such as penicillins as β-lactams and vancomycin as glycopeptides. While new drugs developed recently generally kill bacteria with old mechanisms, which are mostly associated with AMR as bacteria continue to evolve, several new cell wall inhibitory agents had no detectable resistance. Nonetheless, the bottleneck for investigation of killing mechanisms of the new agents resided on the limited access to PG substrates and analogs. Though enzymatic and, more recently, extraction methods provided relatively facile access to Lipid II, thus far they had limited space for modification and no reach to molecules any larger. Chemical synthesis, in comparison, offered far more possibilities for structural modification, as exemplified in sections 3.3.3 and 3.3.4. As our synthetic strategy for PGOs provided a practical way to obtain large PG substrates compared with conventional costly methods,[63, 107] we hope to explore the biological processes of cell wall assembly to provide insight for more efficiently developing antibacterial agents.

References

(1) Fair, R. J.; Tor, Y., Antibiotics and Bacterial Resistance in the 21st Century. *Perspect. Medicin. Chem.* **2014,** *6*, PMC.S14459.

(2) Adeyi, O. O.; Baris, E.; Jonas, O. B.; Irwin, A.; Berthe, F. C. J.; Le Gall, F. G.; Marquez, P. V.; Nikolic, I. A.; Plante, C. A.; Schneidman, M.; Shriber, D. E.; Thiebaud, A. *Drug-resistant infections : a threat to our economic future*; 114679; The World Bank: 2017.

(3) Butler, M. S.; Blaskovich, M. A.; Cooper, M. A., Antibiotics in the clinical pipeline in 2013. *J. Antibiot.* **2013,** *66*, 571.

(4) Munita, J. M.; Arias, C. A., Mechanisms of Antibiotic Resistance. *Microbiol. Spectr.* **2016,** *4* (2), 481-511.

(5) BENZ, R.; BAUER, K., Permeation of hydrophilic molecules through the outer membrane of gram-negativ bacteria. *Eur. J. Biochem.* **1988,** *176* (1), 1-19.

(6) Cox, G.; Wright, G. D., Intrinsic antibiotic resistance: Mechanisms, origins, challenges and solutions. *Int. J. Med. Microbiol.* **2013,** *303* (6), 287-292.

(7) Wright, G. D., Molecular mechanisms of antibiotic resistance. *Chem. Commun.* **2011,** *47* (14), 4055-4061.

(8) Blair, J. M. A.; Webber, M. A.; Baylay, A. J.; Ogbolu, D. O.; Piddock, L. J. V., Molecular mechanisms of antibiotic resistance. *Nat. Rev. Microbiol.* **2014,** *13*, 42.

(9) Wu, H.; Moser, C.; Wang, H.-Z.; Høiby, N.; Song, Z.-J., Strategies for combating bacterial biofilm infections. *Int. J. Oral Sci.* **2014,** *7*, 1.

(10) Martin, J. S. H.; Monaghan, T. M.; Wilcox, M. H., Clostridium difficile infection: epidemiology, diagnosis and understanding transmission. *Nat. Rev. Gastroenterol. Hepatol.* **2016,** *13*, 206.

(11) Beveridge, T. J., Use of the Gram stain in microbiology. *Biotech. Histochem.* **2001,** *76* (3), 111-118.

(12) Silhavy, T. J.; Kahne, D.; Walker, S., The Bacterial Cell Envelope. *CSH Perspect. Biol.* **2010,** *2* (5).

(13) Vollmer, W.; Blanot, D.; de Pedro, M. A., Peptidoglycan structure and architecture. *FEMS Microbiol. Rev.* **2008,** *32* (2), 149-167.

(14) Huang, L.-Y.; Huang, S.-H.; Chang, Y.-C.; Cheng, W.-C.; Cheng, T.-J. R.; Wong, C.-H., Enzymatic Synthesis of Lipid II and Analogues. *Angew. Chem. Int. Ed.* **2014,** *53* (31), 8060-8065.

(15) Ruiz, N., Lipid Flippases for Bacterial Peptidoglycan Biosynthesis. *Lipid Insights* **2016,** *8* (Suppl 1), 21-31.

(16) Waxman, D. J.; Strominger, J. L., Penicillin-Binding Proteins and the Mechanism of Action of Beta-Lactam Antibiotics. *Annu. Rev. Biochem.* **1983,** *52*, 825-869.

(17) Lam, H.; Oh, D.-C.; Cava, F.; Takacs, C. N.; Clardy, J.; de Pedro, M. A.; Waldor, M. K., D-Amino Acids Govern Stationary Phase Cell Wall Remodeling in Bacteria. *Science* **2009,** *325* (5947), 1552-1555.

(18) Lupoli, T. J.; Tsukamoto, H.; Doud, E. H.; Wang, T.-S. A.; Walker, S.; Kahne, D., Transpeptidase-Mediated Incorporation of d-Amino Acids into Bacterial Peptidoglycan. *J. Am. Chem. Soc.* **2011,** *133* (28), 10748-10751.

(19) van Heijenoort, Y.; Gómez, M.; Derrien, M.; Ayala, J.; van Heijenoort, J., Membrane intermediates in the peptidoglycan metabolism of Escherichia coli: possible roles of PBP 1b and PBP 3. *J. Bacteriol.* **1992,** *174* (11), 3549-3557.

(20) Schwartz, B.; Markwalder, J. A.; Wang, Y., Lipid II: Total Synthesis of the Bacterial Cell Wall Precursor and Utilization as a Substrate for Glycosyltransfer and Transpeptidation by Penicillin Binding Protein (PBP) 1b of Eschericia coli. *J. Am. Chem. Soc.* **2001,** *123* (47), 11638-11643.

(21) VanNieuwenhze, M. S.; Mauldin, S. C.; Zia-Ebrahimi, M.; Aikins, J. A.; Blaszczak, L. C., The Total Synthesis of Lipid I. *J. Am. Chem. Soc.* **2001,** *123* (29), 6983-6988.

(22) Wang, N.; Hasegawa, H.; Huang, C.-y.; Fukase, K.; Fujimoto, Y., Synthesis of Peptidoglycan Fragments from Enterococcus faecalis with Fmoc-Strategy for Glycan Elongation. *Chem. Asian J.* **2017,** *12* (1), 27-30.

(23) Zhang, Y.; Fechter, E. J.; Wang, T.-S. A.; Barrett, D.; Walker, S.; Kahne, D. E., Synthesis of Heptaprenyl−Lipid IV to Analyze Peptidoglycan Glycosyltransferases. *J. Am. Chem. Soc.* **2007,** *129* (11), 3080-3081.

(24) Wang, T.-S. A.; Lupoli, T. J.; Sumida, Y.; Tsukamoto, H.; Wu, Y.; Rebets, Y.; Kahne, D. E.; Walker, S., Primer Preactivation of Peptidoglycan Polymerases. *J. Am. Chem. Soc.* **2011,** *133* (22), 8528-8530.

(25) Li, P.; Zhou, C.; Rayatpisheh, S.; Ye, K.; Poon, Y. F.; Hammond, P. T.; Duan, H. W.; Chan-Park, M. B., Cationic Peptidopolysaccharides Show Excellent Broad-Spectrum Antimicrobial Activities and High Selectivity. *Adv. Mater.* **2012,** *24* (30), 4130-4137.

(26) Kuru, E.; Hughes, H. V.; Brown, P. J.; Hall, E.; Tekkam, S.; Cava, F.; de Pedro, M. A.; Brun, Y. V.; VanNieuwenhze, M. S., In Situ Probing of Newly Synthesized

Peptidoglycan in Live Bacteria with Fluorescent D-Amino Acids. *Angew. Chem. Int. Ed.* **2012,** *51* (50), 12519-12523.

(27) Liechti, G. W.; Kuru, E.; Hall, E.; Kalinda, A.; Brun, Y. V.; VanNieuwenhze, M.; Maurelli, A. T., A new metabolic cell-wall labelling method reveals peptidoglycan in Chlamydia trachomatis. *Nature* **2014,** *506* (7489), 507-510.

(28) Liang, H.; DeMeester, K. E.; Hou, C.-W.; Parent, M. A.; Caplan, J. L.; Grimes, C. L., Metabolic labelling of the carbohydrate core in bacterial peptidoglycan and its applications. *Nat. Commun.* **2017,** *8*, 15015.

(29) VanNieuwenhze, M. S.; Mauldin, S. C.; Zia-Ebrahimi, M.; Winger, B. E.; Hornback, W. J.; Saha, S. L.; Aikins, J. A.; Blaszczak, L. C., The First Total Synthesis of Lipid II: The Final Monomeric Intermediate in Bacterial Cell Wall Biosynthesis. *J. Am. Chem. Soc.* **2002,** *124* (14), 3656-3660.

(30) Shih, H.-W.; Chen, K.-T.; Cheng, T.-J. R.; Wong, C.-H.; Cheng, W.-C., A New Synthetic Approach toward Bacterial Transglycosylase Substrates, Lipid II and Lipid IV. *Org. Lett.* **2011,** *13* (17), 4600-4603.

(31) Hesek, D.; Lee, M.; Morio, K.-i.; Mobashery, S., Synthesis of a Fragment of Bacterial Cell Wall. *J. Org. Chem.* **2004,** *69* (6), 2137-2146.

(32) Ye, X.-Y.; Lo, M.-C.; Brunner, L.; Walker, D.; Kahne, D.; Walker, S., Better Substrates for Bacterial Transglycosylases. *J. Am. Chem. Soc.* **2001,** *123* (13), 3155-3156.

(33) Liu, H.; Ritter, T. K.; Sadamoto, R.; Sears, P. S.; Wu, M.; Wong, C.-H., Acceptor Specificity and Inhibition of the Bacterial Cell-Wall Glycosyltransferase MurG. *ChemBioChem* **2003,** *4* (7), 603-609.

(34) Shih, H.-W.; Chang, Y.-F.; Li, W.-J.; Meng, F.-C.; Huang, C.-Y.; Ma, C.; Cheng, T.-J. R.; Wong, C.-H.; Cheng, W.-C., Effect of the Peptide Moiety of Lipid II on Bacterial Transglycosylase. *Angew. Chem. Int. Ed.* **2012,** *51* (40), 10123-10126.

(35) Qiao, Y.; Srisuknimit, V.; Rubino, F.; Schaefer, K.; Ruiz, N.; Walker, S.; Kahne, D., Lipid II overproduction allows direct assay of transpeptidase inhibition by β-lactams. *Nat. Chem. Biol.* **2017,** *13*, 793.

(36) Mahal, L. K.; Yarema, K. J.; Bertozzi, C. R., Engineering Chemical Reactivity on Cell Surfaces Through Oligosaccharide Biosynthesis. *Science* **1997,** *276* (5315), 1125-1128.

(37) Pidgeon, S. E.; Fura, J. M.; Leon, W.; Birabaharan, M.; Vezenov, D.; Pires, M. M., Metabolic Profiling of Bacteria by Unnatural C-terminated D-Amino Acids. *Angew. Chem. Int. Ed.* **2015,** *54* (21), 6158-6162.

(38) Sarkar, S.; Libby, E. A.; Pidgeon, S. E.; Dworkin, J.; Pires, M. M., In Vivo Probe of Lipid II-Interacting Proteins. *Angew. Chem. Int. Ed.* **2016,** *55* (29), 8401-8404.

(39) Siegrist, M. S.; Whiteside, S.; Jewett, J. C.; Aditham, A.; Cava, F.; Bertozzi, C. R., D-Amino Acid Chemical Reporters Reveal Peptidoglycan Dynamics of an Intracellular Pathogen. *ACS Chem. Biol.* **2013,** *8* (3), 500-505.

(40) Qiao, Y.; Lebar, M. D.; Schirner, K.; Schaefer, K.; Tsukamoto, H.; Kahne, D.; Walker, S., Detection of Lipid-Linked Peptidoglycan Precursors by Exploiting an Unexpected Transpeptidase Reaction. *J. Am. Chem. Soc.* **2014,** *136* (42), 14678-14681.

(41) Gautam, S.; Kim, T.; Shoda, T.; Sen, S.; Deep, D.; Luthra, R.; Ferreira, M. T.; Pinho, M. G.; Spiegel, D. A., An Activity-Based Probe for Studying Crosslinking in Live Bacteria. *Angew. Chem. Int. Ed.* **2015,** *54* (36), 10492-10496.

(42) Neumann, K. D.; Villanueva-Meyer, J. E.; Mutch, C. A.; Flavell, R. R.; Blecha, J. E.; Kwak, T.; Sriram, R.; VanBrocklin, H. F.; Rosenberg, O. S.; Ohliger, M. A.; Wilson, D. M., Imaging Active Infection in vivo Using D-Amino Acid Derived PET Radiotracers. *Sci. Rep.* **2017,** *7* (1), 7903.

(43) Mao, D.; Hu, F.; Kenry; Ji, S.; Wu, W.; Ding, D.; Kong, D.; Liu, B., Metal–Organic-Framework-Assisted In Vivo Bacterial Metabolic Labeling and Precise Antibacterial Therapy. *Adv. Mater.* **2018,** *30* (18), 1706831.

(44) Kuru, E.; Tekkam, S.; Hall, E.; Brun, Y. V.; Van Nieuwenhze, M. S., Synthesis of fluorescent D-amino acids and their use for probing peptidoglycan synthesis and bacterial growth in situ. *Nat. Protoc.* **2014,** *10*, 33.

(45) Huang, C.-Y.; Shih, H.-W.; Lin, L.-Y.; Tien, Y.-W.; Cheng, T.-J. R.; Cheng, W.-C.; Wong, C.-H.; Ma, C., Crystal structure of Staphylococcus aureus transglycosylase in complex with a lipid II analog and elucidation of peptidoglycan synthesis mechanism. *Proc. Natl. Acad. Sci. USA* **2012,** *109* (17), 6496-6501.

(46) Huang, S.-H.; Wu, W.-S.; Huang, L.-Y.; Huang, W.-F.; Fu, W.-C.; Chen, P.-T.; Fang, J.-M.; Cheng, W.-C.; Cheng, T.-J. R.; Wong, C.-H., New Continuous Fluorometric Assay for Bacterial Transglycosylase Using Förster Resonance Energy Transfer. *J. Am. Chem. Soc.* **2013,** *135* (45), 17078-17089.

(47) Lebar, M. D.; Lupoli, T. J.; Tsukamoto, H.; May, J. M.; Walker, S.; Kahne, D., Forming Cross-Linked Peptidoglycan from Synthetic Gram-Negative Lipid II. *J. Am. Chem. Soc.* **2013,** *135* (12), 4632-4635.

(48) Lee, W.; Schaefer, K.; Qiao, Y.; Srisuknimit, V.; Steinmetz, H.; Müller, R.; Kahne, D.; Walker, S., The Mechanism of Action of Lysobactin. *J. Am. Chem. Soc.* **2016,** *138* (1), 100-103.

(49) Lee, M.; Hesek, D.; Dik, D. A.; Fishovitz, J.; Lastochkin, E.; Boggess, B.; Fisher, J. F.; Mobashery, S., From Genome to Proteome to Elucidation of Reactions for All Eleven Known Lytic Transglycosylases from Pseudomonas aeruginosa. *Angew. Chem. Int. Ed.* **2017,** *56* (10), 2735-2739.

(50) Ostash, B.; Walker, S., Moenomycin family antibiotics: chemical synthesis, biosynthesis, and biological activity. *Nat. Prod. Rep.* **2010,** *27* (11), 1594-1617.

(51) Sadamoto, R.; Niikura, K.; Sears, P. S.; Liu, H.; Wong, C.-H.; Suksomcheep, A.; Tomita, F.; Monde, K.; Nishimura, S.-I., Cell-Wall Engineering of Living Bacteria. *J. Am. Chem. Soc.* **2002,** *124* (31), 9018-9019.

(52) Ruiz, N., Lipid Flippases for Bacterial Peptidoglycan Biosynthesis. *Lipid Insights* **2015,** *8s1*, LPI.S31783.

(53) Hong, Y.; Liu, M. A.; Reeves, P. R., Progress in Our Understanding of Wzx Flippase for Translocation of Bacterial Membrane Lipid-Linked Oligosaccharide. *J. Bacteriol.* **2018,** *200* (1), e00154-17.

(54) Kuk, A. C. Y.; Hao, A.; Guan, Z.; Lee, S.-Y., Visualizing conformation transitions of the Lipid II flippase MurJ. *Nat. Commun.* **2019,** *10* (1), 1736.

(55) Hakenbeck, R.; Grebe, T.; Zähner, D.; Stock, J. B., β-Lactam resistance in Streptococcus pneumoniae: penicillin-binding proteins and non-penicillin-binding proteins. *Mol. Microbiol.* **1999,** *33* (4), 673-678.

(56) Boneca, I. G.; Chiosis, G., Vancomycin resistance: occurrence, mechanisms and strategies to combat it. *Expert Opin. Ther. Targets* **2003,** *7* (3), 311-328.

(57) Hakenbeck, R.; Brückner, R.; Denapaite, D.; Maurer, P., Molecular mechanisms of *β*-lactam resistance in Streptococcus pneumoniae. *Future Microbiol.* **2012,** *7* (3), 395-410.

(58) Holtje, J. V., Growth of the stress-bearing and shape-maintaining murein sacculus of Escherichia coli. *Microbiol. Mol. Biol. Rev.* **1998,** *62* (1), 181-203.

(59) Wong, K. K.; Pompliano, D. L., Peptidoglycan biosynthesis - Unexploited antibacterial targets within a familiar pathway. *Adv. Exp. Med. Biol.* **1998,** *456*, 197-217.

(60) Typas, A.; Banzhaf, M.; Gross, C. A.; Vollmer, W., From the regulation of peptidoglycan synthesis to bacterial growth and morphology. *Nat. Rev. Microbiol.* **2012,** *10* (2), 123-136.

(61) Schneider, T.; Kruse, T.; Wimmer, R.; Wiedemann, I.; Sass, V.; Pag, U.; Jansen, A.; Nielsen, A. K.; Mygind, P. H.; Raventós, D. S.; Neve, S.; Ravn, B.; Bonvin, A. M. J. J.; De Maria, L.; Andersen, A. S.; Gammelgaard, L. K.; Sahl, H.-G.; Kristensen, H.-H., Plectasin, a Fungal Defensin, Targets the Bacterial Cell Wall Precursor Lipid II. *Science* **2010,** *328* (5982), 1168-1172.

(62) Ling, L. L.; Schneider, T.; Peoples, A. J.; Spoering, A. L.; Engels, I.; Conlon, B. P.; Mueller, A.; Schaberle, T. F.; Hughes, D. E.; Epstein, S.; Jones, M.; Lazarides, L.; Steadman, V. A.; Cohen, D. R.; Felix, C. R.; Fetterman, K. A.; Millett, W. P.; Nitti, A. G.; Zullo, A. M.; Chen, C.; Lewis, K., A new antibiotic kills pathogens without detectable resistance. *Nature* **2015,** *517* (7535), 455-459.

(63) Lee, M.; Hesek, D.; Mobashery, S., Synthetic Efforts in Preparations of Components of the Bacterial Cell Wall. In *Chemical Glycobiology*, American Chemical Society: 2008; Vol. 990, pp 54-78.

(64) Cho, S.; Wang, Q.; Swaminathan, C. P.; Hesek, D.; Lee, M.; Boons, G.-J.; Mobashery, S.; Mariuzza, R. A., Structural insights into the bactericidal mechanism of human peptidoglycan recognition proteins. *Proc. Natl. Acad. Sci. USA* **2007,** *104* (21), 8761-8766.

(65) Ifuku, S.; Miwa, T.; Morimoto, M.; Saimoto, H., Preparation of highly chemoselective N-phthaloyl chitosan in aqueous media. *Green Chem.* **2011,** *13* (6), 1499-1502.

(66) Binette, A.; Gagnon, J., Regioselective Silylation of N-Phthaloylchitosan with TBDMS and TBDPS Groups. *Biomacromolecules* **2007,** *8* (6), 1812-1815.

(67) Hermanson, G. T., Chapter 10 - Fluorescent Probes. In *Bioconjugate Techniques (Third edition)*, Academic Press: Boston, 2013; pp 395-463.

(68) Dumbre, S.; Derouaux, A.; Lescrinier, E.; Piette, A.; Joris, B.; Terrak, M.; Herdewijn, P., Synthesis of Modified Peptidoglycan Precursor Analogues for the Inhibition of Glycosyltransferase. *J. Am. Chem. Soc.* **2012,** *134* (22), 9343-9351.

(69) Burgess, A.; Vigneron, S.; Brioudes, E.; Labbé, J.-C.; Lorca, T.; Castro, A., Loss of human Greatwall results in G2 arrest and multiple mitotic defects due to deregulation of the cyclin B-Cdc2/PP2A balance. *Proc. Natl. Acad. Sci. USA* **2010,** *107* (28), 12564-12569.

(70) McCloy, R. A.; Rogers, S.; Caldon, C. E.; Lorca, T.; Castro, A.; Burgess, A., Partial inhibition of Cdk1 in G2 phase overrides the SAC and decouples mitotic events. *Cell Cycle* **2014,** *13* (9), 1400-1412.

(71) Chang, S.; Cohen, S. N., High frequency transformation of Bacillus subtilis protoplasts by plasmid DNA. *Molec. Gen. Genet.* **1979,** *168* (1), 111-115.

(72) Wang, H.; Wang, R.; Cai, K.; He, H.; Liu, Y.; Yen, J.; Wang, Z.; Xu, M.; Sun, Y.; Zhou, X.; Yin, Q.; Tang, L.; Dobrucki, I. T.; Dobrucki, L. W.; Chaney, E. J.; Boppart, S. A.; Fan, T. M.; Lezmi, S.; Chen, X.; Yin, L.; Cheng, J., Selective in vivo metabolic cell-labeling-mediated cancer targeting. *Nat. Chem. Biol.* **2017,** *13*, 415.

(73) van Oosten, M.; Schäfer, T.; Gazendam, J. A. C.; Ohlsen, K.; Tsompanidou, E.; de Goffau, M. C.; Harmsen, H. J. M.; Crane, L. M. A.; Lim, E.; Francis, K. P.; Cheung, L.; Olive, M.; Ntziachristos, V.; van Dijl, J. M.; van Dam, G. M., Real-time in vivo imaging of invasive- and biomaterial-associated bacterial infections using fluorescently labelled vancomycin. *Nat. Commun.* **2013,** *4*, 2584.

(74) Wang, W.; Lin, L.; Du, Y.; Song, Y.; Peng, X.; Chen, X.; Yang, C. J., Assessing the viability of transplanted gut microbiota by sequential tagging with D-amino acid-based metabolic probes. *Nat. Commun.* **2019,** *10* (1), 1317.

(75) Thaxton, C. S.; Georganopoulou, D. G.; Mirkin, C. A., Gold nanoparticle probes for the detection of nucleic acid targets. *Clin. Chim. Acta* **2006,** *363* (1), 120-126.

(76) Baptista, P.; Pereira, E.; Eaton, P.; Doria, G.; Miranda, A.; Gomes, I.; Quaresma, P.; Franco, R., Gold nanoparticles for the development of clinical diagnosis methods. *Anal. Bioanal. Chem.* **2008,** *391* (3), 943-950.

(77) Verma, M. S.; Rogowski, J. L.; Jones, L.; Gu, F. X., Colorimetric biosensing of pathogens using gold nanoparticles. *Biotechnol. Adv.* **2015,** *33* (6, Part 1), 666-680.

(78) Aldewachi, H.; Chalati, T.; Woodroofe, M. N.; Bricklebank, N.; Sharrack, B.; Gardiner, P., Gold nanoparticle-based colorimetric biosensors. *Nanoscale* **2018,** *10* (1), 18-33.

(79) Chang, C.-C.; Chen, C.-P.; Wu, T.-H.; Yang, C.-H.; Lin, C.-W.; Chen, C.-Y., Gold Nanoparticle-Based Colorimetric Strategies for Chemical and Biological Sensing Applications. *Nanomaterials* **2019,** *9* (6), 861.

(80) Turkevich, J.; Stevenson, P. C.; Hillier, J., A study of the nucleation and growth processes in the synthesis of colloidal gold. *Discuss. Faraday Soc.* **1951,** *11* (0), 55-75.

(81) Liu, X.; Atwater, M.; Wang, J.; Huo, Q., Extinction coefficient of gold nanoparticles with different sizes and different capping ligands. *Colloids Surf. B. Biointerfaces* **2007,** *58* (1), 3-7.

(82) Storhoff, J. J.; Elghanian, R.; Mucic, R. C.; Mirkin, C. A.; Letsinger, R. L., One-Pot Colorimetric Differentiation of Polynucleotides with Single Base Imperfections Using Gold Nanoparticle Probes. *J. Am. Chem. Soc.* **1998,** *120* (9), 1959-1964.

(83) Zhan, N.; Palui, G.; Kapur, A.; Palomo, V.; Dawson, P. E.; Mattoussi, H., Controlling the Architecture, Coordination, and Reactivity of Nanoparticle Coating Utilizing an Amino Acid Central Scaffold. *J. Am. Chem. Soc.* **2015,** *137* (51), 16084-16097.

(84) Akrami, M.; Balalaie, S.; Hosseinkhani, S.; Alipour, M.; Salehi, F.; Bahador, A.; Haririan, I., Tuning the anticancer activity of a novel pro-apoptotic peptide using gold nanoparticle platforms. *Sci. Rep.* **2016,** *6*, 31030.

(85) Ramya, A. N.; Joseph, M. M.; Nair, J. B.; Karunakaran, V.; Narayanan, N.; Maiti, K. K., New Insight of Tetraphenylethylene-based Raman Signatures for Targeted SERS Nanoprobe Construction Toward Prostate Cancer Cell Detection. *ACS Appl. Mater. Interfaces* **2016,** *8* (16), 10220-10225.

(86) Feng, J.; Shen, Q.; Wu, J.; Dai, Z.; Wang, Y., Naked-eyes detection of Shigella flexneri in food samples based on a novel gold nanoparticle-based colorimetric aptasensor. *Food Control* **2019,** *98*, 333-341.

(87) Li, Z.; Askim, J. R.; Suslick, K. S., The Optoelectronic Nose: Colorimetric and Fluorometric Sensor Arrays. *Chem. Rev.* **2019,** *119* (1), 231-292.

(88) Zhu, L.; Li, S.; Shao, X.; Feng, Y.; Xie, P.; Luo, Y.; Huang, K.; Xu, W., Colorimetric detection and typing of E. coli lipopolysaccharides based on a dual aptamer-functionalized gold nanoparticle probe. *Microchimica Acta* **2019,** *186* (2), 111.

(89) Alizadeh, N.; Memar, M. Y.; Moaddab, S. R.; Kafil, H. S., Aptamer-assisted novel technologies for detecting bacterial pathogens. *Biomed. Pharmacother.* **2017,** *93*, 737-745.

(90) Park, K. S., Nucleic acid aptamer-based methods for diagnosis of infections. *Biosens. Bioelectron.* **2018,** *102*, 179-188.

(91) Takahashi, M., Aptamers targeting cell surface proteins. *Biochimie* **2018,** *145*, 63-72.

(92) Ray, P. C.; Khan, S. A.; Singh, A. K.; Senapati, D.; Fan, Z., Nanomaterials for targeted detection and photothermal killing of bacteria. *Chem. Soc. Rev.* **2012,** *41* (8), 3193-3209.

(93) Ahmed, A.; Rushworth, J. V.; Hirst, N. A.; Millner, P. A., Biosensors for Whole-Cell Bacterial Detection. *Clin. Microbiol. Rev.* **2014,** *27* (3), 631-646.

(94) Iqbal, S. S.; Mayo, M. W.; Bruno, J. G.; Bronk, B. V.; Batt, C. A.; Chambers, J. P., A review of molecular recognition technologies for detection of biological threat agents. *Biosens. Bioelectron.* **2000,** *15* (11), 549-578.

(95) Holzinger, M.; Le Goff, A.; Cosnier, S., Nanomaterials for biosensing applications: a review. *Front. Chem.* **2014,** *2* (63).

(96) Wang, Y.-X.; Ye, Z.-Z.; Si, C.-Y.; Ying, Y.-B., Application of Aptamer Based Biosensors for Detection of Pathogenic Microorganisms. *Chinese J. Anal. Chem.* **2012,** *40* (4), 634-642.

(97) Hong, K. L.; Sooter, L. J., Single-Stranded DNA Aptamers against Pathogens and Toxins: Identification and Biosensing Applications. *Biomed Res. Int.* **2015,** *2015*, 31.

(98) Liu, Y.; Wang, J.; Song, X.; Xu, K.; Chen, H.; Zhao, C.; Li, J., Colorimetric immunoassay for Listeria monocytogenes by using core gold nanoparticles, silver nanoclusters as oxidase mimetics, and aptamer-conjugated magnetic nanoparticles. *Microchimica Acta* **2018,** *185* (8), 360.

(99) Xu, Z.; Bi, X.; Huang, Y.; Che, Z.; Chen, X.; Fu, M.; Tian, H.; Yang, S., Sensitive colorimetric detection of Salmonella enteric serovar typhimurium based on a gold nanoparticle conjugated bifunctional oligonucleotide probe and aptamer. *J. Food Saf.* **2018,** *38* (5), e12482.

(100) Boucher, H. W.; Talbot, G. H.; Bradley, J. S.; Edwards, J. E.; Gilbert, D.; Rice, L. B.; Scheld, M.; Spellberg, B.; Bartlett, J., Bad Bugs, No Drugs: No ESKAPE! An Update from the Infectious Diseases Society of America. *Clin. Infect. Dis.* **2009,** *48* (1), 1-12.

(101) Marimuthu, K.; Venkatachalam, I.; Khong, W. X.; Koh, T. H.; Cherng, B. P. Z.; Van La, M.; De, P. P.; Krishnan, P. U.; Tan, T. Y.; Choon, R. F. K.; Pada, S. K.; Lam, C. W.; Ooi, S. T.; Deepak, R. N.; Smitasin, N.; Tan, E. L.; Lee, J. J.; Kurup, A.; Young, B.; Sim, N. T. W.; Thoon, K. C.; Fisher, D.; Ling, M. L.; Peng, B. A. S.; Teo, Y.-Y.; Hsu, L. Y.; Lin, R. T. P.; Ong, R. T.-H.; Teo, J.; Ng, O. T.; for the Carbapenemase-Producing Enterobacteriaceae in Singapore Study, G., Clinical and Molecular Epidemiology of Carbapenem-Resistant Enterobacteriaceae Among Adult Inpatients in Singapore. *Clin. Infect. Dis.* **2017,** *64* (suppl_2), S68-S75.

(102) DeMeester, K. E.; Liang, H.; Jensen, M. R.; Jones, Z. S.; D'Ambrosio, E. A.; Scinto, S. L.; Zhou, J.; Grimes, C. L., Synthesis of Functionalized N-Acetyl Muramic

Acids To Probe Bacterial Cell Wall Recycling and Biosynthesis. *J. Am. Chem. Soc.* **2018,** *140* (30), 9458-9465.

(103) Calabretta, P. J.; Hodges, H. L.; Kraft, M. B.; Marando, V. M.; Kiessling, L. L., Bacterial Cell Wall Modification with a Glycolipid Substrate. *J. Am. Chem. Soc.* **2019,** *141* (23), 9262-9272.

(104) Senter, P. D., Potent antibody drug conjugates for cancer therapy. *Curr. Opin. Chem. Biol.* **2009,** *13* (3), 235-244.

(105) Alley, S. C.; Okeley, N. M.; Senter, P. D., Antibody–drug conjugates: targeted drug delivery for cancer. *Curr. Opin. Chem. Biol.* **2010,** *14* (4), 529-537.

(106) Saha, K.; Agasti, S. S.; Kim, C.; Li, X.; Rotello, V. M., Gold Nanoparticles in Chemical and Biological Sensing. *Chem. Rev.* **2012,** *112* (5), 2739-2779.

(107) Welzel, P., Syntheses around the Transglycosylation Step in Peptidoglycan Biosynthesis. *Chem. Rev.* **2005,** *105* (12), 4610-4660.

Appendix A

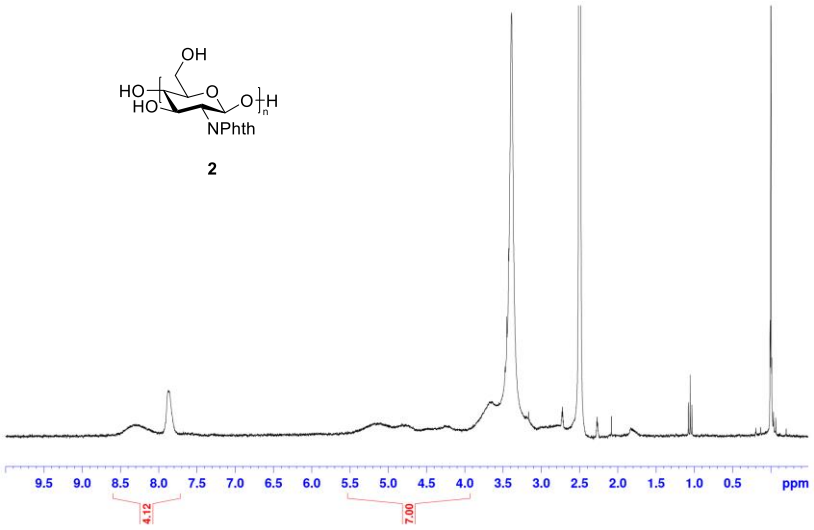

Figure a1. ^{1}H NMR spectrum for **2** (400 MHz, DMSO)

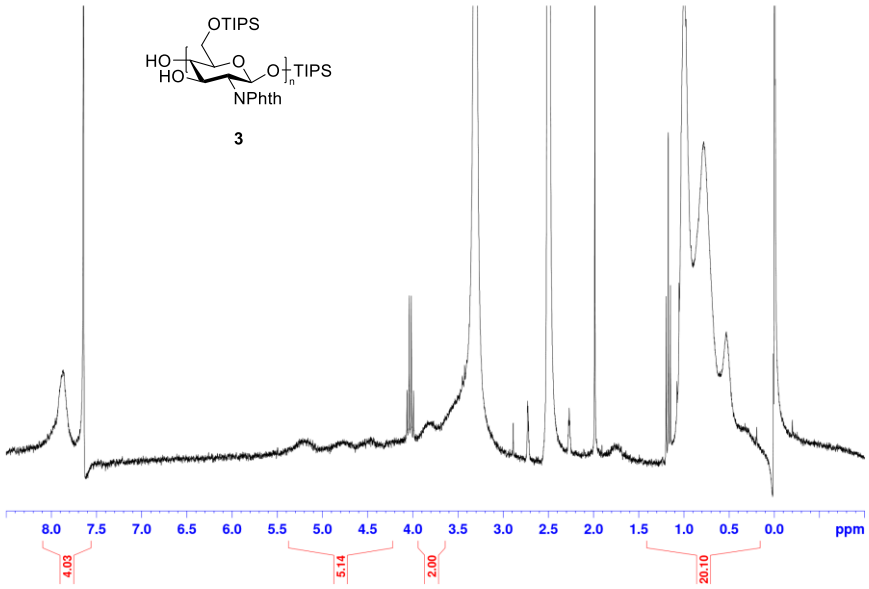

Figure a2. ^{1}H NMR spectrum for **3** (400 MHz, DMSO)

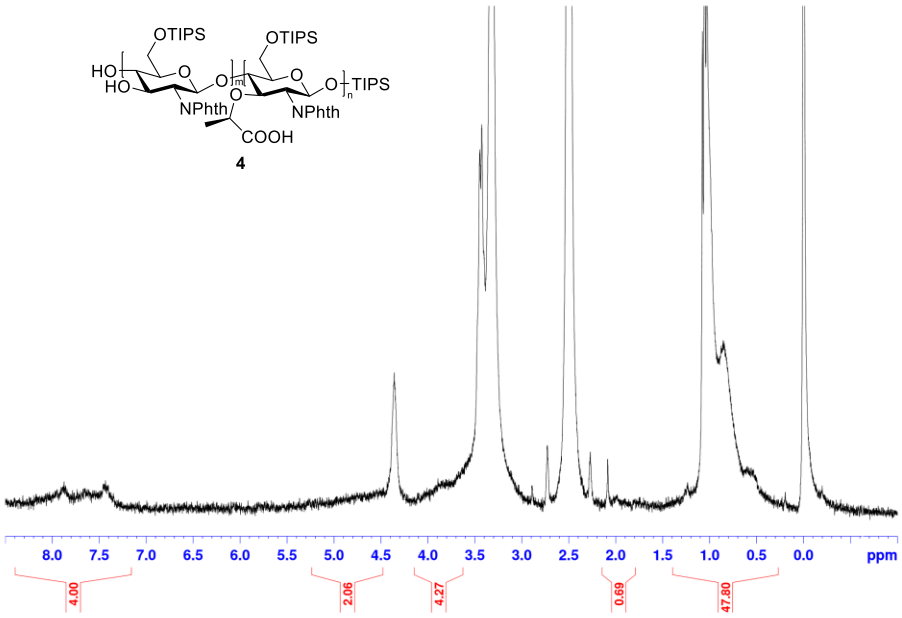

Figure a3. ^{1}H NMR spectrum for **4** (400 MHz, DMSO)

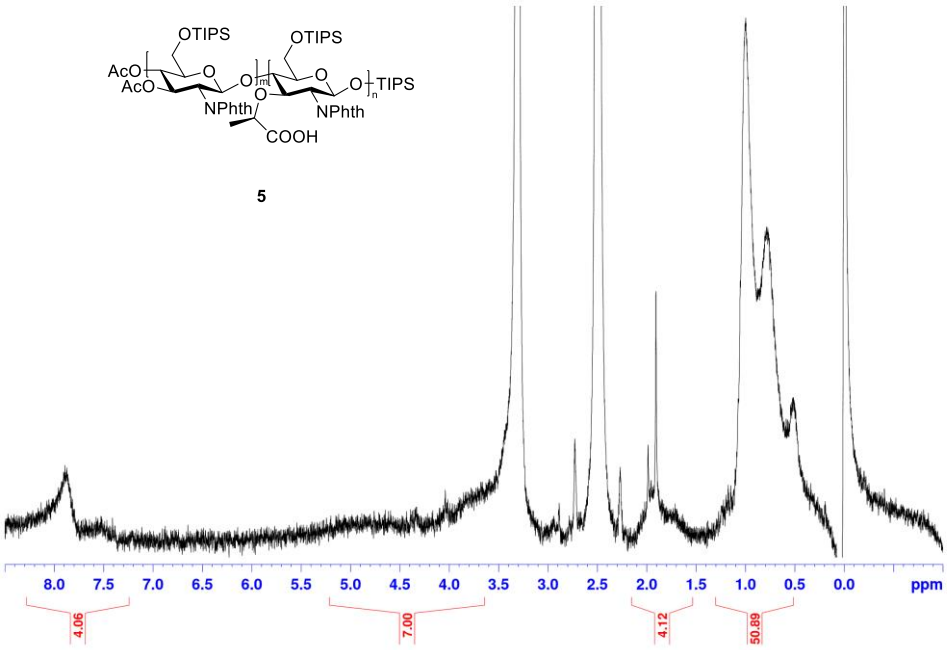

Figure a4. ^{1}H NMR spectrum for **5** (400 MHz, DMSO)

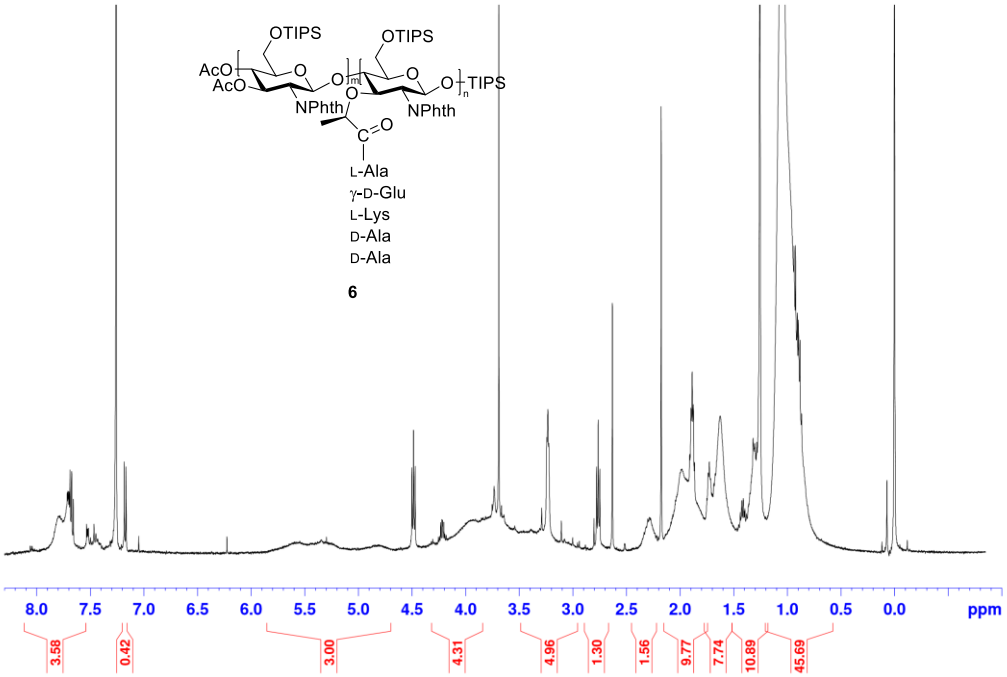

Figure a5. ^{1}H NMR spectrum for **6** (400 MHz, DMSO)

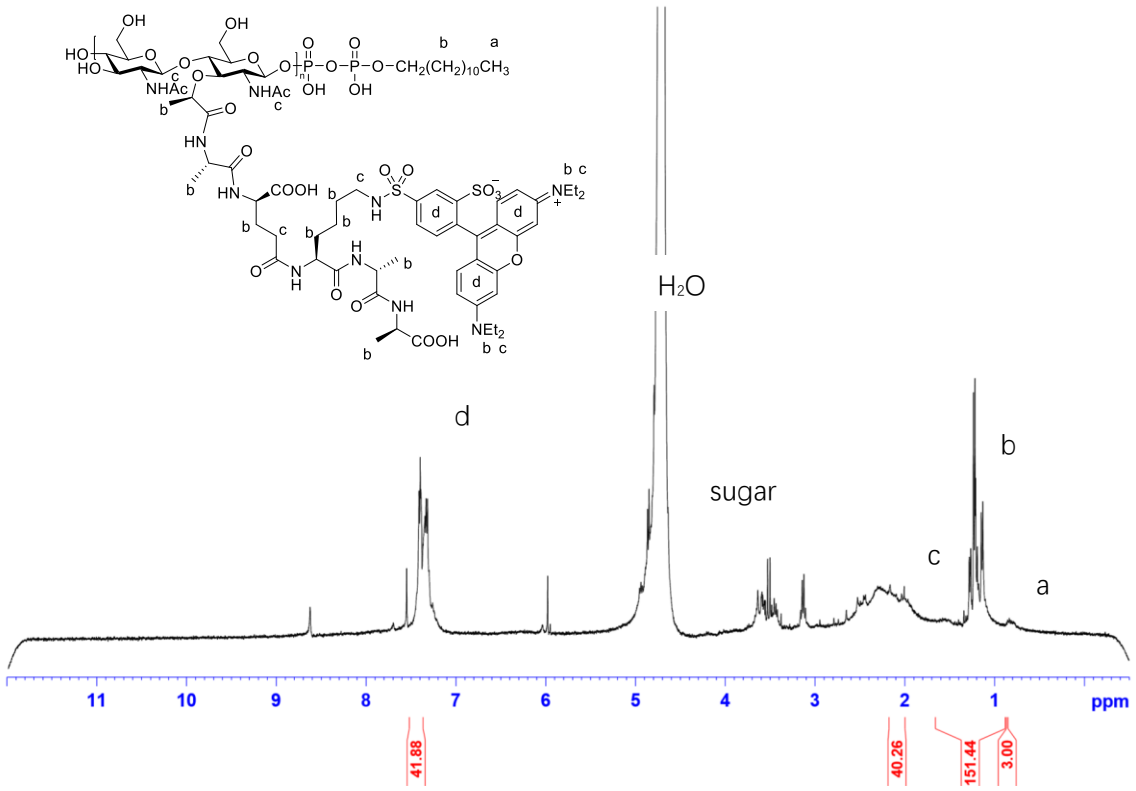

Figure a6. ^{1}H NMR spectrum of fluorescently labeled **9** used for STED confocal microscopy (400 MHz, D_2O).

The methyl end of lipid moiety (0.8-0.9, **a**) has been calibrated to be 3 protons (1 lipid as base for calculation)

Aromatic protons (7-8, **d**) were only from rhodamine (9 per molecule), and 42 protons in total matched 4.6 rhodamine moieties per polymer on average.

Alkyl protons (0.9-1.5, **b**) were from lipid (24 per molecule), rhodamine (6 per molecule) and peptide (20 per molecule), and 151 protons matched 5.0 peptide moieties per polymer on average

Acetyl protons (2-2.2, **c**) were from NAG/NAM (3 per molecule) and glutamate on peptide (2 per molecule), and 40 protons matched 10.0 sugar moieties per polymer on average.

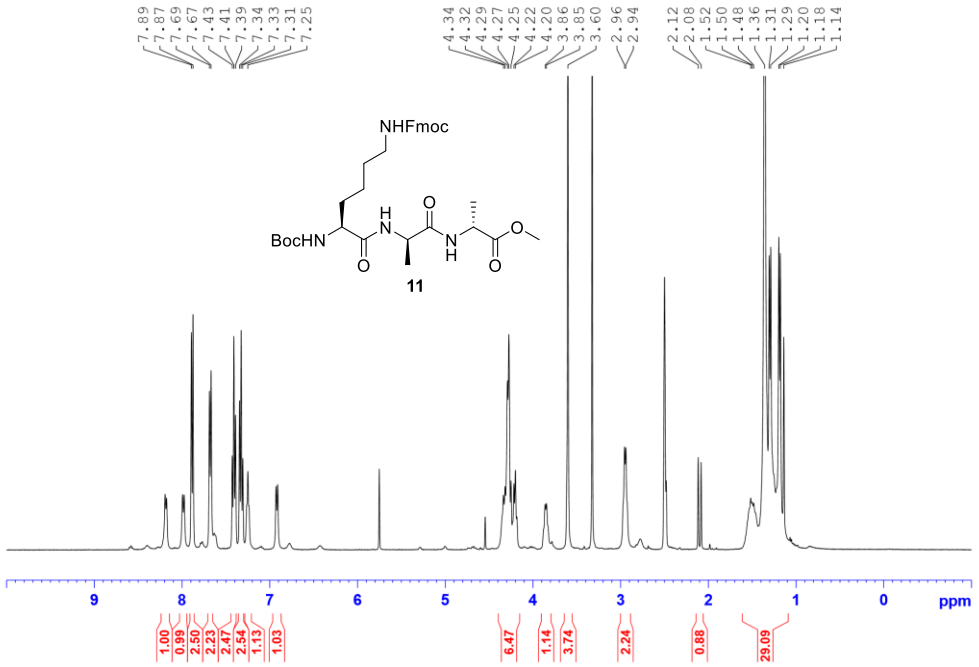

Figure a7. ^{1}H NMR spectrum for **11** (400 MHz, DMSO)

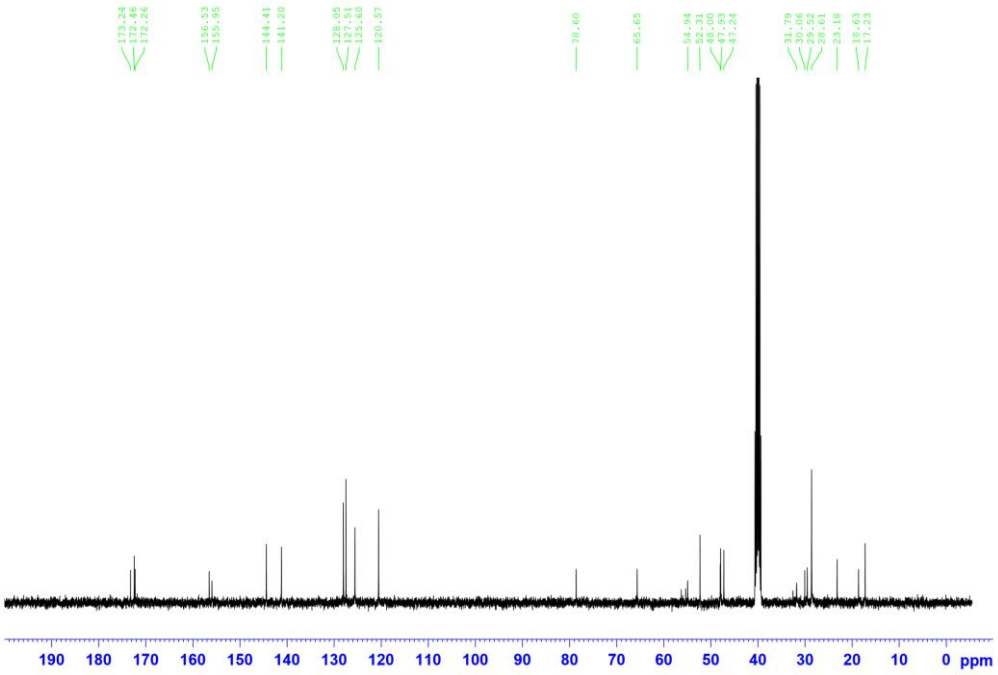

Figure a8. ^{13}C NMR spectrum for **11** (101 MHz, DMSO)

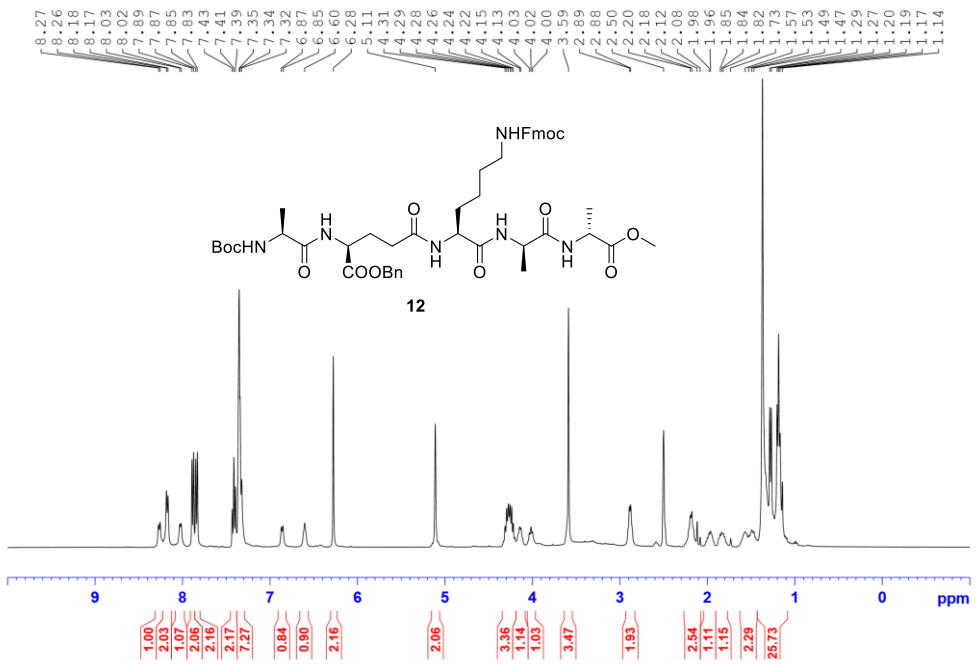

Figure a9. ^{1}H NMR spectrum for **12** (400 MHz, DMSO)

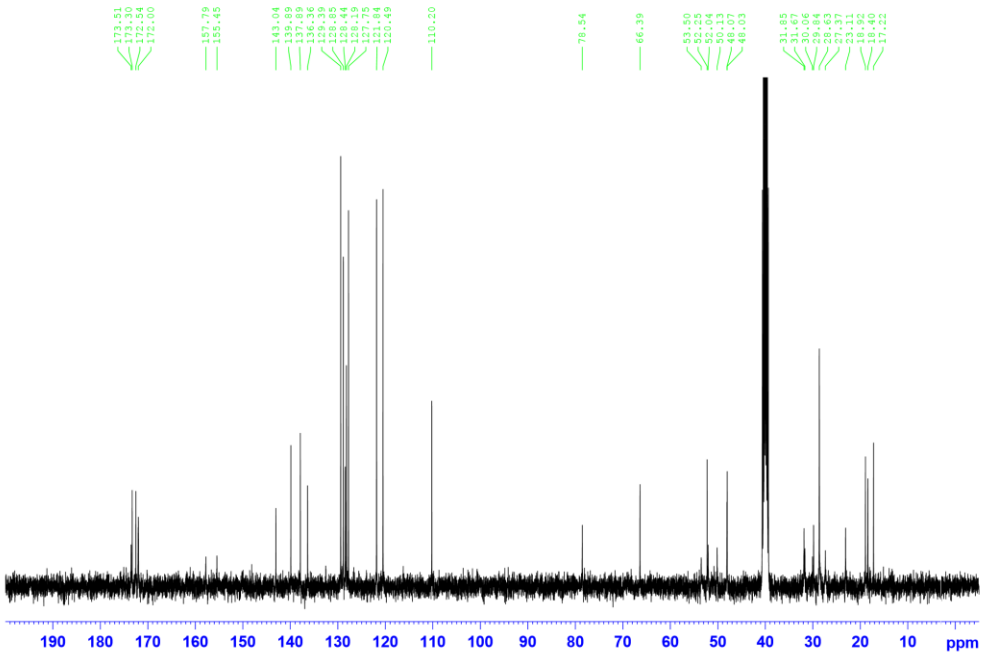

Figure a10. ^{13}C NMR spectrum for **12** (101 MHz, DMSO)

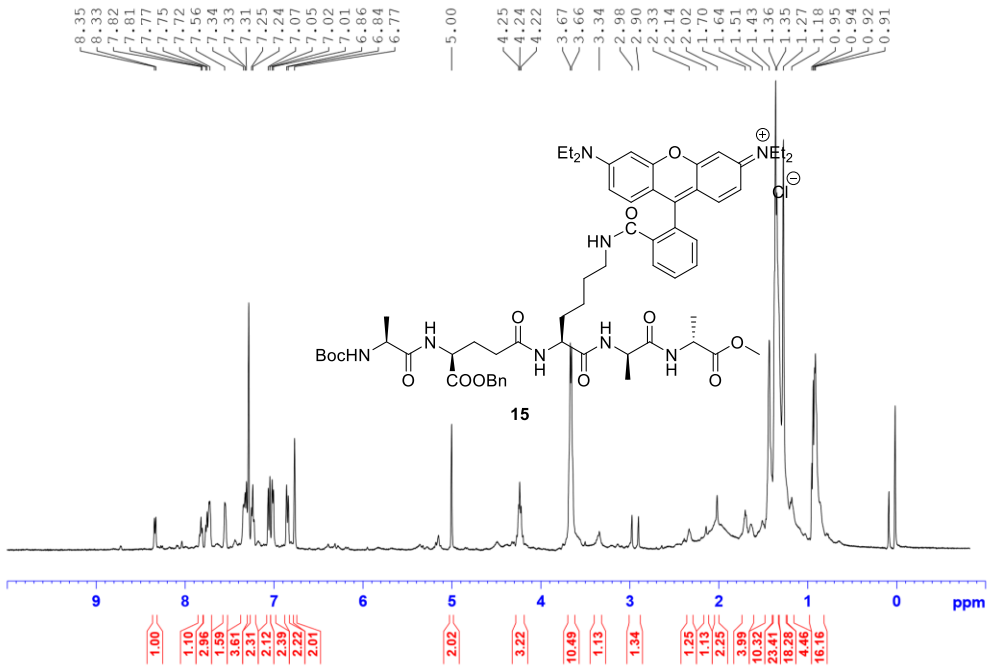

Figure a11. ^{1}H NMR spectrum for **15** (500 MHz, Chloroform-*d*)

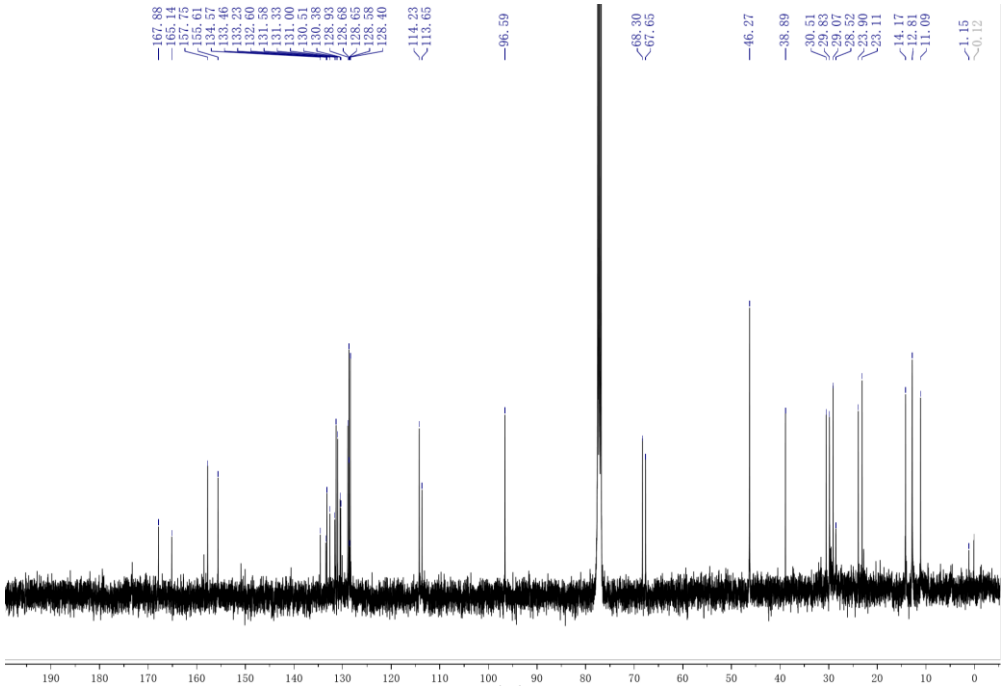

Figure a12. ^{13}C NMR spectrum for **15** (101 MHz, Chloroform-*d*)

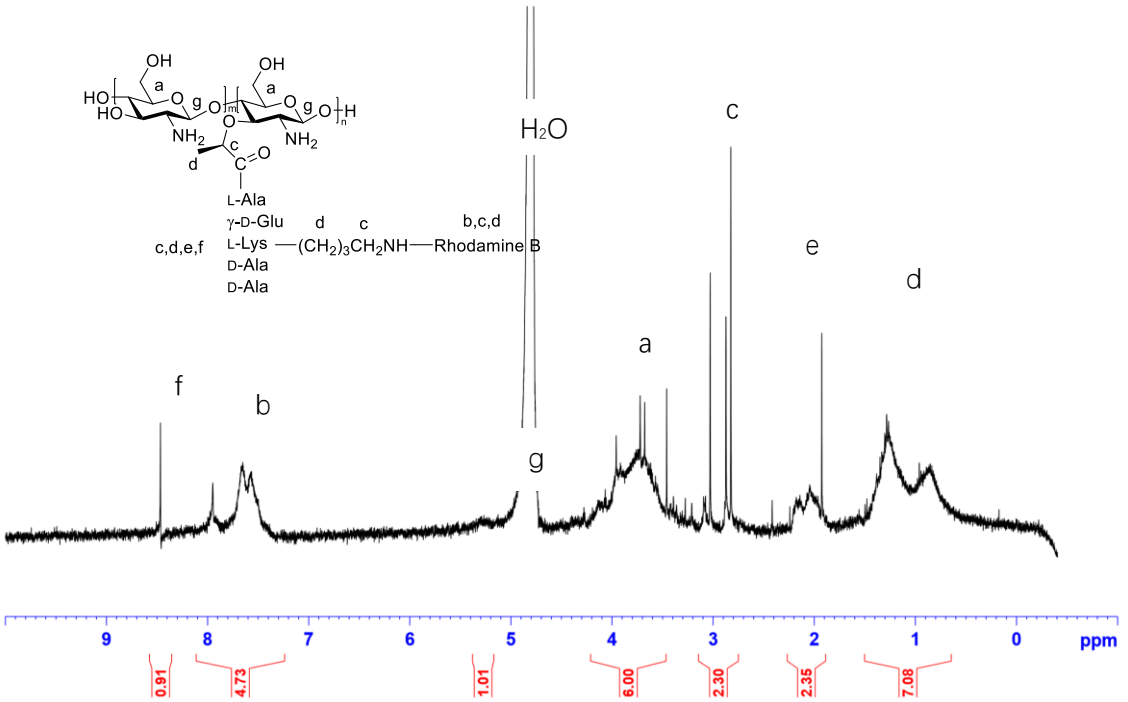

Figure a13. ^{1}H NMR spectrum for rhodamine labeled Chitosan-peptide **16** (500 MHz, D_2O)

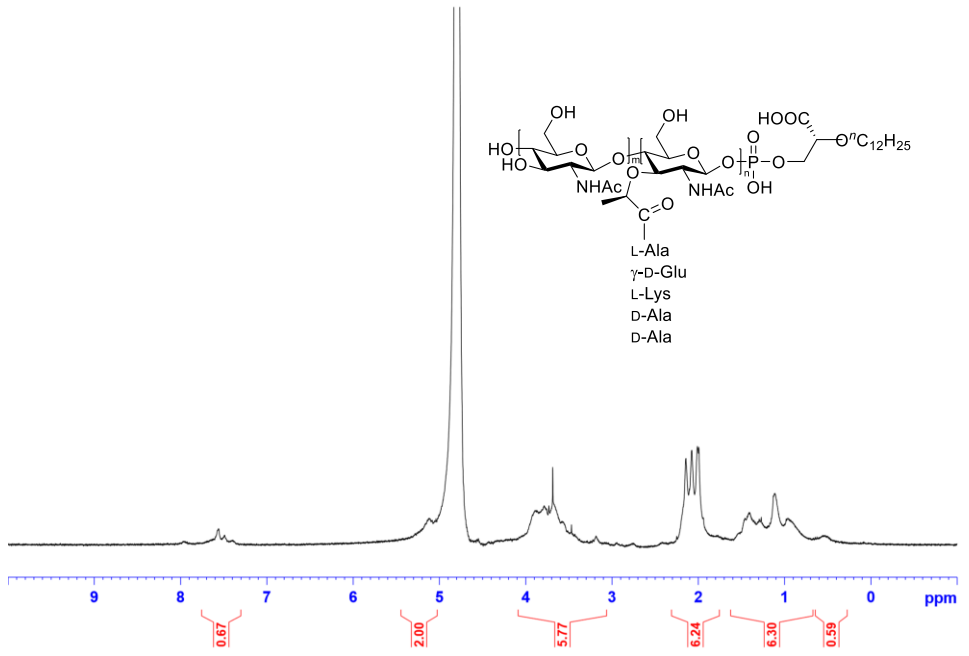

Figure a14. ^{1}H NMR spectrum for **17** (500 MHz, D_2O)

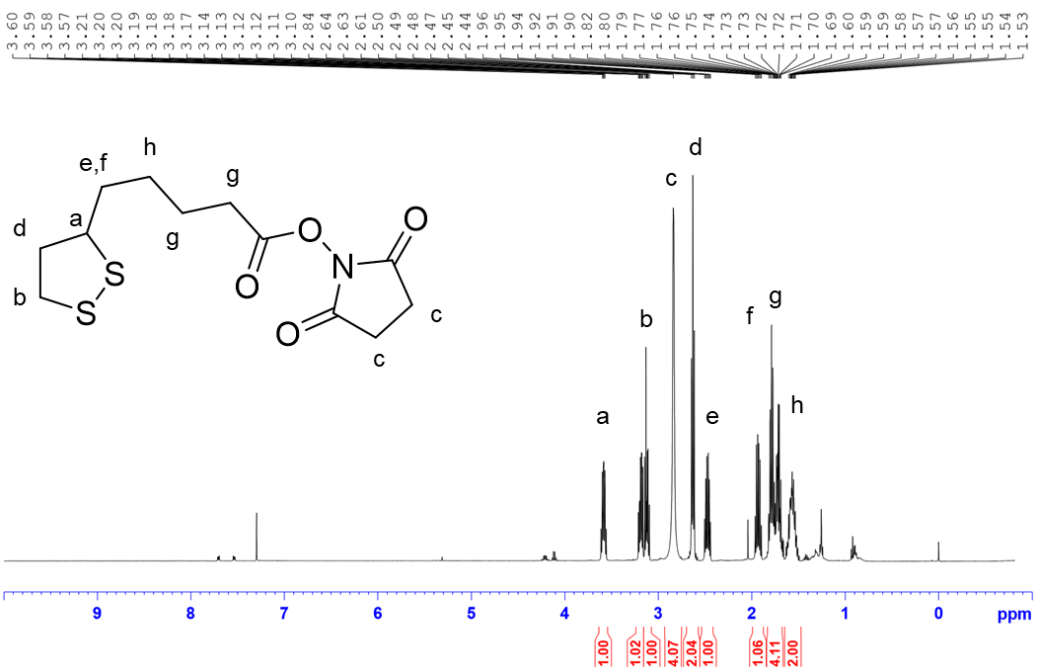

Figure a15. ^{1}H NMR spectrum for **18** (500 MHz, $CDCl_3$)

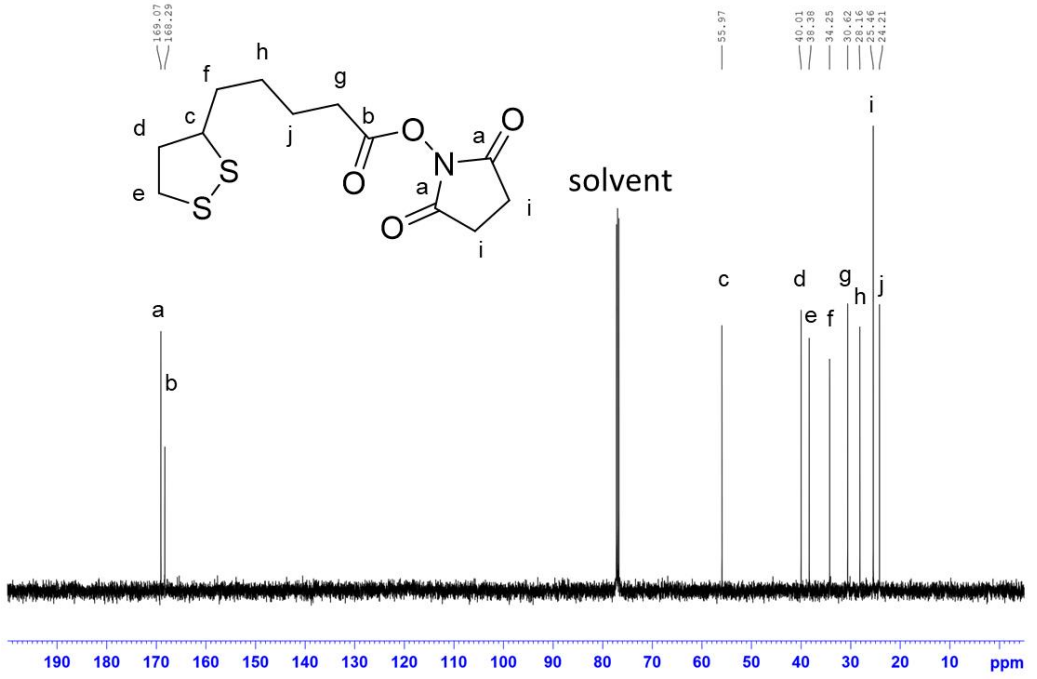

Figure a16. ^{13}C NMR spectrum for **18** (125 MHz, $CDCl_3$)

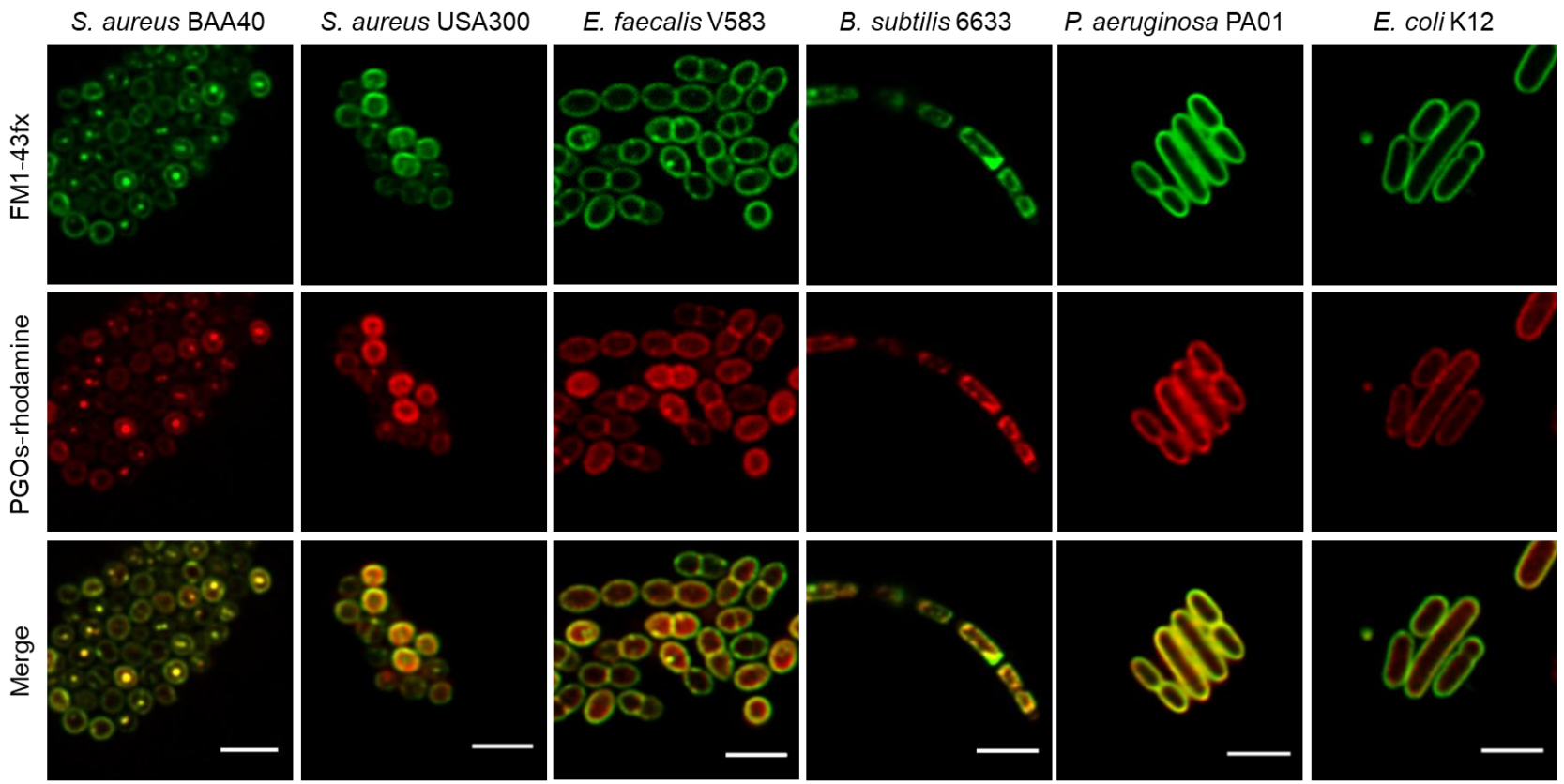

Figure a17. Fluorescence STED confocal studies of 6 different bacteria strains. Green color marked fluorescence from the membrane dye FM 1-43fx, red color marked fluorescence from the PGO-rhodamine, and yellow color indicated colocalization of the two fluorophores in bacterial cells. Scale bar = 2 μm.

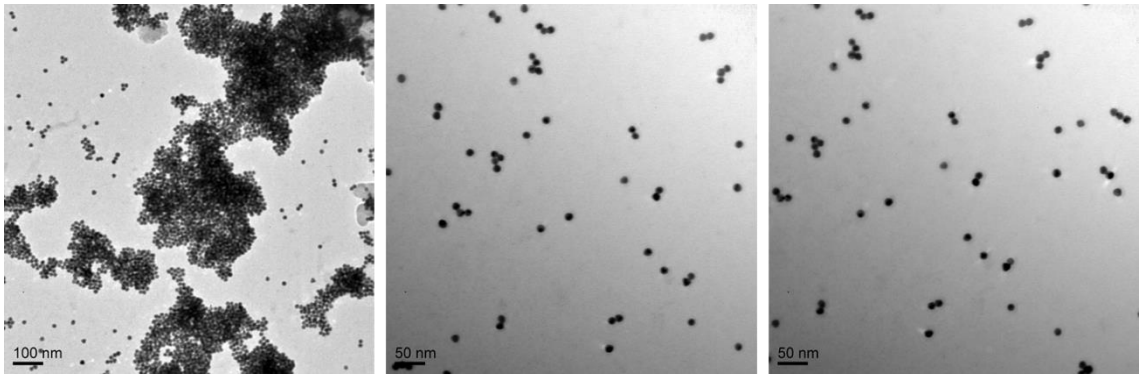

Figure a18. Broader view of AuNP in solution.

List of Publications

1. "Catalyst-Controlled Stereoselective O-Glycosylation: Pd(0) vs Pd(II)" Yao, H.; Zhang, S.; Leng, W.-L.; Leow, M.-L.; Xiang, S. He, J.-X.; Liao, H.; Le Mai Hoang, K.; Liu, X.-W. *ACS Catal.* **2017**, *7*, 5456-5460.
2. "Asymmetric syntheses of 8-oxabicyclo[3,2,1]octane and 11-oxatricyclo[5.3.1.0]undecane from glycals" Liao, H.; Leng, W.-L.; Le Mai Hoang, K.; Yao, H.; He, J.-X.; Voo, A. Y. H.; Liu, X.-W. *Chem. Sci.* **2017**, *8*, 6656-6661.
3. "A minimalist approach to stereoselective glycosylation with unprotected donors" Le Mai Hoang, K.; He, J.-X.; Báti, G.; Chan-Park, M. B.; Liu, X.-W. *Nat. Commun.* **2017**, *8*, 1146.
4. "Oxadiazabicyclooctenone as a versatile monomer for the construction of pH sensitive functional polymers via ROMP" Mallick, A.; Xu, Y.; Lin, Y.; He, J.-X.; Chan-Park, M. B.; Liu, X.-W. *Polym. Chem.* **2018**, *9*, 372-377.
5. "Venturing beyond Donor-Controlled Glycosylation: New Perspectives toward Anomeric Selectivity" Leng, W.-L.[#]; Yao, H.[#]; He, J.-X.[#]; Liu, X.-W. *Acc. Chem. Res.* **2018**, *51*, 628-639. ([#] equal contribution)
6. "CHAPTER 2 Methodologies in Chemical Syntheses of Carbohydrates." Leng, W.-L.[#]; He, J.-X.[#]; Yao, H.[#]; Liu, X.-W. *Synthetic Glycomes,* (The Royal Society of Chemistry) **2019**, pp 15-45. ([#] equal contribution)

7. "Stereo- and regioselective glycosylation with protection-less sugar derivatives: an alluring strategy to access glycans and natural products" Báti, G.[#]; He, J.-X.[#]; Pal, K. B.[#]; Liu, X.-W. *Chem. Soc. Rev.* **2019**, *48*, 4006-4018. ([#] equal contribution)
8. "Synthetic Biohybrid Peptidoglycan Oligomers Enable Pan-Bacteria-Specific Labeling and Imaging: *In Vitro* and *In Vivo*" He, J.-X.; Le Mai Hoang, K.; Kho, S. H.; Guo, Z.; Zhong, W.; Thappeta, K. R. V.; Zamudio-Vázquez, R.; Hoo, S. N.; Xiong, Q.; Duan, H.; Yang, L.; Chan-Park, M. B.; Liu, X.-W. *Chem. Sci.* **2020**, DOI: 10.1039/C9SC06345E.